KELP FOREST MODULE DEVELOPMENT FOR A REGIONAL OCEAN MODEL AND ITS USE FOR BIOGEOCHEMISTRY AND ECOLOGY IMPACTS.

by

MATHEUS FAGUNDES

(Under the Direction of C. Brock Woodson)

ABSTRACT

Kelp forests are present across a quarter of all coastlines and are essential vegetated ecosystems. These ecosystems are susceptible to extreme events and climate change, but also modify the physics of in the water column and, consequently, the biogeochemistry and ecology. Although scientists have understood the importance of kelp forests and have studied these domains extensively both in the field and in the laboratory, these studies only provide snapshots or isolated views of kelp forest dynamics. More recently, ocean modeling efforts have been made to address the spatial and temporal variability of the dynamics of these ecosystems, especially for understanding the interaction of nearshore currents and changes in the biogeochemistry in the water column. However, to date kelp forests have not been fully incorporated in to couped hydrodynamic-biogeochemical models. In this dissertation, I develop a 3-D hydrodynamic model for kelp forests in a regional ocean model, add a biogeochemistry model that represents the primary process for kelp forests, and demonstrate the impact of stressors on kelp forests and the effects on local physics and biogeochemistry.

INDEX WORDS: kelp modeling, model development, biogeochemistry, ecology, coastal engineering applications

KELP FOREST MODULE DEVELOPMENT FOR A REGIONAL OCEAN MODEL AND ITS USE FOR BIOGEOCHEMISTRY AND ECOLOGY IMPACTS.

by

MATHEUS FAGUNDES

B.Sc., Universidade Federal do Maranhao, Brazil, 2016

M.Sc., University of Georgia, 2018

A Dissertation Submitted to the Graduate Faculty of The University of Georgia in Partial Fulfillment of the Requirements for the Degree

DOCTOR OF PHILOSOPHY

ATHENS, GEORGIA

2023

KELP FOREST MODULE DEVELOPMENT FOR A REGIONAL OCEAN MODEL AND ITS USE FOR BIOGEOCHEMISTRY AND ECOLOGY IMPACTS.

by

MATHEUS FAGUNDES

Major Professor: C. Brock Woodson

Committee: Brian Bledsoe
David Emory Stooksbury
Renato Castelão

Electronic Version Approved:

Ron Walcott
Vice Provost for Graduate Education and Dean of the Graduate School
The University of Georgia
August 2023

DEDICATION

Eu gostaria de começar a agradecer aos meus pais, Maria Christina e Marco Antonio, e minhas irmas, “Tata” e “Anas Craras”, que sempre me apoiaram os meus sonhos. Minha vida começou no meio do “Brasilzao” rodeado por fazendas. Meus pais mesmo não tendo muitas condições queriam que a gente tivesse o melhor em educação para que um dia a gente fosse alguém na vida. A típica pessoa no estado aonde eu nasci faria veterinária, zootecnia ou agronomia como profissão. Quando eu tive a vontade de fazer Oceanografia, muitos me disseram que isso seria loucura. Coincidentemente, o primeiro programa de Oceanografia na Universidade Federal do Maranhão estava abrindo no semestre seguinte e era aonde eu tinha meu tio Esnel. Meu tio Esnel me acolheu em sua casa nos próximos 5 anos dessa minha jornada. Não somente minha graduação, mas como a minha estadia no Maranhão com o meu tio me fez crescer como pessoa e olhar o mundo de outra forma. Agradecer meus professores que também tiveram um papel importante na minha decisão de que caminho da Oceanografia seguir. Ao o meu orientador Dr. Torres, e aos professor Dr. Pezzi no INPE e Dra. Parise na UFMA por me derem as ferramentes necessários para o meu crescimento na carreira de modelagem numérica.

Aos meus familiares que mesmo estando longe, vocês também participaram desse meu processo Um agradecimento ao meu primo, João Vitor por passar vários anos natal e ano novo comigo nos anos que não poderia ir ao Brasil.

E claro que não poderia de agradecer imensamente meu orientador Dr. Woodson pelos 7 anos de aprendizagem, batendo cabeça, e sendo paciente comigo nos momentos que eu achava que estava certo. O senhor me mostrou muito como olhar os problemas na ciência de outra maneira e

me deu desafios que eu achava que nunca poderia terminar como, por exemplo, meu mestrado e agora meu doutorado.

Por último, a pessoa mais especial na minha vida minha avó, que por mais que a senhora não esteja aqui saiba que sempre penso na senhora e nos nossos momentos. Eu gostaria muito que a senhora pudesse estar vendo aonde eu cheguei, porem a vida não eh do jeito que a gente quer, mas espero que aonde a senhora estiver que a senhora esteja muito orgulhosa de mim.

"Last but not least", gostaria de agradecer a mim mesmo por ter me aguentado e ter conseguido chegar aonde eu cheguei de forma atabalhoada. Obrigado Matheus do passado por continuar nessa jornada de ensino e estudos. Mas você deveria ter trabalhado mais por que agora tô sofrendo com tanto coisa.

ACKNOWLEDGEMENTS

I want to say thank you to Dr. Woodson for being the most patient person at times. I was being stubborn, also believing in my potential way back to my masters when I only had a dream to become a great scientist in physical oceanography. You showed me the beauty of looking at problems from different perspectives. Thank you for trusting that I had enough knowledge of ocean modeling that I could do the work you wanted someone to do.

I was able to do my Ph.D. thanks to the support of NSF research grant and the Engineering department at UGA.

My project had lots of help from other collaborators. First of all, the local fishing cooperatives from the Federación Regional de Sociedades Cooperativas de la Industria Pesquera (FEDECOOP), the civil association Comunidad y Biodiversidad in Baja California, and the California Department of Fish and Wildlife for giving support and helping in the data collection that I was able to use to validate my models. Secondly, Dr. Micheli and Dr. Monismith at Stanford University and Dr. Valle-Levinson at the University of Florida.

Also, my peers in my lab were always ready to debate and listen to my crazy ideas and show me even better angles to my problems. Additionally, Zhuofei Huo at GACRC that I do not know how many times I emailed and annoyed him with my issues in my model compilations.

Last but not least, I thank my committee for suggesting courses I should take to improve my background in statistics and for the tips for some of the results I found in my dissertation.

TABLE OF CONTENTS

LIST OF TABLES

Page

LIST OF FIGURES

Page

CHAPTER 1

INTRODUCTION

In recent years, modeling efforts have started moving towards eddy and submesoscale resolution for Global Climate Models (GCMs; Giorgi *et al.* 2009). However, coastal processes are still poorly represented (Holt *et al.* 2017), for example sediment transport, internal tides, and aquatic vegetation are rarely accounted for in GCMs. The growing need for higher resolution projections at coastal scales has been described as one of the great scientific challenges by both the Climate Research Programme and NOAA (WCRP, 2021; GSL, 2022). Yet, recent improvements in higher resolution projections have been primarily atmosphere-focused. In order to understand the effects of coastal processes on climate change, nearshore dynamics such as flow-vegetation interactions need to be incorporated in these earth system models.

Blue carbon ecosystems such as kelp forests and salt marshes also remain largely unrepresented in GCMs, yet their impacts are vast. Blue Carbon ecosystems impact both the carbon cycle (Macreadie *et al.* 2019) and coastal residence time (Liu *et al.* 2019), and create high dissolved oxygen environments (Gerard, 1986). Kelp forest ecosystems, in particular, are present in 25% of the world's coastlines (Duarte, 2017; Macreadie *et al.* 2019; Wernberg *et al.* 2019) and are the largest coastal vegetated ecosystems in the world (Filbee-Dexter & Wernberg, 2020). Kelp forests export over 40% of the total carbon produced from all Blue Carbon ecosystems (Duarte, 2017). While they are important for carbon sequestration (Macreadie *et al.* 2019), kelp forests also shelter macroinvertebrates, fish, and mammals (Dayton, 1985), maintain high dissolved oxygen

(DO) (Frieder *et al.* 2012) and high pH (Krause-Jensen *et al.* 2016), and increase residence time (Jackson, 1984; Gaylord *et al.* 2007).

Besides their ecological value, kelp forests are also important economically, generating over $1 billion annually (Kim *et al.* 2017). For example, human consumption, pharmaceuticals, and biofuel (Buschmann *et al.* 2017). Kelp forests have also been suggested as a bio-engineering alternative to manage carbon in the atmosphere (Duarte *et al.* 2013). Additionally, they have also been studied to understand their effect on nearshore erosion as kelp forests can damp currents and waves before arriving to the shore (Løvås & Tørum, 2001). Culturally, they play an important role in the Indigenous Australian culture (Thurstan *et al.* 2018).

Although, kelp forest effects on hydrodynamics and transport have been studied extensively in laboratory experiments (Rosman *et al.* 2010; Rosman *et al.* 2013) and *in situ* (Walter *et al.* 2012; Leary *et al.* 2017; Monismith *et al.* 2022), little effort has been placed on developing a hydrodynamic model that represents kelp in the water column and its effects on global climate. So far, models either only account for the influence of vegetation at the bottom of the domain (Wu *et al.* 2017), or they are offline models that do not allow feedback between the hydrodynamic and biogeochemical models (Frieder *et al.* 2022). This proposal seeks to develop a model capable of representing a 3-D kelp forest including kelp canopy (hereafter *canopy*) in a high-resolution hydrodynamic model as well as impacts on biogeochemistry of its surroundings. Chapter 2 of this proposal includes an overview of the topics related to kelp forests and lays out further motivation for the research. I address three fundamental research questions in this dissertation comprising Chapters 3-5 respectively:

1. Can a hydrodynamic module be developed to simulate kelp forests in a regional ocean model? If so, can this model represent the canopy and its turbulence generated in that region?
2. What are the impacts of kelp respiration and net primary productivity within kelp domains? How does pH look like in relation to Apparent Oxygen Utilization in kelp forests? Can kelp forests create a climate refugia against hypoxia and acidification in the future?
3. How does fragmentation affect the physics and biogeochemistry in kelp forests regions?

In Chapter 6, I summarize and reflect on results, highlight contributions to ocean modeling, oceanography, engineering, and climate modeling from my dissertation and outline future research and development directions.

CHAPTER 2

LITERATURE REVIEW

2.1 KELP DESCRIPTION

Kelp forests are dense stands of macroalgae found in areas of rocky substrate (Bolton, 2010) and cover 25% of coastlines globally (Wernberg *et al.* 2018; Fig. 2.1). Individual kelp plants can grow from 5 m to up to 200 m depth (Žuljević *et al.* 2016) depending on different physical factors and nutrients availability; and thus, kelp ecosystems can have net primary production (NPP) 10-fold higher than phytoplankton in some coastal and polar regions (Pessarrodona *et al.* 2022). These macroalgae also generate a three-dimensional structure that changes the physical (Jackson, 1984) and biogeochemical (Jackson, 1977) conditions in their surrounding environment. The abundance of food sources and protection against currents make kelp forests an excellent shelter for macroinvertebrates, fish, and mammals (Dayton, 1985; Rafaelli & Hawkins, 1999). However, these ecosystems are susceptible to seasonal variations, external physical impacts (i.e., storm surges, El Niño, marine heatwaves; Dayton & Tegner, 1984; Dayton, 1985; Gaylord *et al.* 2007; Arafeh-Dalmau et al 2020; Monismith *et al.* 2022), and climate change (Reed *et al.* 2016) that can lead to dense forests or complete absence of kelp (urchin barrens; Rogers-Bennett et al 2019).

Kelps have been studied all over the world (Wernberg *et al.* 2018). They are commonly categorized as cold region species (Bolton, 2010). However, some species are found in warm regions (Braga & Yoneshigue-Valentin, 1996). Bolton (2010) recognized over 100 species throughout the world, where the northeast Pacific is the most diverse of all regions. Kelps in

subtidal areas can be divided into three categories according to how they grow (Wernberg *et al.*, 2018): a) kelps that have flexible stipes and spread over the sea floor not reaching more than a couple of meters off the bottom (Fig. 2.2a); b) kelp that have erect stipes that can form kelp beds with canopies but do not reach the surface (Fig. 2.2b), and c) kelps that have gas-filled bladders that allow them to reach their canopy to the surface (Fig. 2.2c).

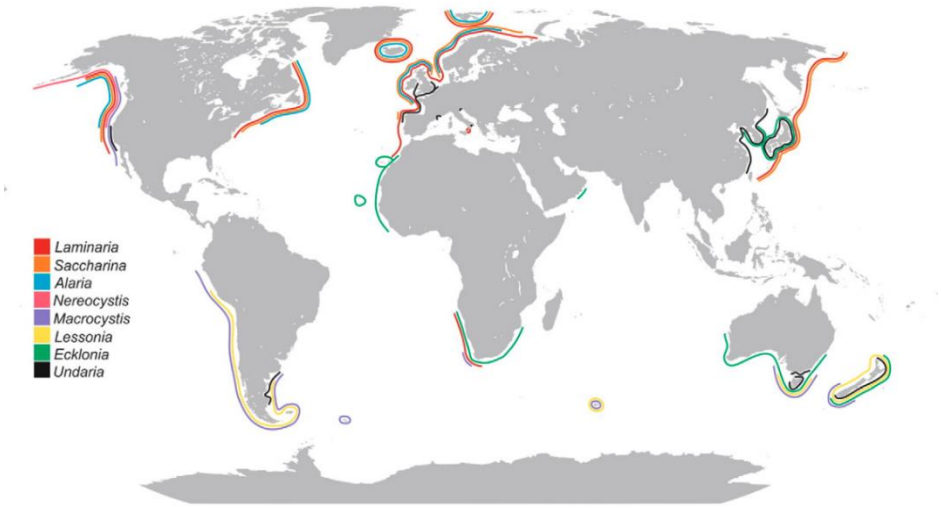

Figure 2.1- General types of kelp forests and their locations around the world. Source: Teagle *et al.* 2017.

Even though these macroalgae cover ¼ of the world's coastlines, they have particular environmental requirements to survive and colonize other regions. For example, according to Wernberg *et al.* (2018), temperatures below 15°C are optimum for growth and gametogenesis. Kelp inhabit rocky tidal areas because they require a hard substrate for their holdfast which is similar to a root structure for seagrasses and terrestrial plants. These regions are also characterized by turbulent waters that bring inorganic carbon and nutrients to their stipes and blades. Graham *et al.* (2007) found kelps in depths as deep as 150 m from the surface where nutrients result from

upwelling in the Galapagos region. Žuljević *et al.* (2016) found kelps in depths greater than 70 m, where the cold waters probably come from Western Mediterranean deep waters.

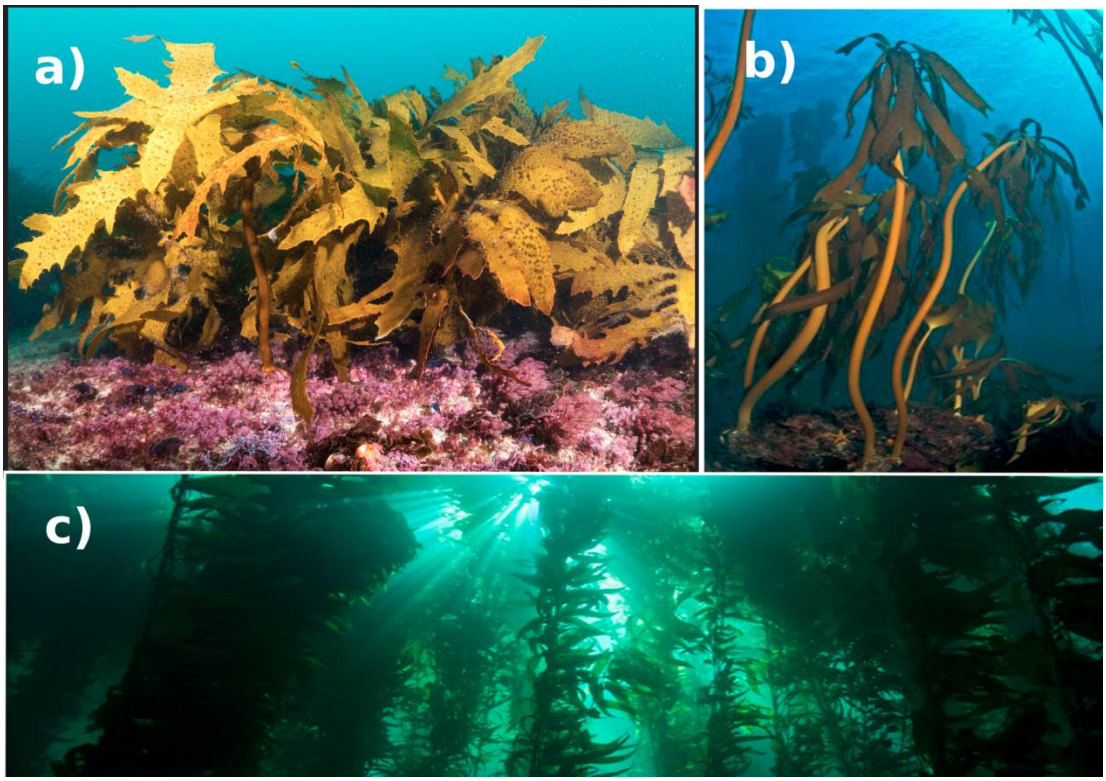

Figure 2.2 - Types of kelp forests a) *Ecklonia radiata*. (Source: https://www.flickr.com/photos/johnwturnbull/49088656047); b) *Laminaria pallid*a. (Source: https://www.marineprotectedareas.org.za/kelp-forests); and c) *Macrocystis pyrifera*. (Source: https://oceanservice.noaa.gov/facts/kelp.html)

Kelp forests are one of the most productive coastal ecosystems in the world (Pessarrodona *et al.* 2022). In addition, some studies show higher net primary productivity (NPP) in kelp forests than in the phytoplankton (Smale *et al.* 2016; Rassweiler *et al.* 2018). For instance, Rodgers & Shears (2016) found NPP to be almost 800 g C m^{-2} yr^{-1} in northern New Zealand for understory kelp (see Fig. 3), whereas the NPP decreased close to the bottom to almost 300 g C m^{-2} yr^{-1}. These

values were similar to those reported by Smale *et al.* (2020) in the United Kingdom for *L. hyperborea*, a similar species type examined by Rodgers & Shears (2016). Furthermore, Smale *et al.* (2016), studying *L. hyperborea,* showed that over 75% of the total NPP within the domain was stored in the canopy. Reed *et al.* (2009) used frond densities to estimate NPP for *Macrocystis pyrifera* (giant kelp) in Southern California (see Fig. 4). They found NPP of 1825 g C m^{-2} yr^{-1}. Castorani *et al.* (2021) concluded that the decline of the canopy from giant kelp due to climate change events could reduce the total ecosystem NPP.

In addition to carbon sequestration, kelps ecosystems are crucial for local biogeochemistry. For example, kelp forests can regulate and sustain high pH in Arctic summers, which is beneficial to calcifying organisms (Krause-Jensen *et al.* 2016). The same authors determined that kelp forests could increase pH by 0.18 pH units and decrease pCO_2 by 10 ppm per day during the ten days observed. Dissolved oxygen (DO), however, showed no trend beyond normal diurnal oscillations. Murie & Bourdeau (2020) observed an increase in pH of almost 0.15 pH units and a decrease in pCO_2 by almost 150 ppm over two years. However, these authors found that the kelp canopy region had the most change compared to the bottom of the kelp forests.

Kelps, in particular, giant kelps (*Macrocystis pyrifera*), have the highest photosynthetic capacity in the first meter of the surface where the canopy is present (Gerard, 1986; Traiger *et al.* 2022). Gerard (1986) also found that photosynthetic capacity was the most optimized below the surface, where radiation was limited. Jackson (1977) found that changes in dissolved oxygen (DO) for canopy-forming kelp were between 3 to 6 m below the surface in contrast to previous studies. He also observed that the highest concentration was during the upwelling season, and the lowest nitrate (NO_3) concentration was at the surface during maximum growth. He suggested that the lowest NO_3 at the surface occurred due to the high photosynthetic rate in the canopy. Traiger *et al.*

(2022) measured nutrients and physical parameters inside and outside the kelp forest in Monterey Bay during the Summer of 2019. Biogeochemical variables varied with depth, time of the day, and flow type (e.g., high or low). Predominantly, DO and pH were higher inside the kelp forest than outside during the day. For example, DO and pH declined with depth during high flow and daytime within the kelp forest. During the night at low flow, subsurface pH was higher than the surface in the kelp forest.

Internal waves and coastal currents are also affected in the water column when entering kelp forest domain (Jackson, 1984; Mork, 1996; Jackson, 1998). For example, Jackson (1984) observed damping of internal waves propagating through giant kelp. In addition, he observed a slowdown of low-frequency waves and a damping of high-frequency waves. Mork (1996) found that kelp forests damped around 80% of the total wave energy due to an integrated effect of varying depths and kelp fronds in Norway. Finally, Jackson (1998) used observations to comprehend velocity patterns in and around a kelp bed in southern California. He concluded that alongshore velocities became almost null inside the kelp while cross-shore velocities were not modified when entering the kelp bed. Rosman *et al.* (2007) found similar velocity reductions to Jackson (1998) in a field study from Northern Monterey Bay. In addition, Rosman *et al.* (2007) pointed out that semidiurnal and diurnal velocities can be damped up to 5-fold, and cross-shore currents can be damped up to 4-fold depending on surface canopy and kelp forest density. As a result, turbulence levels were low in the water column except during some periods when it was high at the bottom and in canopy regions.

Many efforts have investigated how high drag from giant kelp impact currents and turbulence (Rosman *et al.* 2010; Rosman *et al.* 2013). For example, Rosman *et al.* (2010) wanted to understand how surface canopy and kelp density could affect currents, turbulent kinetic energy

(TKE), and total drag in the water column. They used a laboratory setup that was dynamically scaled to represent the real world. Unidirectional currents forced the laboratory experiment. They found that the configuration with surface canopy showed the most significant changes for time-averaged velocity and in the water column. However, the differences between sparse and dense kelp with surface canopy were insignificant for the same variables. The bulk drag calculated was most significant for the surface canopy configuration. The dense configuration had a drag coefficient 5-fold larger than the sparse configuration. More recently, Rosman *et al.* (2013) used the same laboratory configuration as Rosman *et al.* (2010), except they added surface elevation. The primary study was to observe flow-wave-kelp interactions under controlled conditions. Surface currents for both flow-kelp and flow-wave-kelp experiments showed a reduction due to the surface canopy. The drag parameter was lower for almost the entire water column for the no-waves experiment. Turbulence production was more significant for the wave experiments than the current experiment at the surface. The authors hypothesized that TKE is larger at the surface due to the presence of the canopy and where biomass is most significant. Monismith *et al.* (2022) hypothesized that variability in kelp biomass could affect flows. To assess this theory, they used two sites (Punta Prieta and Morro Prieta) in Isla Natividad in Baja, California, MX (Fig. 2.3). Their 2-½ year dataset included two distinct biomass periods (no kelp and high kelp density) (Fig. 2.4).

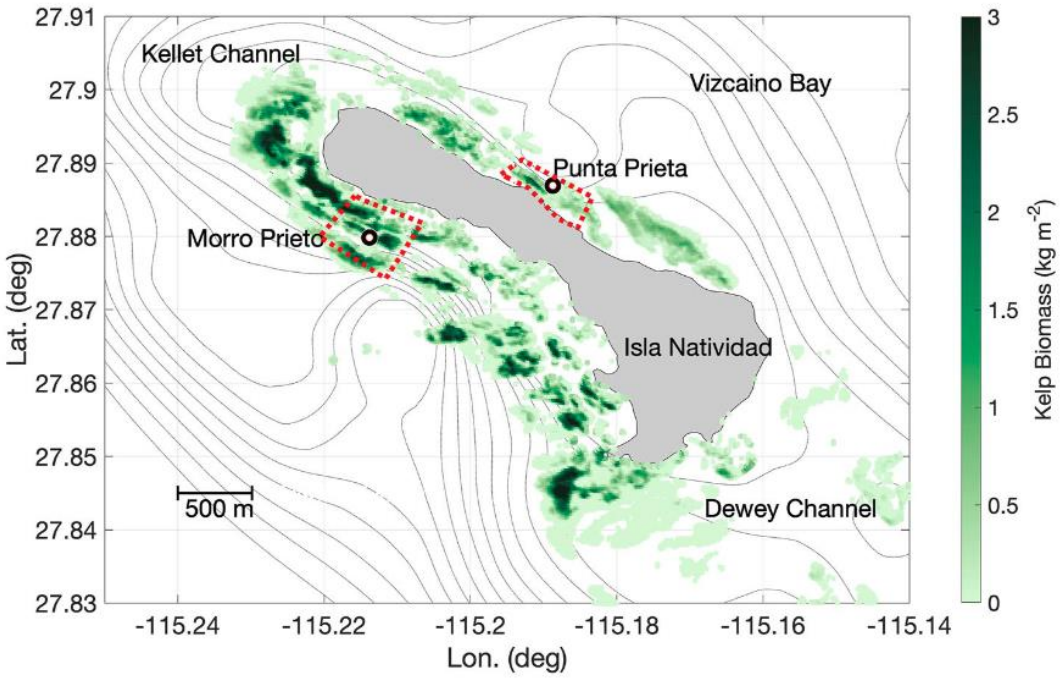

Figure 2.3 – Map showing the position of the long-term moorings. Source: Monismith *et al.* 2022a.

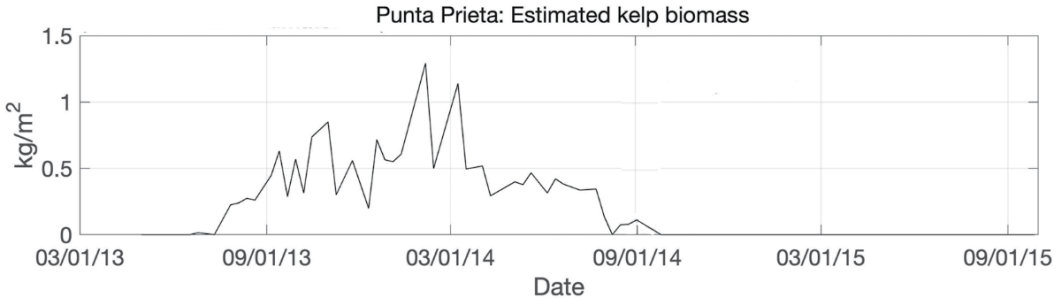

Figure 2.4 – Satellite-derived kelp biomass estimate for Punta Prieta – MX. Source: Monismith *et al.* 2022a.

Currents were measured every 1 minute or 10 minutes using Acoustic Doppler Profilers (ADPs) with 0.5 m bins. Of the two sites, Punta Prieta (PP) is more tidally driven than Morro Prieta (MP). During the period with biomass greater than 0.5 kg/m^2, currents decreased dramatically. In addition, the two main tidal constituents, M2 and K1, were significantly reduced for PP. They concluded that currents did not decrease further when the kelp biomass was greater than 0.5 kg/m^2. Besides flow modifications, kelp forests can also inhibit headland upwelling and increase flow ducting as shown in a study conducted off two headlands around Isla Natividad, MX (Valle-Levinson *et al.* 2022). Sampling using a towed Acoustic Doppler Current Profiler (ADCP) covered one complete tidal cycle. Where kelp biomass canopy was dense, headland upwelling was suppressed, and flow magnitude increased between patches of kelp due to flow ducting. They speculated that flow ducting in fragmented kelp forests could increase safe spaces or refuges for various species.

2.2 **ECOLOGICAL IMPACTS OF KELP FORESTS**

Kelp forests are known for being a shelter for various species and have abundant food sources for fish (Efird & Konar, 2014), crustaceans (Coates *et al.* 2014), and snails (Teagle *et al.* 2017). Kelps are also food for grazers (Dayton, 1985), planktonic larvae (Duggins *et al.* 1989), and suspension feeders (Duggins & Eckman, 1994). Teagle *et al.* (2017) synthesized the ecological function of kelps and biodiversity in different kelp species worldwide. They divided the kelp into three assemblages (see Fig. 2.5): holdfast, stipe, and blade.

Figure 2.5 – Schematic depicting the 3 possible habitats on kelps. Source: http://www.clipartpanda.com/clipart_images/label-the-diagram-as-you-41751015

They further found out that in the holdfast region over 70% of biota are predominantly amphipods and polychaetes. Larger predators such as lobster and crabs also, make part of the holdfast ecology region. Sessile invertebrates and flora are generally the species composition within the stipe region where the scarcity of fauna results from unstable kelp blades. However, epibiont organisms colonize blades. Fish species also inhabit these rich ecosystems.

Efird & Konar (2014) wanted to understand the relationship between fish clusters in patchy kelp forests. They conducted a study in Alaska using four surface canopy kelps and four common fish families, and found that fish assemblages correlated more to understory kelp than with surface canopy-forming kelp. Another significant conclusion was that fish location explained 90% of the fish abundance differences.

Bender *et al.* (1998) reviewed over 20 studies relating habitat loss and population density in land and concluded that population density will be affected depending on the region these

population is found. Bodkin (1988) studied how the abundance and diversity of fish clusters would be affected by the removal of *Macrocystis pyrifera* along the California coast. This study divided the region into experimental and control areas, where he conducted benthic and fish surveys. Fish abundance declined, and benthic species changes stayed similar before clearing the experimental site. As a result, the total biomass decreased by more than half after clearing. While complete removal of a kelp forest region can happen, fragmentation naturally occurs in kelp forests and, therefore, can better explain population size.

Additionally, large-scale events (e.g.: El Niño and heatwaves) can affect kelp forests, resulting in recruitment decline, reduced dispersion, and a decrease in larvae abundance (Barber & Chavez, 1986; Zeidberg & Hamner, 2002; Kim *et al.* 2007; Rogers-Bennett *et al.* 2016). Rogers-Bennett *et al.* (2016) found that larvae and newly settled red abalone were affected by the 2014 ('warm blob') and 2015 (El Niño) events, following the wiped-out of the kelp forest along the west US coast (Low *et al.* 2022a). Adult abalone can also be affected in kelp forests regions due to the large scale events. For example, on the West coast of the US, adult abalone abundance declined during El Niño (Raimondi *et al.* 2002). In contrast, there was a positive correlation between the seasonality of the kelp density and the recruitment of invertebrate species in different locations of the kelp forest during a period of weak El Niño (Almanza *et al.* 2012). Another critical variable for ecology impacts is the patch size. Patch size greatly affects the size of edge and interior habitats for different species. Deza & Anderson (2010) used a similar approach as Bodkin (1988) for another region off the California coast. They wanted to understand the relationship between the recruitment of fish and kelp patch size. They observed that the change in the density of rocky fishes due to fragmentation was negligible at a small scale. However, at a larger scale, fragmentation is essential for recruitment.

2.3 AQUATIC VEGETATION MODELING

Modeling of nearshore environments has received more attention in recent years. Increases in computational power and the creation of tools such as the Coupled Ocean-Atmosphere-Wave-Sediment-Transport (*COAWST*) model (Warner *et al.* 2008) have helped scientists to better understand coastal processes and nearshore environments and their interaction with sediment and vegetation. For example, the vegetation module in *COAWST* (*COAWST*-VEG) allows the simulation of three-dimensional flow-vegetation interactions (Beudin *et al.* 2017) and vegetation and sediment transport interactions (Donatelli *et al.* 2018). This module was initially used to understand hydrodynamics in seagrass and salt-marsh environments (Kalra *et al.* 2017; Donatelli *et al.* 2018). However, other aquatic vegetation could benefit from this module available, for example, mangroves and kelps.

Kelp forests have been extensively studied for their importance in biological, physical, and biogeochemistry processes. Despite their global importance, most models describing kelp forest ecosystems have been related to their life cycle and biogeochemical importance (Solidoro *et al.* 1997; Broch & Slagstad, 2012; Hadley *et al.* 2015)., Frieder *et al.* (2022) recently developed an offline 3D seaweed model that simulates nutrients and macroalgal growth. However, a significant shortcoming of this study is that the seaweed model is coupled offline, precluding a representation of flow-kelp-biogeochemical feedbacks. An offline model is a model that does not interact directly with the actual model. For instance, the offline model only receives “fixed” datasets (e.g.: outputs from models or observational data) that are used to calculate a variable (e.g.: pH), and consequently, does not affect in any way the original values used. To date, the hydrodynamic changes due to canopy-forming kelp have only been studied using laboratory experiments (Rosman *et al.* 2010) and imposing a higher drag at the bottom in a hydrodynamic model (Wu *et*

al. 2017). Thus, a hydrodynamic model that can represent canopy-forming kelps in an ocean circulation model is needed.

Kelp forests like seagrasses adds an extra force called drag force ($F_{d,v}$) term in the Navier-Stokes equation. For example, assuming the along-shore (v) momentum term of the Reynolds-Averaged Navier-Stokes (RANS) equations under the Boussinesq approximation:

$$\frac{\partial v}{\partial t} + \frac{\partial vu}{\partial x} + \frac{\partial vv}{\partial y} + \frac{\partial vw}{\partial z} + fu = -\frac{1}{\rho_0}\frac{\partial P}{\partial y} - \frac{\partial}{\partial z}(\overline{u'w'} - \nu\frac{\partial v}{\partial z}) + D_v + F_v \quad \textbf{(1)}$$

The spatially averaged vegetation drag force for the alongshore velocity ($F_{d,v}$) neglecting cross shore velocity can be written as:

$$F_{d,veg,v} = \frac{1}{2} C_d b_v P_v v\sqrt{v^2} \quad \textbf{(2)}$$

Where P_v is plant density, b_v is the width of kelp, and C_D is the drag coefficient for an individual plant. However, this module was developed for seagrasses environments which do not extend through the water depth or develop canopies. However, kelp forests can have extensive canopies that cover the last meter or so to the surface **(**Traiger *et al.* 2022). As a result, some limitations are then found for kelp forests with canopies (Fig. 2.6). For example, the module developed by Beudin *et al.* (2017) does not account for change in space between individual plants. To date, the effects of surface canopies on currents have only been studied in laboratory settings **(**Rosman *et al.* 2013**)**.

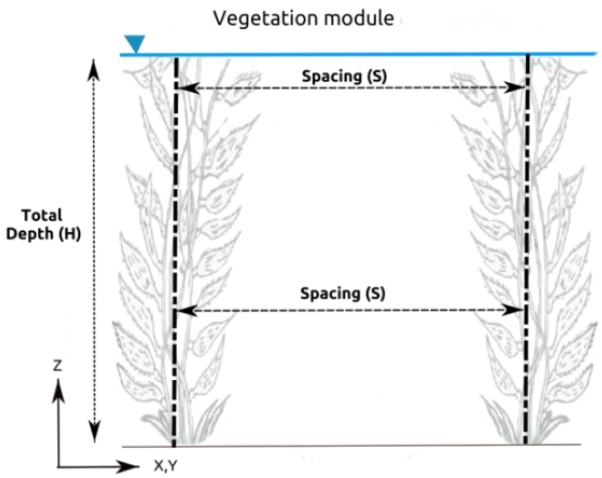

Figure 2.6 - Diagram of how the original module could simulate vegetation in *COAWST* (a).

The vegetation module requires plant height (m), plant density (plants/m^2), plant diameter (m), and plant thickness (m). The other settings are number of vegetation types, Young's modulus (10^7), vegetation mass density (1000.0), additional horizontal viscosity coefficient (0.0), and drag coefficient for each individual plant. My first research chapter builds upon the previous work done by Beudin *et al.* (2017) and develops the vegetation module further to account for kelp canopy through a decrease in spacing between individual plants and applies this method to kelp forest domains in *COAWST.*

2.4 DISSOLVED OXYGEN AND pH MODELING

Kelp forests also provide shelter to macroinvertebrates (Dayton, 1985), uptake carbon (Macreadie *et al.* 2021), are highly productive (Gerard, 1986), and elevate pH and Dissolved Oxygen (DO) relative to surrounding areas (Frieder *et al.* 2012). Koweek et al. (2017) mentioned the importance of kelp forests in creating a natural climate refuge for organisms. However, Traiger et al. (2022) concluded that kelp forests would have a limited role in protecting benthic organisms

against hypoxia and acidification in regions where upwelling happens but could be significant in areas with low flow exchange (e.g., bays). They also suggested that canopy regions have the most impact in modifying pH and DO compare to offshore locations, and these changes were likely to due to photosynthesis and respiration by *M. pyrifera* and not phytoplankton. For instance, Pfister *et al.* (2019) analyzed samples in the Northern CCS both inside and outside kelp forests at 1 m depth, and found differences of almost 2.5 mg/L and 0.2 units for DO and pH, respectively. In Central California, Koweek *et al.* (2017) found a difference inside kelp of over 0.5 pH units between the top and bottom. Traiger *et al.* (2022) found that daily variability inside kelp could be as high as 7 mg/L and 0.36 pH units for a Central California region, similar to Frieder *et al.* (2012).

Although these studies were essential to understanding variability in biogeochemical properties of kelp forest regions, they only provide views of a single location, not capturing the big picture of the domains. Thus, based on Traiger *et al.* (2022), a biogeochemistry model to represent kelp respiration and kelp net primary production would be helpful to understand the impact on local biogeochemistry. The only biogeochemical model developed for *M. pyrifera* was recently published by Frieder *et al.* (2022). This model while robust is focused on biomass growth of kelp forest through the nitrogen cycle, and therefore, not giving a perspective for DO change due to the high-drag environment created by kelp forests. The most representative model for DO, but still not for vegetation specifically, was published by Scully (2013). This simple DO model was used to investigate the impact of river discharge, water temperature, and wind speed on hypoxia in Chesapeake Bay. They used an advection-diffusion equation and an extra term to represent respiration in their domain (eq. 2).

$$\frac{\partial DO}{\partial t} + (\frac{u\partial}{\partial x} + \frac{v\partial}{\partial y} + \frac{w\partial}{\partial z})DO = \frac{\partial}{\partial z}K_z\frac{\partial DO}{\partial z} - Respiration \quad \textbf{(2)}$$

Where $\frac{\partial DO}{\partial t}$ is the time rate of change of DO, the second term is the advection of DO, the terms on the right side are the vertical diffusion, spatially and temporally constant nocturnal respiration rate (mmol O_2/m^3/day). DO concentration has been reported to have an indirect relationship with pH (Chen *et al.* 2017). These authors proposed that through the decomposition of organic matter (eq. 3) they could reconstruct dissolved inorganic carbon (DIC) and total alkalinity (TA) from DO:

$$(CH_2O)_{106}(NH_3)_{16}H_3PO_4 + 138O_2 \rightarrow 106CO_2 + 122H_2O + 17H^+ + 16NO_3^- + H_2PO_4^- \quad \textbf{(3)}$$

As a result, they could determine pH. This approach done by Chen *et al.* (2017) while applied to the open ocean could also be applied to understand the change in pH due to the changes in the water column caused by kelp forest. My second research chapter (Chapter 4) focuses on developing a DO model for kelp forest, coupling it with the kelp forest module developed in Chapter 3 and applying the methods developed Chen *et al.* (2017). These two biogeochemical models coupled with the hydrodynamic model developed for kelp forests in the previous chapter, can give the perspective of the physical impact of kelp forests in these two important processes for organisms.

2.4 FRAGMENTATION IN KELP FOREST DOMAINS

Climate change (Murie & Bourdeau, 2020) and extreme events (Edwards, 2004; Cavanaugh *et al.* 2019) have been extensively studied as impacts on ecosystems (Pandolfi *et al.* 2003; Wernberg *et al.* 2013). One of the effects of these events is fragmentation (Edwards, 2004).

However, most of the research done for fragmentation is focused on patch scales, not entire areas (Fahrig, 2003). Fragmentation is expected to increase for vegetation on land and in the water due to climate change and other anthropogenic impacts (Bryan-Brown *et al.* 2020; Murie & Bourdeau, 2020). On land, habitat fragmentation creates more edge environments which in turn affects species movement (Elias, 2013) and these habitats eventually can collapse (Fig. 2.7).

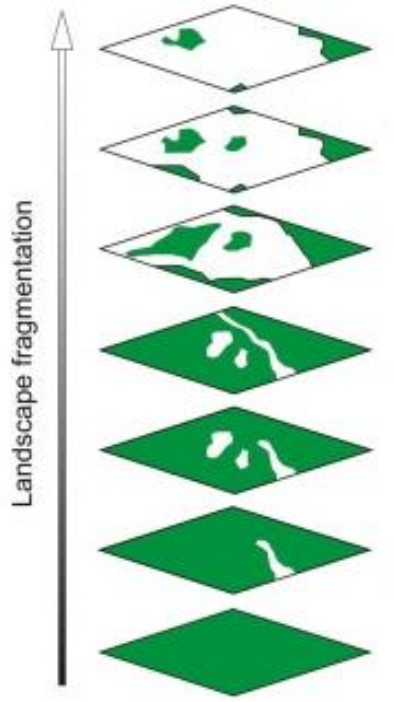

Figure 2.7 - Process of habitat fragmentation from initial to collapse of habitat. Modified from: Elias, 2013.

For kelp forests this is no different. Seasonal variations and external physical impacts (e.g., storm surges, heatwaves, and El Niño; (Dayton & Tegner, 1984; Dayton, 1985; Gaylord *et al.* 2007; Arafeh-Dalmau et al 2020; Monismith *et al.* 2022) modify kelp forest domains (e.g.: change in kelp forest density and patch sizes; Beas-Luna *et al.* 2020; Gordon *et al.* 2020). Dayton & Tegner (1984) found that stronger winter storms during the 1983 El Niño destroyed patches of understory kelps. Edwards & Estes (2006) showed that during the 1997-98 El Niño year, the losses of *Macrocystis pyrifera* were generalized across the west coast of the US. Furthermore, higher

temperatures due to the El Niño event also show increased kelp mortality (Dayton & Tegner, 1984; Edwards & Estes, 2006). High sea surface temperature (SST) also indicates potential nutrient depletion, resulting in a decline in kelp canopy (Dayton & Tegner, 1984). The limited nutrients do not allow kelp to repair from damage after storms **(**Dayton & Tegner, 1984). More recently, Monismith *et al.* (2022) demonstrated through the calculation of kelp biomass using satellite estimates the complete removal of biomass around Isla Natividad, Mexico, after a hurricane. Although, kelp forests are sensitive to large scale physical impacts, and therefore, increase patchiness, they have also been observed to increase in area in some other regions of the globe (Krumhansl *et al.* 2016; fig. 2.8).

Laboratory and modeling studies have been used to study landscape fragmentation effects on flows for both on land (Poëtte *et al.* 2017; Bannister *et al.* 2022) and in water (Nepf, 1999; Liu *et al.* 2021). Poëtte *et al.* (2017) observed an increase in velocity at the canopy height amd as the patches were farther apart the flow changed from a single edge to multiple flows. Liu *et al.* (2021) that the single patch had an enhancement in the wake entrainment with the increase in vegetation density. Valle-Levinson *et al.* (2022) observed formation of flow ducting between two different patch sizes in Punta Prieta - MX.

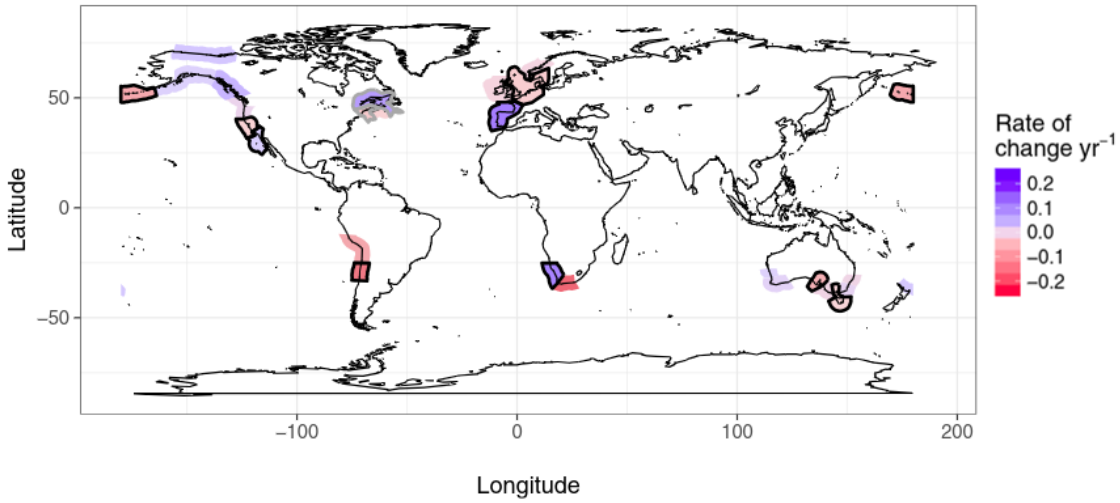

Figure 2.8 – Rate of change per year for kelp forests regions. Modified from Krumhansl *et al.* 2016.

While fragmentation in ecosystems on land represent more of a physical change, in the nearshore vegetation the fragmentation process can affect local and global biogeochemistry that in turn affects local biota and carbon uptake. Fragmentation studies have been either focusing on the impact of these large-scale events on the kelp distribution (Arafeh-Dalmau *et al.* 2019) or the effects on ecology (Efird *et al.* 2014). These ecology studies focused on the result (e.g.: movement or change in population after fragmentation) but did not measure the changes in the stressors such as temperature, DO, and pH especially for sessile organisms, for example, marine invertebrates (abalone, snails) at the bottom. My third research chapter (Chapter 5) explores the impact of different levels of fragmentation on local currents, turbulence, stratification, and biogeochemistry by utilizing the combined hydrodynamic module developed in chapter 3 and biogeochemistry module developed in chapter 4.

CHAPTER 3

KELP FOREST MODEL DEVELOPMENT IN A REGIONAL OCEAN MODEL[1]

[1] Fagundes, Matheus; Micheli, F.; Monismith, S. G.; Valle-Levinson, A.; Woodson, C. B. To be submitted to *the journal Geoscientific Model Development.*

ABSTRACT

Kelp forests are essential ecosystems in coastal regions around the world. However, studies have yet to simulate these ecosystems in either regional ocean or global climate models. This paper describes and validates a model that simulates hydrodynamics and turbulence within kelp forests in *Coupled Ocean-Atmosphere-Wave-Sediment-Transport model (COAWST V3.3*). I used 2-1/2 years of *in situ* data covering periods with and without kelp forests around Isla Natividad (Baja CA, Mexico) which allowed us to validate the model for the main tidal constituents. I developed a simple but efficient linear regression approach to simulate kelp canopies (hereafter *canopy*) in *COAWST*. I tested different vegetation drag coefficients and compared simulations with our canopy model against the standard vegetation module in *COAWST*. Results show that while both models simulate the velocities observed in the *in situ* dataset, *canopy* model was able to simulate for the first time turbulence kinetic energy generated due to kelp canopy as observed in laboratory experiments. This new kelp model provides opportunities to understand how turbulence affects ecology, physics, and biogeochemistry within kelp domains.

3.1 INTRODUCTION

Kelp forest ecosystems occupy almost 7 x 10^6 km^2 globally, when accounting for polar regions, of the world's coastlines (Duarte, 2017; Macreadie *et al.* 2019; Wernberg *et al.* 2019), representing the largest coastal vegetated ecosystem in the world. These macroalgae live in nutrient-rich habitats such as Eastern Boundary currents (EBUs) and provide significant carbon sequestration (Britton *et al.* 2016; Low *et al.* 2021, Eger *et al.* 2023). While kelp forests are important for carbon sequestration (Macreadie *et al.* 2019), kelp forests also have local biological (Gaylord *et al.* 2002*)* and physical impacts (Gaylord *et al.* 2007) that have been observed *in situ*

(Walter *et al.* 2012; Leary *et al.* 2017; Monismith *et al.* 2022) and in laboratory experiments (Rosman *et al.* 2010; Rosman *et al.* 2013). Considering that kelp forests have ecological, biogeochemical, and physical importance, comparative efforts to simulate these ecosystems in ocean models have been limited. Up to now, only one study has attempted to include the physical response of flows due to kelp forests into an ocean model, and it did not specifically account for variation in kelp canopy (Wu *et al.*2017).

Kelp forests are found worldwide (Delille *et al.* 2009; Krause-Jensen *et al.*2016) composed of 5 recognized types based on dominant genus: Ecklonia, Nereocystis, Lessonia, Laminaria, and Macrocystis (Rafaelli & Hawkins, 1999). Along the west coast of North America, the predominant species is the giant kelp *Macrocystis* spp. (Steneck *et al.* 2002). *Macrocystis* spp. are found in general between 2 to 30 meters in the water column (Jackson & Winant, 1983) forming dense underwater forests (Steneck *et al.* 2002) (Fig. 3.1). Kelp forests are normally recognized for their importance as shelter for macroinvertebrates, fish, and mammals (Dayton, 1985; Rafaelli & Hawkins, 1999). Furthermore, kelp forests have a large impact on carbon storage or net primary productivity (NPP). A kelp forest can uptake up to 4-fold more carbon per year than a boreal forest (Reed & Brzezinski, 2009) or phytoplankton production in upwelling zones (Behrenfeld & Falkowski, 1997). Kelp forests account for almost 5% of the total global blue carbon and 1/3 of the total carbon sequestered in coastal regions (Filbee-Dexter & Wernberg, 2020; Eger *et al.* 2023). Similarly, kelp forests are physically important as they alter currents and mixing in subtidal nearshore environments of temperate and high latitudes (Dayton, 1985; Rafaelli & Hawkins, 1999).

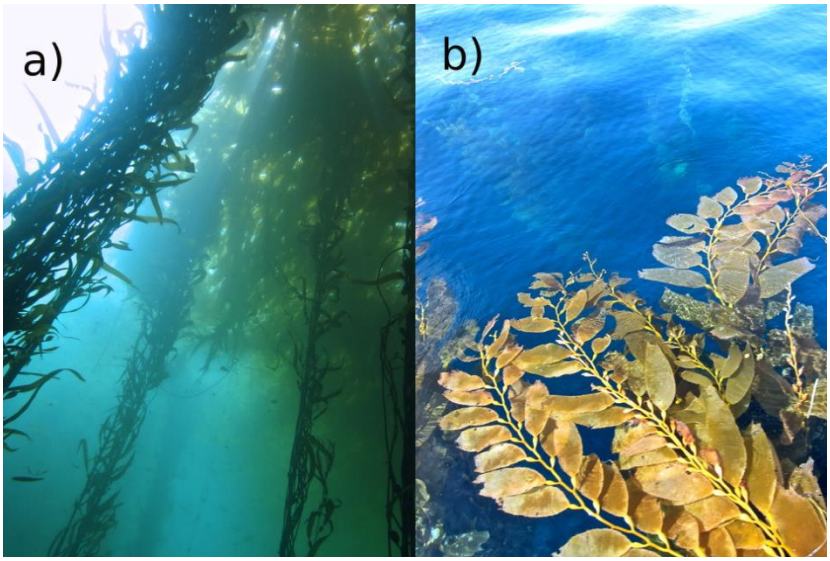

Figure 3.1 - Underwater formation of *M. Pyrifera* (a) and surface canopies at the surface (b). Source: Photo taken by Charles Boch.

Previous studies to understand the effect of kelp forests on currents focused on particular regions along California Current System (CCS; e.g.: Jackson, 1984; Monismith *et al.* 2022), scaled laboratory experiments (e.g.: Rosman *et al.* 2010), or high-resolution simulation of kelp beds (e.g.: Wu *et al.* 2017). While these studies helped better understand flow-vegetation interactions in these complex ecosystems, they did not capture the entire range of effects that kelp forests have on the biology, biogeochemistry, and currents. In this present study, a high-resolution semi-idealized hydrodynamic model coupled with a vegetation module is used to create and validate a kelp (stipes + canopy) module to allow for studies on the effects of kelp forests, not only on the hydrodynamics, but also the resultant effects on biogeochemical cycling and larval transport.

3.2 THEORY

The alongshore (v) momentum term of the Reynolds-Averaged Navier-Stokes (RANS) equations under the Boussinesq approximation (Beudin *et al.* 2017):

$$\frac{\partial v}{\partial t}+\frac{\partial vu}{\partial x}+\frac{\partial vv}{\partial y}+\frac{\partial vw}{\partial z}+fu=-\frac{1}{\rho_0}\frac{\partial P}{\partial y}-\frac{\partial}{\partial z}(\overline{u'w'}-\nu\frac{\partial v}{\partial z})+D_v+F_v \quad \textbf{(1)}$$

where $\frac{\partial v}{\partial t}$ is the unsteady term, $\frac{\partial(vu)}{\partial t}+\frac{\partial(vv)}{\partial t}+\frac{\partial(vw)}{\partial t}$ are the advection terms, *f* is the Coriolis parameter, $-\frac{1}{\rho_0}\frac{\partial P}{\partial y}$ is the pressure gradient in the *y*-direction, ρ_0 is the reference density of seawater, $\overline{u`w`}$ is the vertical flux of horizontal momentum by turbulent velocity fluctuations, $\nu\frac{\partial v}{\partial z}$ is the molecular viscosity, D_v is the horizontal diffusive term, and the last term (F_v) is a forcing term that includes the effects of vegetation on the flow. The spatially averaged vegetation drag force for the alongshore velocity neglecting cross shore velocity can be written as:

$$F_{d,veg,v}=\frac{1}{2}C_d b_v P_v v\sqrt{v^2} \quad \textbf{(2)}$$

Where P_v is plant density, b_v is the width of kelp, and C_D is the drag coefficient for an individual plant. The code for the vegetation module in *COAWST* was originally written to represent seagrasses which do not extend to the water surface, and therefore, no canopy was needed. However, kelp forests can have extensive canopies that cover the last meter or so to the surface **(**Fig. 1; Traiger *et al.* 2022). To date, the effects of surface canopies on currents have only been studied in laboratory settings (Rosman *et al.* 2013).

Two simulations are presented in this paper: The first simulation is running the *COAWST* vegetation module with no changes (*standard* hereafter) (Fig. 3.2-a) and the second is modifying the code to account for kelp canopy (*canopy*) (Fig. 3.2-b). The *standard* simulation assumes that plant diameter (*pd*) and plant thickness (*pt*) are constant from the seafloor to the surface. The *canopy* simulation assumes a linear increase in *pd* and *pt* in the last meter of the water column

(Fig. 3.2; Utter & Denny, 1996). The *canopy* module then simulates the effects of kelp stipes fronds getting close to each other (S) as they spread out on the surface due to being longer than the water depth (Fig. 3.1b) by indirectly changing *pd* and *pt* and consequently the effects on the currents in a kelp forest.

I fit a linear regression to simulate kelp canopies starting from 1 m below the surface. This modification in the vegetation model code captures the increase in kelp spacing (*S*) at the surface between individual kelp plants (eq. 3). For our scenario, this gives *pt* and *pd* equal to 2.3 at the surface forming a virtually solid boundary. The coefficients in (3) can be varied to adjust for the density, extent the of the canopy, or water depth accordingly, the values below relate to the specific setup for our model test case:

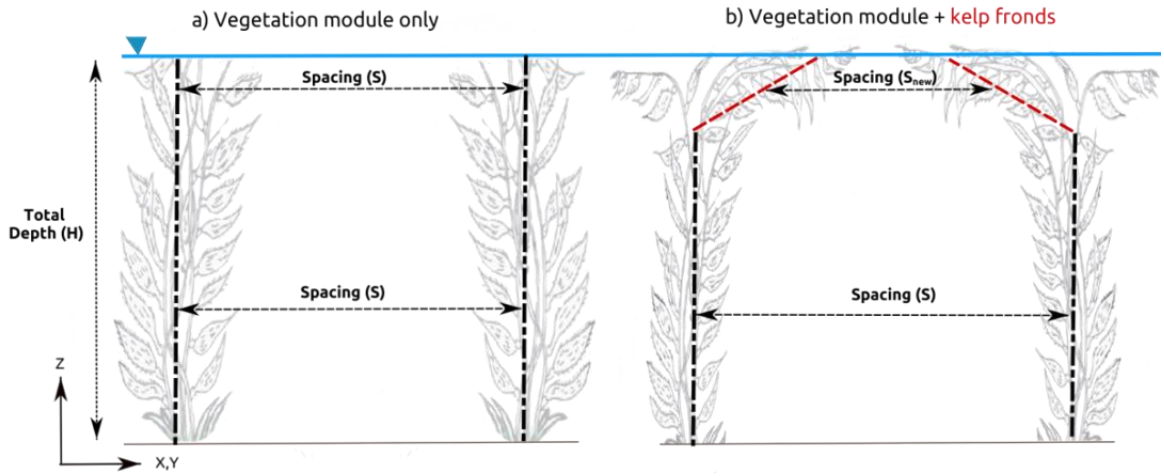

Figure 3.2 - Schematic of the two simulations in *COAWST*.

$$\begin{cases} pt = pd = 0.3m & if\ h \leq H - 1m \\ pt = pd = 2.3h - 27.3 & if\ h > H - 1m \end{cases} \quad (3)$$

3.3 METHODS

3.3.1 Area of Study

This study focuses on kelp forests surrounding Isla Natividad in the Vizcaino Bay region of Baja California, MX. Baja California is affected by large scale forcings such as El Niño (Trenberth, 1997) and marine heat waves (Cavanaugh *et al.* 2010; McPherson *et al.* 2021). Mesoscale forcings such as California Current characterized by low salinity, low temperature, high dissolved oxygen (DO) and California Undercurrent (CU) that is saltier, higher temperature and low in dissolved oxygen, also play a major role in the physical environment of this region (Mancilla-Peraza *et al.* 1993). Seasonally, there is strong stratification in the upper 20 meters of the water column, and conditions are influenced by wind-driven upwelling that brings water temperatures as low as 8°C, salinity (~33.8), and low DO (<5.5 ml/l) to the surface during spring/summer. During winter, waters can reach 16°C, salinity (~34), and DO around 5 ml/l (Mancilla-Peraza *et al.* 1993). Around Isla Natividad, winds, waves (surface and internal), tides, and kelp forests drive the dynamics (Woodson, 2018; Valle-Levinson *et al.* 2022) at relatively small spatial and temporal scales (e.g: < 1 km, < 24 h). For instance, the shape of kelp forests can modify tides and dampen headland upwelling (Valle-Levinson *et al.* 2022).

Isla Natividad is a 7 km long island south of Isla Cedros in Central Baja California, Mexico (Schlenger *et al.* 2021) located between 115°15'W-115°6'W and 27°48'N-27°55'12''N (Fig. 3.3). The island is bounded by Kellet Channel on the north and Dewey Channel on the south (Mancilla-Peraza *et al.* 1993), and is surrounded year-round by kelp forests (*Macrocystis Pyrifera*) which provide shelter for organisms including abalones (*Haliotis* spp.; Micheli *et al.* 2012). Isla Natividad has two distinct local ocean regions on each side of the island (Woodson, 2018). On the southeastern side, Morro Prieto can reach mean temperature of 16°C and mean DO of 6 mg/l at 12 m while on the northwestern side, Punta Prieta has waters that are typically 3°C warmer and mean DO of 7.5 mg/l (Boch *et al.* 2018) at the same depth. Because of the economic and ecological

importance of abalone, the fishing cooperative, Buzos Y Pescadores, in Isla Natividad established 2 marine reserves that have been monitored since 2006 (Boch *et al.* 2018; Micheli *et al.* 2012). One of the marine reserves is located near Punta Prieta and has sensors at 7 m and 12 m depth (Boch *et al.* 2018)**.**

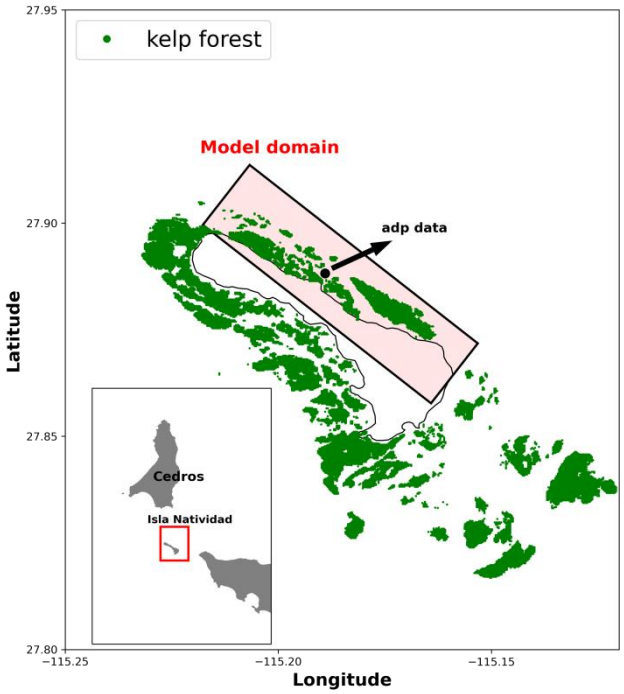

Figure 3.3 - Map of Isla Natividad indicating regional location and areas covered with kelp. Black circle indicates location of ADP data used in this study.

3.3.2 Forcing

The mooring at Punta Prieta (Fig. 3.3) was chosen for evaluating the vegetation models in *COAWST* for four reasons, a) long term data are available (Woodson *et al.*, 2018), b) the 2015-16 heat wave caused complete removal of kelp **(**Fig. 3.4**)** giving the opportunity to understand the environment without kelp (Monismith *et al.* 2022), c) it is within a marine reserve (Micheli *et al.*

2012), and d) flows are generally tidal and alongshore as opposed to currents around Morro Prieto (Boch *et al.* 2018).

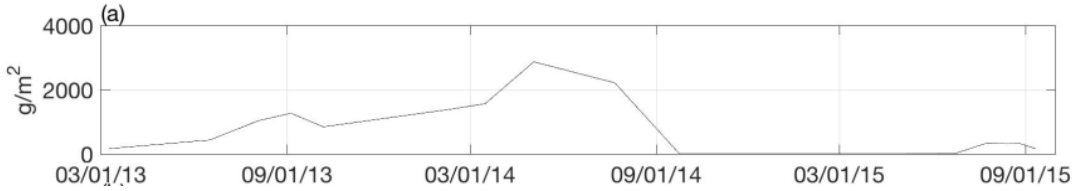

Figure 3.4 - Averaged kelp biomass around Isla Natividad, MX. Source: Monismith *et al.* (2022).

In situ current data were collected every 0.5 meter starting from 0.65 meters above the bottom to the surface (~14 m) from 2013-2016 (Fig. 3.5). The depth of the ADP data used for this simulation was from 2.65-12.65 meters from the bottom to remove errors in the first couple meters due to side-lobe interference. Depth-averaged velocities were calculated after removing errors from bottom and surface (Fig. 3.5). Both E-W and N-S velocities increased in the 2015 period (Fig. 3.5) when there was no kelp biomass observed (Fig. 3.4) while in 2014, the highest kelp biomass observed for the 2-1/2 year record, velocities were ~2-fold slower (Monismith *et al.* 2022).

Currents were rotated into along- and cross-shore axes using Principal Component Analysis (PCA; Campbell & Atchley 1981; Emery & Thompson 2004). The rotated velocities were separated by season (Fig. 3.6). Based on Fig. 3.4 and Fig. 3.6, the cross-shore and alongshore Winter 2015 (henceforth adp15) and Spring 2014 (adp14) velocity records are used for no-kelp and kelp analyses. The adp15 data set was used to validate *COAWST* without the vegetation module prior to implementing it for the adp14 dataset (e.g. to estimate drag coefficients in the absence of kelp).

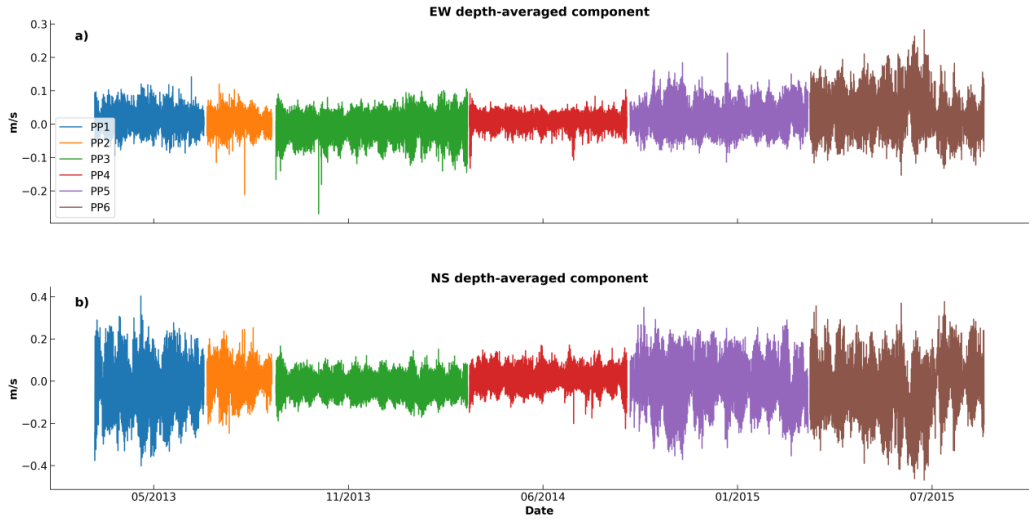

Figure 3.5 - EW and NS depth-averaged components of velocity for 6 different periods at Punta Prieta (PP), Isla Natividad, MX.

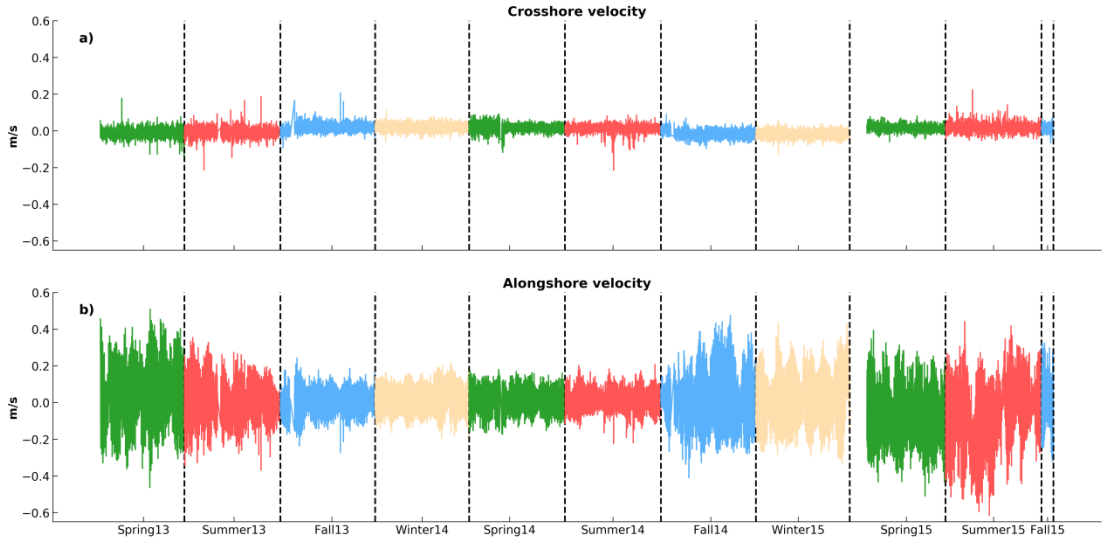

Figure 3.6 - Rotated cross-shore and alongshore velocities separated by season.

Both, cross-shore and alongshore velocities from adp15 and adp14 were harmonically analyzed using a python version of T-TIDE (Pawlociwicz *et al.* 2002**;** Figs. 3.7, 3.8**)** before being used to force *COAWST* and to validate the vegetation module, respectively.

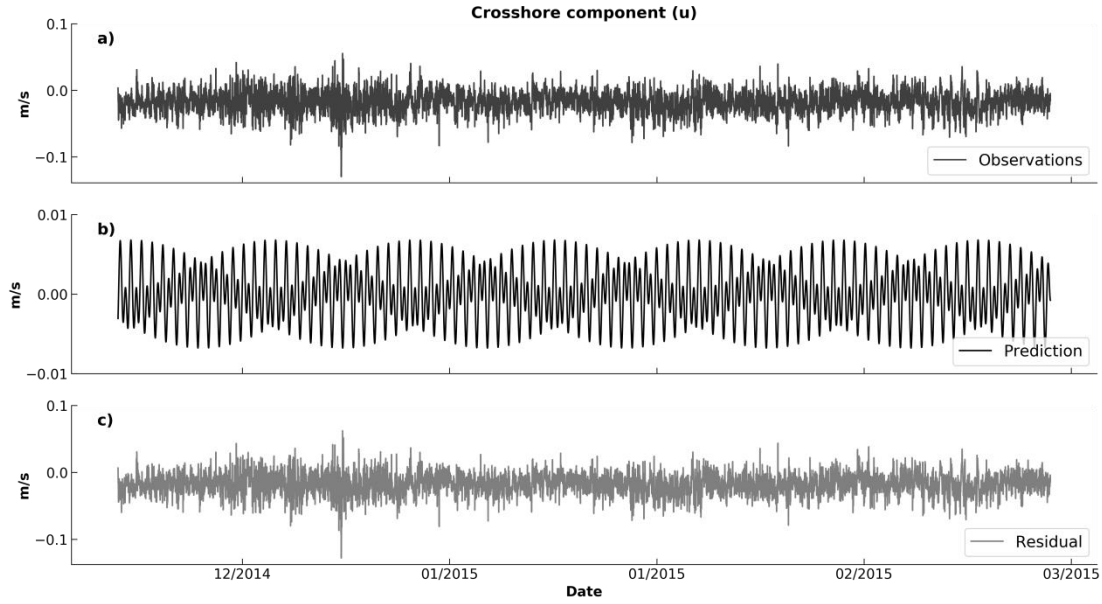

Figure 3.7 - Cross-shore component for winter 2015 in PP. From top to bottom: Observations (a) based on Fig. 3.5, prediction using t-tide (b), data residuals (c).

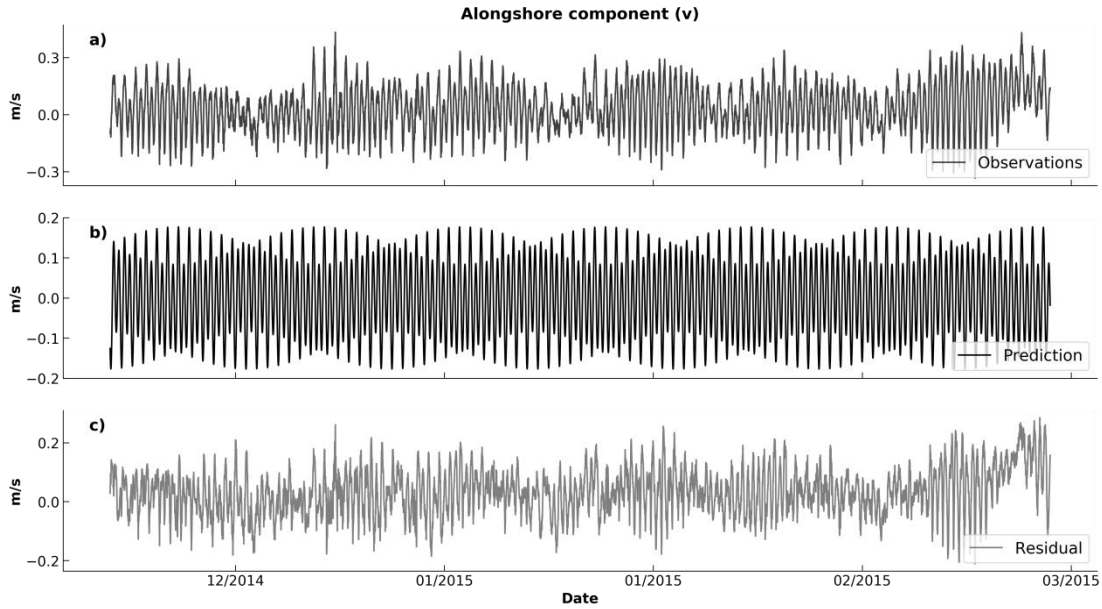

Figure 3.8 - Along-shore component for winter 2015 in PP. From top to bottom: Observations (a) based on Fig. 5, prediction using t-tide (b), and data residuals (c).

3.3.3 Numerical Model Description

The model used in this study was the *Coupled Ocean-Atmosphere-Wave-Sediment-Transport model (COAWST V3.3*; Warner *et al.* 2008). The ocean component of *COAWST* is the *Regional Ocean Modeling System (ROMS)* (Haidvogel *et al.* 2008). ROMS is a 3-D, free-surface model, which solves the primitive equations using hydrostatic and Boussinesq approximations with topography-following sigma layers (Shchepetkin and McWilliams, 2005; Haidvogel *et al.* 2008). For the momentum equations, splines vertical advection and logarithmic bottom friction were selected to keep stability and better represent the environment, respectively. The model used the Mellor-Yamada level 2.5 turbulence closure scheme (MY-2.5). All boundaries (N, S, E, W) were open to allow along- and cross-shore flows. A periodic boundary condition was applied for free-surface, a Flather condition for 2D u- and v-momentum, and a Radiation-Nudging condition for 3D u- and v-momentum. The barotropic time-step was set at 10 s. Bottom roughness (z_{ob}) was 0.03 m and surface roughness (z_{os}) was 0.4 m with a no-slip condition along the bottom to provide a best fit for the no-kelp simulations to observed velocity profiles. The model had 40 sigma-layers splitting the 13 meters of water column with surface stretching (θ_s)= 1, bottom stretching (θ_b)= 2, and thermocline depth (Tcline) = 0. The domain was approximately 14 km long by 3 km wide **(**Fig. 3.9**)** with a grid size of 25 meters x 25 meters. The model was initialized at rest with a well-mixed domain where temperature and salinity are 19°C and 34, respectively (Low *et al.* 2021). The model was forced every 10 min with depth-averaged tidal fits from adp15 (Monismith *et al.* 2022). Hydrodynamic conditions of the domain were simulated for 3 months, however, the first 30 days provided dynamic adjustment of the currents. The vegetation module was activated accounting for the drag due to the kelp forests in the simulations using the *standard* and *canopy* modules (Beudin *et al.* 2017). Results are presented for the second month of each simulation.

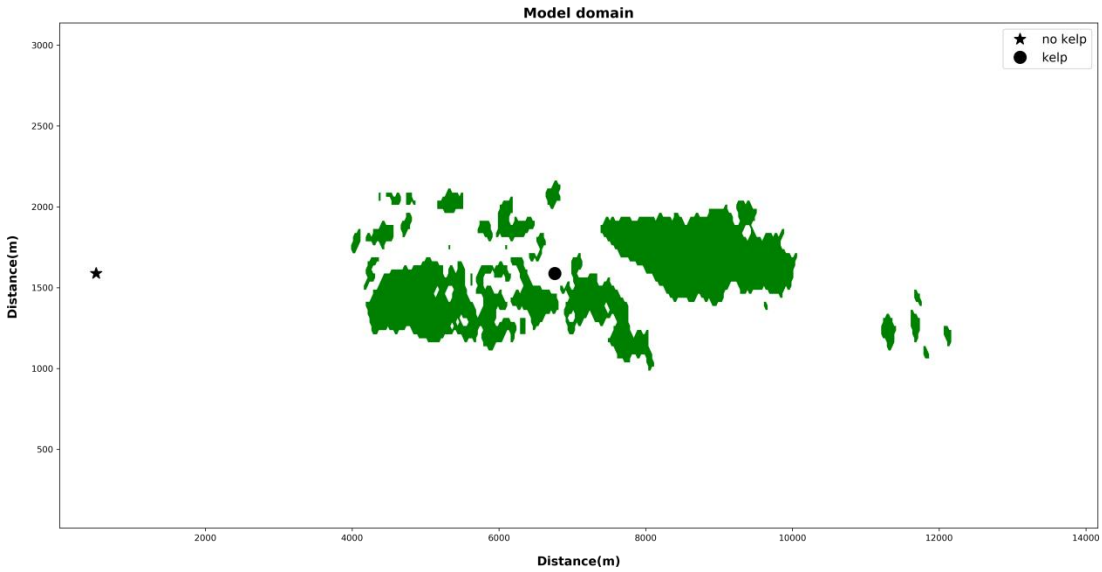

Figure 3.9 - Model domain. No kelp station (star) is used to validate the idealized model and kelp station (circle) is to validate the vegetation module in *COAWST*.

3.3.4 Vegetation module parameters

The vegetation module is a standard component in *COAWST* (Beudin *et al.* 2017). This module receives *u* and *v* from *ROMS* and returns both the drag force (F_d) and vertical turbulent mixing (Beudin *et al.* 2017). The vegetation module requires 4 parameters: plant height (m), plant density (plants/m^2), plant diameter (m), and plant thickness (m) (Table 3.1). The other settings are number of vegetation types, Young's modulus (10^7), vegetation mass density (1000.0), additional horizontal viscosity coefficient (0.0), and drag coefficient for each individual plant (0.05-0.6).

Table 3.1 - Vegetation module initial parameters.

	Plant height(m)	**Plant Density (plants/m^2)**	**Plant diameter (m)**	**Plant thickness (m)**
Standard	13	0.9*	0.3	0.3
Canopy			*See equation 1*	*See equation 1*

*(GAYLORD *et al.* 2007).

3.3.5 Time-averaged velocity

The output velocity data were used to calculate the time-averaged velocity ($\bar{u}$). To compute $\bar{u}$, alongshore and cross-shore velocities were used to calculate velocity component in the domain, and then, integrated in time:

$$|V| = \sqrt{\bar{u}^2 + \bar{v}^2} \qquad \textbf{(4)}$$

$$\bar{u} = \frac{1}{T}\int_0^T u dt \qquad \textbf{(5)}$$

3.3.6 Model Skill

A quantitative model skill was presented by Willmott (*1981*) (eq. 6)*:*

$$WS = 1 - \frac{\sum_{i=1}^{N}(m_i - o_i)^2}{\sum_{i=1}^{N}(|m_i - \bar{o}| + |o_i - \bar{o}|)^2} \qquad \textbf{(6)}$$

where *m* is the variable modeled being compared against the observed variable (*o*), the index *i* represents each depth for our case. It takes the sum of difference for each point squared and divides by sum of the absolute variability of the model and observed variable in relation to the mean of the observed variable squared. A Willmott Skill equal to 0 (WS = 0), means complete disagreement, and, *WS* = 1 means exact match between simulations and observations. This

verification has been applied in other model simulations (Warner *et al.* 2005b; Liu *et al.* 2009). Before calculating *WS*, the model was interpolated to the depths of the *adp* dataset. Time-averaged velocities for the domain with vegetation module off and the *no kelp station* in Fig. 3.8 were the same, and therefore, I used *no kelp station* for the validation. *Kelp station* (Fig. 3.9) was used and compared against adp14 where kelp biomass was the highest (Fig. 3.4).

3.3.7 Bulk Drag calculations

Field estimates of kelp forest drag coefficients represent the bulk drag effect of multiple kelp plants. For example, in a 1-D linear momentum balance,

$$\frac{\partial u}{\partial t} + C_D^B \frac{U\,|U|}{h} = -g\frac{\partial \eta}{\partial x} \qquad \textbf{(7)}$$

After some manipulation:

$$C_D^B = -\frac{h(\frac{\partial u}{\partial t} + \frac{\partial \eta}{\partial x})}{U\,|U|} \qquad \textbf{(8)}$$

Applying the centered difference method for $\frac{\partial u}{\partial t}$ and $\frac{\partial \eta}{\partial x}$, yields:

$$C_D^B = \frac{-\frac{h}{2\Delta t}(u_j^{t+1} - u_j^{t-1}) - \frac{hg}{2\Delta t}(\eta_{j+1}^t - \eta_{j-1}^t)}{\bar{u}\,|\bar{u}|} \qquad \textbf{(9)}$$

The bulk drag coefficient, C_D^B (eq. 9), is the net coefficient for the entire region of influence, which is not necessarily the drag force on an individual kelp plant, C_D^i. In the *COAWST* model, the drag coefficient input is for an individual plant, C_D^i. Therefore, to evaluate model input, I changed C_D^i and used the model to estimate C_D^B. Computing C_D^B does two things, 1) shows that the drag on

an individual kelp plant is not the same as the bulk drag coefficient, and 2) allow us to parameterize the kelp model. In total, there were 12 simulations varying C_D^i from 0.05 to 0.6. A threshold for velocities less than 0.05 m/s was imposed in order to get reasonable estimates of C_D^B during calculations.

3.3.8 Turbulent Kinetic Energy (TKE)

Turbulent kinetic Energy (TKE) is generally described by the intensity of the turbulent motion. The nearshore environment is believed to be an important region that dissipates TKE (Carter *et al.* 2005). Like bottom boundary conditions in a nearshore environment, vegetation also increases TKE (Rosman *et al.* 2010; Kalra *et al.* 2017). For example, a laboratory study demonstrated that while kelp increased TKE in the water column when compared to no kelp, the largest turbulence occurred when the kelp had a dense surface canopy (Rosman *et al.* 2010). TKE was calculated by *ROMS* and normalized by the total velocity. The TKE calculation was computed only for a cross-section area where kelp forest region was present.

3.4 RESULTS

Before starting the analysis of the kelp forest model, the model needs to adjust to a stable condition using a spin-up period to remove transient dynamics due to initial startup. For this simulation, I use sea surface elevation as the spin-up variable (Fig. 3.10). Because the no kelp simulation only has alongshore and cross-shore velocities as forcings, the period needed to stabilize was a little less than a month (Fig. 10-a), when kelp was added the spin-up period increased to closer to a month (Fig. 3.10-b). The amplitude of the sea surface height (SSH) stayed at 0.02 m and 0.001 m for no kelp and vegetation module on, respectively. There was no difference in SSH amplitude and time for the system to stabilize for both simulations *standard* and *canopy*.

When the vegetation module is added there is a destructive influence on the simulated range of SSH, this represents up to 40% reduction in amplitude.

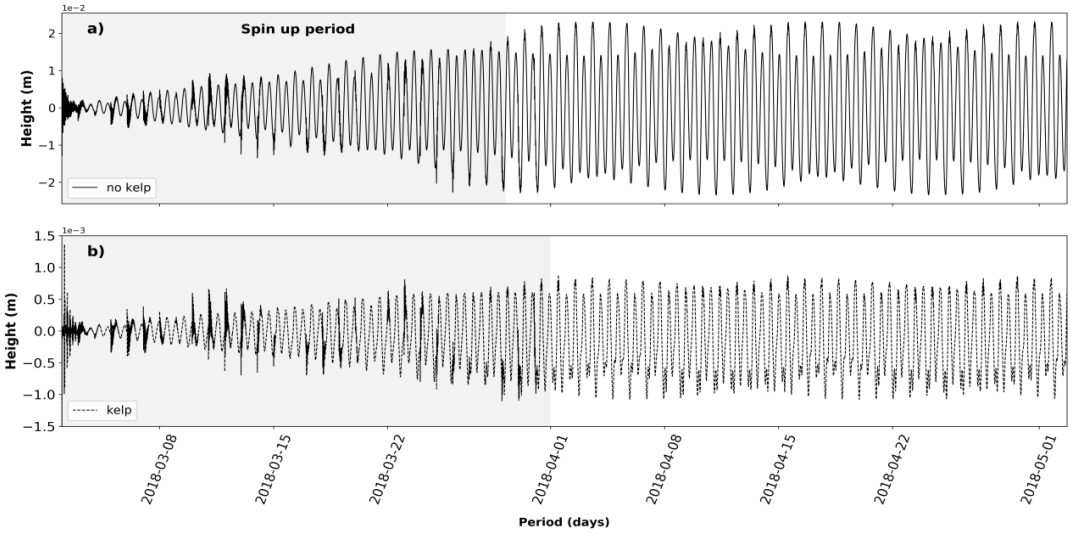

Figure 3.10 - Spin-up of the model domain for no kelp and inside kelp.

For the remaining analysis, the model was interpolated to the points of the *adp* dataset. The no kelp model showed good agreement with *adp15* (Fig. 3.11). Validation of the time-averaged currents was only possible up to 10.15 m from the bottom due to invalid values measured by the *adp15* instrument. The model overestimated the velocity over the first 4 m, underestimated to up to 9 m, and overestimated for the remainder of the data available. The absolute maximum difference was 0.008 m/s between model velocity and those observed at 6 m. The skill for the time-averaged velocity in the no kelp model run compared to *adp15* was 98.8%. A high *WS* indicates a good agreement with the variability of the observed dataset.

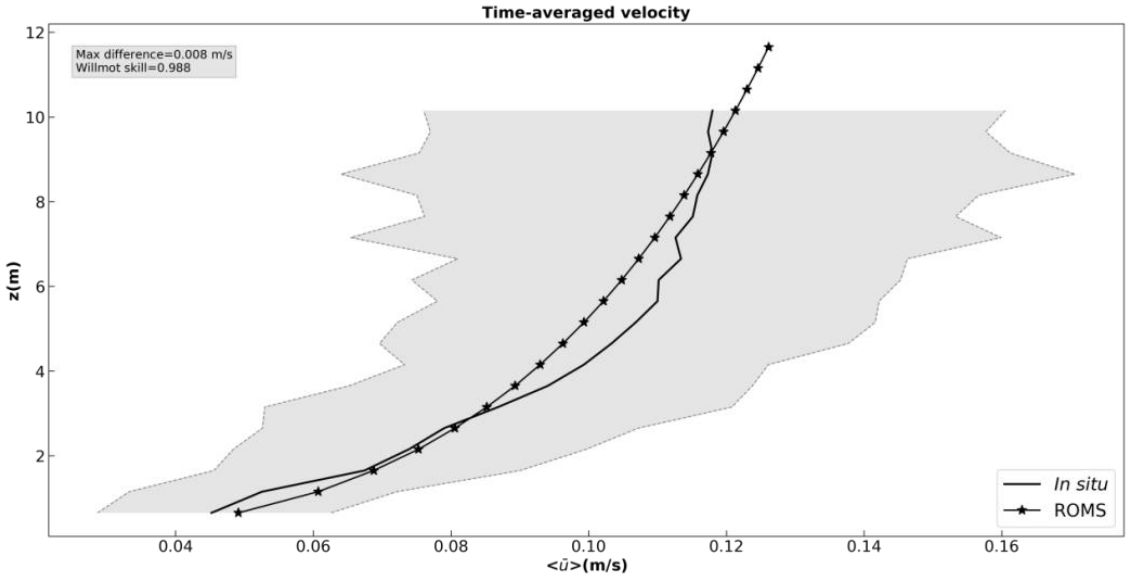

Figure 3.11 - Time-averaged profile comparison between *adp* data and model run without *vegetation* model. The gray region shows the 95% CI and mostly represents variation in velocity due to tides. Y-axis is above the bottom.

For both configurations with kelp, modeled time-averaged velocities decreased with the increase of $C_{d,veg}$ as expected (Fig. 3.12). The *standard* configuration showed a slightly higher time-averaged velocity than *canopy* throughout all case scenarios. This difference was more pronounced in the last 4 m to the surface. $C_{d,veg}$ was a way to change the fit of the velocities in the kelp simulation. Changes of 0.05 for $C_{d,veg}$ were considered a safe and fast approach to fit the best scenario while not having to simulate too many scenarios. The best fit scenarios were $C_{d,veg}$ = 0.35 (Fig. 3.12-g) and $C_{d,veg}$= 0.4 (Fig. 3.12-h) for the *canopy* and *standard* models, respectively. At $C_{d,veg}$= 0.35, the *standard* model provided a better fit than *canopy* between 7-9 m but overestimated the velocity below 6 m more than *canopy*. The scenario $C_{d,veg}$= 0.4 showed overestimation for both simulations below 6 m where both models had the same velocities, the *standard* module had the same variability at the surface as the *canopy* module in the $C_{d,veg}$= 0.35. The higher value for the

standard module also represents the effect of not applying the effects of the kelp canopy over the entire water column.

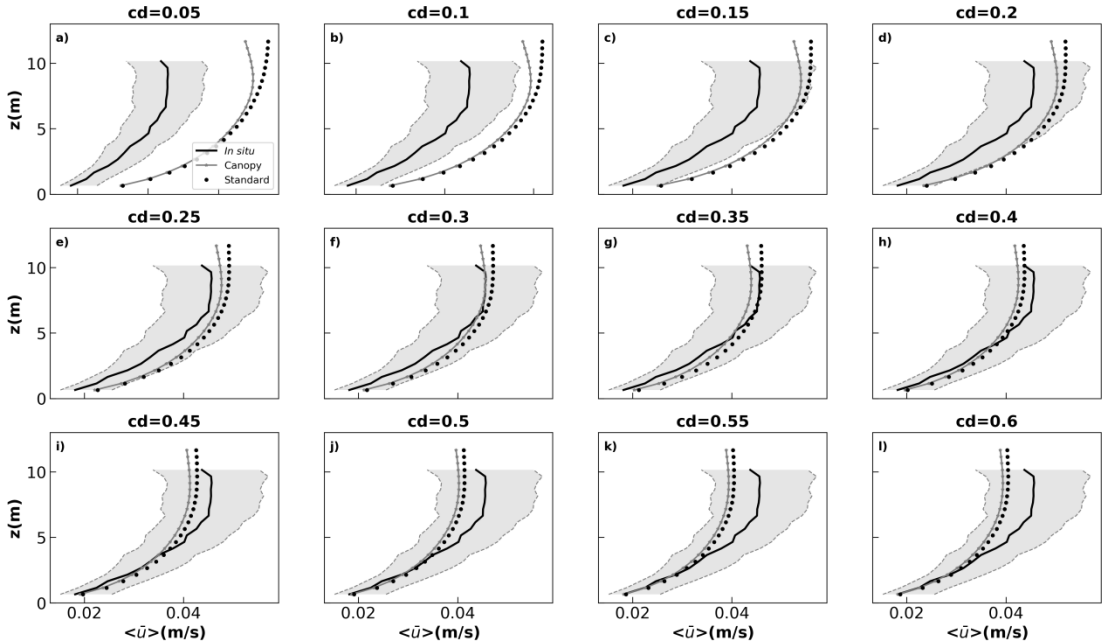

Figure 3.12 - Time-averaged profiles comparison between adp data and for *standard* and *canopy*. The gray region shows the 95% CI for the effects of the tides. Y-axis is above the bottom.

Table 3.2 shows *WS* calculated for the best $C_{d,veg}$ of each configuration. The water column was divided into upper and lower regions for this assessment to understand the impact of the code modification but also assess over the entire water column to check the overall fit. The division at 5 m was done because the *in situ* data only extends to 10 m. Over the entire water column *WS* was not different. Between the two regions, both simulations had greatest skill in the first 5 m which is observable in Fig. 3.12g-h. The *standard* model was slightly better near the bottom. The largest difference was observed in the upper 5 m where *canopy* model had the most skill (*WS* = 0.767), this difference is due to a slightly better fit between 5-6 m and between 8-9 m where it seems the velocity still feels the canopy acting on the surface velocities.

Table 3.2 - WS for the two best vegetation drag for both *standard* and *canopy* models.

	top*	**down****	**total*****
Standard	0.721	0.972	0.983
Canopy	0.767	0.967	0.983

* Calculated using values where depth is greater than 5. ** Calculated using values where depth is less or equal 5. ***Calculated for all the water column.

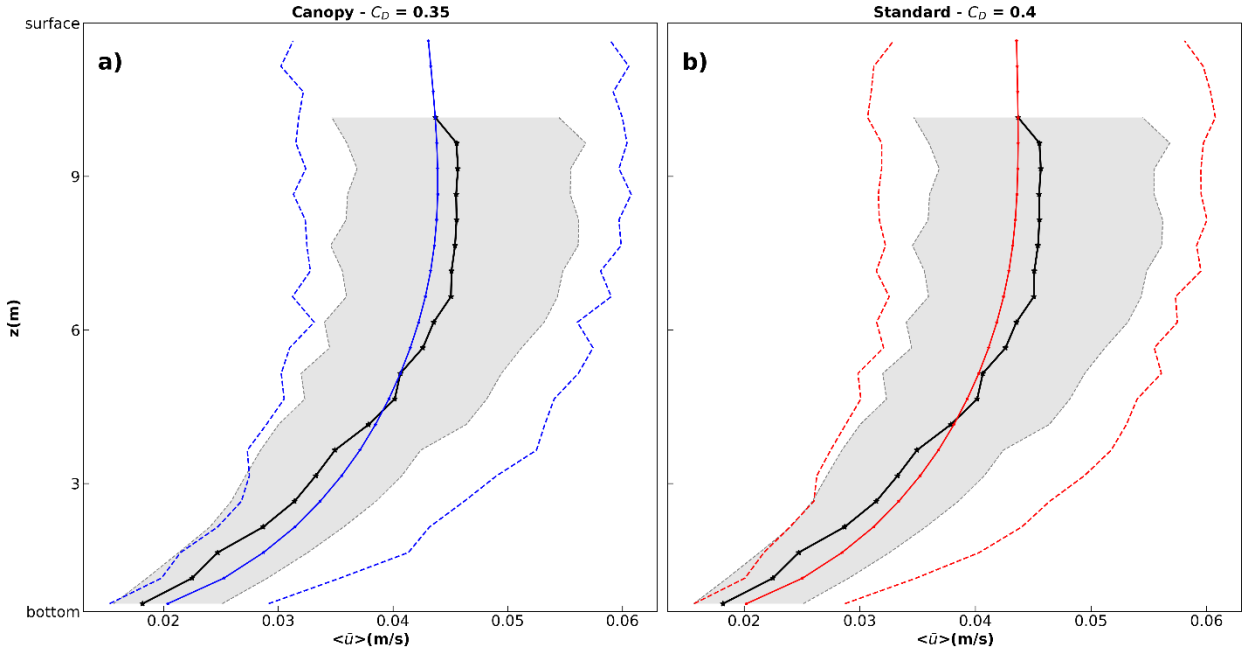

Figure 3.13 - Time-averaged profiles comparison between adp data and for *standard* and *canopy*. Dashed lines in blue (a) and red (b) represent the variability of *canopy* and *standard*, respectively. *The* gray region shows the 95% CI for the effects of the tides. Y-axis is above the bottom.

The two best models fit, and their variability is shown (Fig. 3.13). Both represent better the lower bound up to 3 meters above the bottom. After that, they started deviating from the variability observed in the adp dataset. This deviation, however, is not too strong. Utilizing WS to compare modules variability versus the observed dataset, I found WS equals 0.942 for the *canopy* on the

lower bound side (left of the mean time-averaged velocity) and WS equals 0.936 for the *standard* on the same bound. Although the *standard* module represented slightly better on the upper bound (WS= 0.909) than the *canopy* module (WS= 0.904), this difference is not too significant to assume that the *standard* module is better at representing the upper bound of the variability.

WS scores separated by 0.01 m/s bins are shown in Fig. 3.14. Both *canopy* and *standard* simulate similar along- and cross-shore velocities when compared against *in situ* datasets. *WS* values range from 0.25-0.93 for alongshore velocities (Fig. 3.14a) and 0.19-0.47 for cross-shore velocities (Fig. 3.14b). As expected, alongshore *WS* showed better comparison than cross-shore. One possible reason is that cross-shore velocities at the Punta Prieta site are also affected by internal waves and tides, while alongshore velocities are purely surface tides. As a result, alongshore velocities are compared better with observations at higher velocities than velocities closer to zero where there can be more uncertainty in both the model and measured velocities. Cross-shore velocities are best simulated between 0.04 and 0.05 m/s.

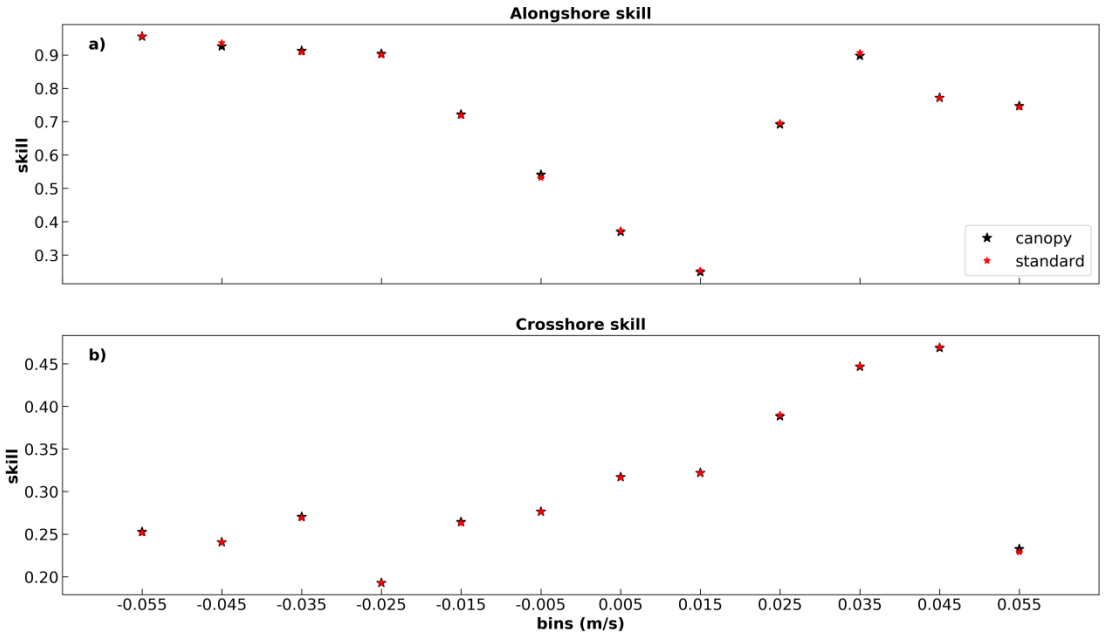

Figure 3.14 - WS for alongshore (a) and cross-shore (b) for *canopy* and *standard* simulations split by 0.01 m/s bins.

Mean bulk drag (C_D^B) increased as vegetation drag ($C_{d,veg}$) increased for both simulations (Table 3.3). The variability also increases as $C_{d,veg}$ becomes large. The C_D^B calculated for *canopy* is slightly larger for all $C_{d,veg}$ used. C_D^B for the best simulations were the same 0.084 and had the same variability $\pm$0.072. These values are within the values for dense kelp forests (C_D^B = 0.18) and sparse kelp forests (C_D^B= 0.07) in a laboratory study (Rosman *et al.* 2010). The values were also in agreement with Monismith *et al.* (2022) for the adp15 data used for this simulation (C_D^B~ 0.04).

Table 3.3 - Median bulk drag coefficient and 95% CI calculated from **equation 7** for *standard* and *canopy*.

	Cd_{veg} = 0.05	**Cd_{veg} = 0.10**	**Cd_{veg} = 0.15**	**Cd_{veg} = 0.20**	**Cd_{veg} = 0.25**	**Cd_{veg} = 0.30**	**Cd_{veg} = 0.35**	**Cd_{veg} = 0.40**	**Cd_{veg} = 0.45**	**Cd_{veg} = 0.50**	**Cd_{veg} = 0.55**	**Cd_{veg} = 0.60**
$Standard_{cd}$	.032± 0.016	.048± 0.028	.060± 0.037	.067± 0.045	.073± 0.052	.078± 0.059	.082± 0.065	**.084± 0.072**	.087± 0.078	.090± 0.084	.092± 0.090	.095± 0.093
$Canopy_{cd}$	.036± 0.018	.052± 0.030	.064± 0.040	.071± 0.048	.077± 0.056	.081± 0.063	**.084± 0.070**	.087± 0.077	.090± 0.085	.093± 0.091	.096± 0.094	.098± 0.094

The estimates of bulk drag (C_D^B) improves as Reynolds number (Re) increases (Fig. 3.15). Depth-averaged velocity was binned from 0.01 m/s to 0.09 m/s with 0.01 m/s intervals. C_D^B also has a Re dependency as expected. The medians for the two models are not statistically different. The C_D^B estimations are higher and less precise for smaller Re values (e.g: $10^{5.5}$ to $10^{5.8}$), and as the depth-averaged velocity increases bulk drag estimates are closer to what has been observed in the literature (Rosman *et al.* 2010; Monismith *et al.* 2022).

While the time-averaged profiles and bulk drag estimation are similar between both models, the difference in the mean velocity and its variability observed from the last two meters to the surface is quite different (Fig. 3.16). Overall, the largest differences are on the edges of the kelp forest region. The *standard* model had higher velocity and variability than *canopy* model in the last 2 m near the surface (Fig. 3.16a-b), resulting from the addition of kelp canopy in the latter model. *Canopy* had slightly higher velocity just below the kelp canopy especially on the edges (Fig. 3.16a). This decrease in time-averaged velocity at the surface and an increase at the bottom has been previously observed in laboratory for dense kelp with canopy (Rosman *et al.* 2010; Rosman *et al.* 2013).

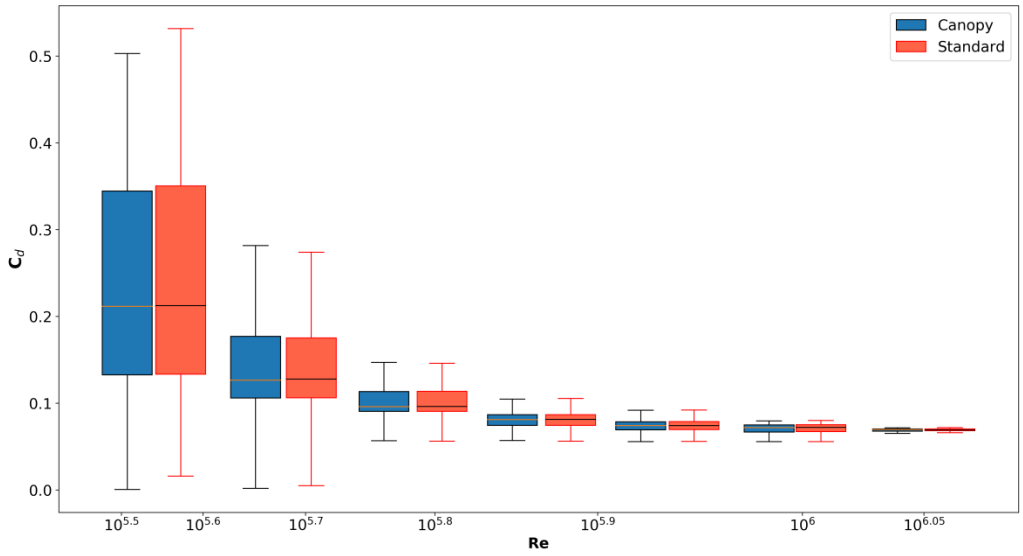

Figure 3.15 - Bulk drag versus Reynolds number for depth-averaged velocities at each 0.01m/s interval for both *canopy* and *standard*.

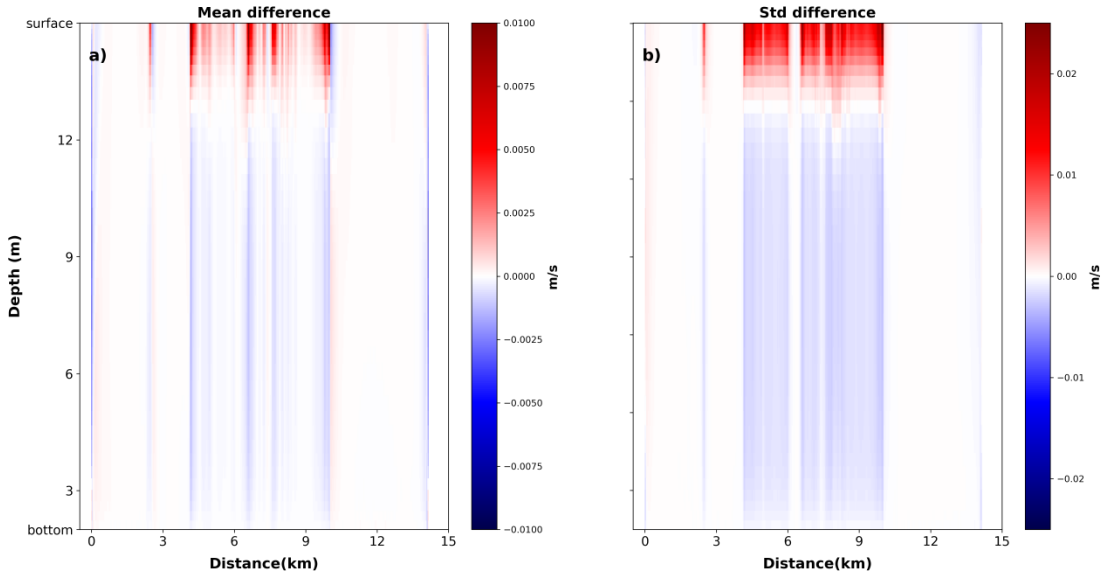

Figure 3.16 - Mean (a) and standard deviation (b) of velocities difference between *standard* and *canopy*. Alongshore slice at 1500m.

Absolute time-averaged cross-shore (Fig. 3.17a) and alongshore (Fig. 3.17b) velocities for the *canopy* simulation illustrate the ducting of flow around patches of kelp (Valle-Levinson et al

2022). Velocities in the kelp were disregarded, and where kelps are present in the model are shown in brown. There is an increase in mean time-averaged cross-shore speed along the outer and inner edges of the kelp forest (Fig. 3.17a). The highest absolute cross-shore velocities are located between kelp forests at 6.8 and 7.4 km. Acceleration of flow along the edges of kelp forests has been previously observed (Jackson & Winant, 1983; Jackson, 1998; Graham, 2003). In addition, the flow channeling between kelp gaps has been described recently for the same region (Valle-Levinson *et al.* 2022). The absolute time-averaged alongshore speeds decrease to almost zero between 1 and 1.5 km (Fig. 17b). The giant patch in front of this section is the cause of these velocities being almost null. The alongshore section shows flow channeling between 1.5 and 2 km. Flow channeling is stronger closer to the 2 km region and for depths between 8.5 m and the surface. Velocities are higher on the outer edge (approximately at 2.2 km) where there is no large patch that inhibits flows in that area. As a result, our model could also be applied to understand the effects on nutrient uptake (Gaylor *et al.* 2007), larvae dispersal (Graham, 2003), and connectivity among beds (Gaylord *et al.* 2006). In addition, Valle-Levinson *et al.* (2022) hypothesized that these regions could provide localized sites of fertilization and safe spaces for various species.

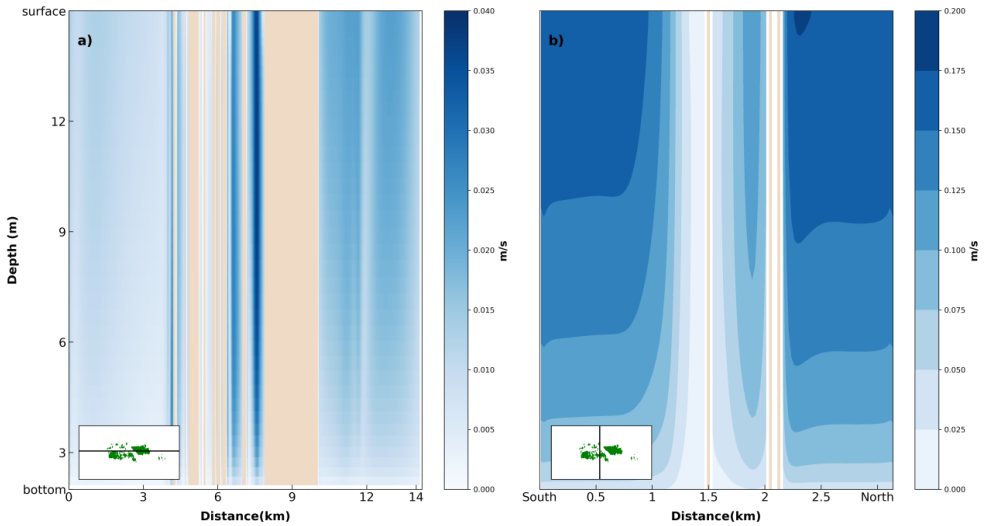

Figure 3.17 - Absolute time-averaged cross-shore (a) and alongshore (b) velocities for *canopy* module simulation. Brown region indicates where kelp forest module is present in the model.

Profiles of normalized TKE (hereafter TKE) for *standard*, *canopy*, and canopy with 50% coverage (instead of 100%) at the surface (*canopy50*) further illustrate the effects of kelp canopy on flows (Fig. 3.18). TKE was relatively the same from 0.5 m up to 7 m above the bottom for both the *standard* and *canopy* models. The *standard* profile is close to a linear function as expected for free surface flows. Similar mean TKE profiles were observed for no kelp and no canopy scenarios in a laboratory experiment (Rosman *et al.* 2010). The *canopy* simulation showed a TKE peak 2-fold higher than Rosman *et al.* (2010) while *canopy50* showed values similar to this laboratory study for a dense canopy scenario. I believe this is because of the spacing at the surface in the *canopy* scenario acting as almost a solid boundary at the surface generating more friction, and therefore, more TKE. While the profiles in the Rosman *et al.* (2010) do not show the bump observed in the simulations, I observed that the peaks, for both sparse and dense with kelp fronds, are always deeper than the actual kelp fronds located at the surface which is also observed in both simulations *canopy* and *canopy50*. TKE then decreases within the canopy.

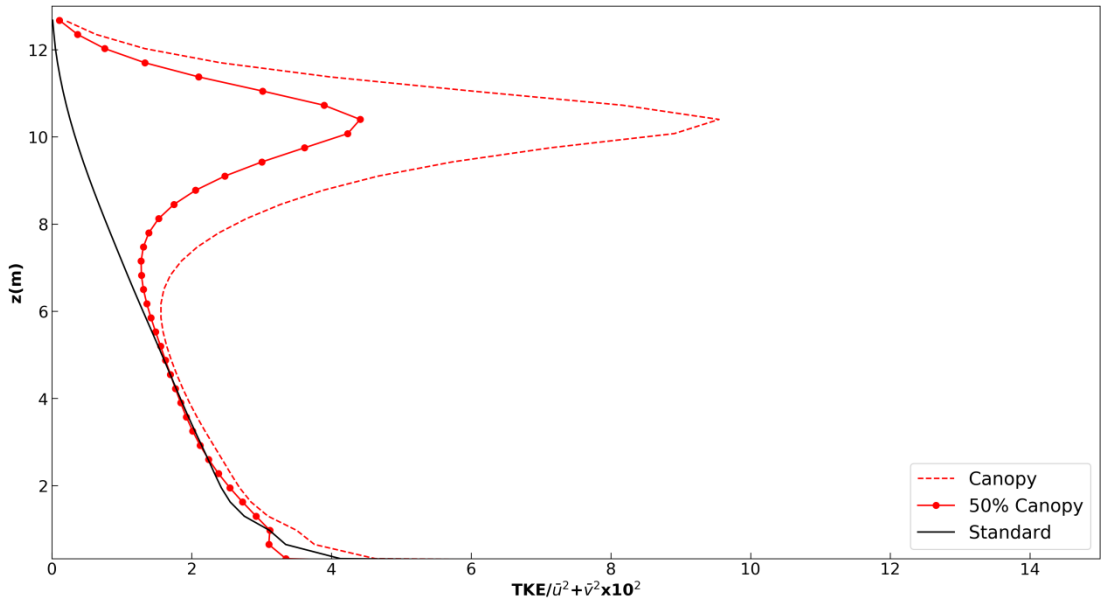

Figure 3.18 - Averaged normalized TKE only in the kelp forest region. Alongshore slice at 1500m.

3.5 DISCUSSION

The Coupled Ocean-Atmosphere-Wave-Sediment transport (*COAWST*) modeling system has been successfully applied to characterize wave-flow-seagrass interactions. The new module described in this paper, expands *COAWST* capability to simulate flow-vegetation interactions for canopied vegetation, specifically kelp forests. This module not only simulates the time-averaged tidal-driven currents in the presence of kelp forests but also the wake (turbulent kinetic energy) generated by kelp fronds as observed in laboratory experiments (Rosman *et al.* 2010).

The influence of kelp forests on currents have been modeled previously (Wu *et al.* 2017; Frieder *et al.* 2022). However, these models did not explicitly account for the presence of a canopy or were run offline and thus did not provide feedback to the regional model. In this study I were able to implement changes in flow and turbulence caused by kelp forests in a regional ocean model that provide feedback on the flows themselves. This was possible because of the vegetation module

developed by Beudin *et al.* (2016) and our modifed approach to simulate kelp canopy. In a previous study, the effects on currents by the drag generated due to kelp forests was only implemented at the bottom of the domain (Wu *et al.* 2017). Like this study, they also observed damping in the tidal velocity for regions where kelp beds were present. The most recent study documenting kelp forest simulation (Frieder *et al.* 2022) not only added the changes in the flows in the water column but also simulated growth and death of kelp forests, making their model more robust them the one present here for simulating kelp effects over longer time frames. However, the shortcoming of their model was that they used an offline Large Eddy Simulation (LES) forced by model outputs, and therefore, no direct feedback in the regional ocean model. While I understand our kelp forest simulation uses a static kelp forest domain and does not show a more realistic kelp forest seasonal cycle, it does represent well the domain when kelp density is zero and when kelp density is high (0.9 plants/m^2). This module can be expanded to be used to understand the two way interaction between kelp forests, currents, and biogeochemistry, for example, and could be modified to vary parameters through time to account for growth and decay of kelp forests over seasonal and interannual cycles.

The module presented here shows good agreement for the time-averaged velocity at Punta Prieta for the 2015 period when kelp was absent (Monismith *et al.* 2022). The differences observed mainly in the middle of the water column between our model and the *in situ* dataset could have been because the simulation was only forced with the two main tidal constituents for the domain and did not include wind and wave effects on currents (Monismith *et al.* 2022). However, while the largest difference between model and *in-situ* dataset occurs in the middle of the water column, I believe this difference could be due to two possible issues: a) model settings, for example, the sigma layers being coarser in the middle of the water column, or b) not having a solid coast on the

south boundary representing the island which could change the cross-shore velocities in the water column (Russell & Vennell, 2017). The upper 2 m of the water column cannot be compared due to ADP instrument capabilities pointed out by Monismith *et al.* (2022). This upper 2 m is strongly influenced by winds and waves that increase the velocity (see Fig. 7 in Monismith *et al.* 2022) and for our case I did not consider these two other processes.

When kelp is present, time-averaged velocity profiles show a rapid decrease in the last meter to the surface. Neither the *standard* nor *canopy* modules captured the change in the last 2 m of the water column observed in the *in situ* datasets. This has been pointed out that when kelp is present at the PP site, the velocities are wave-induced (Monismith *et al.* 2022) which is not imposed in the domain. Consequently, both models simulate similar patterns up to 10 meters by changing the vegetation drag by only 0.05. However, even if measurements for the last two meters are not reliable, I observe that the *in situ* data shows a tendency to slow down in the canopy region. The canopy region is formed due to the spread out of kelp fronds in the upper 2 m (Jackson, 1984), resulting in a dense region with larger drag than the rest of the kelp environment (Rosman *et al.* 2010), almost like a semi-wall. Although, our *canopy* approach does not account for changes in kelp orientation with currents, it shows better results in the canopy region than the *standard* module (Fig. 12-h).

The nearshore environment is believed to be an important region that dissipates TKE (Carter *et al.* 2005). Like bottom boundary conditions in a nearshore environment, vegetation also increases TKE (Rosman *et al.* 2010; Kalra *et al.* 2017). For example, kelp forests have a great effect on the various physical, chemistry, and biological processes due to the turbulence near the canopy region (Rosman *et al.* 2010). To our knowledge, this is the first time a hydrodynamic model was able to model TKE in the water column caused by canopies.

The density of *M. pyrifera* plants varies significantly throughout the year (Monismith *et al.* 2022). Reed *et al.* (2009) found that the lowest densities were during the end of winter season while the highest were during summer. The same authors found that the spacing between canopies decrease to its minimum during fall and increase during winter. For our simulations, I found that plant density ~ 0.9 plants m^{-2} (Reed *et al.* 2009) and *canopy50* produced the best scenario for summer periods, and therefore, the best fit to TKE estimates. Consequently, a study to develop a time-varying change in canopy spacing is needed to understand the impact of fronds for seasonal and yearly variability in kelp domains. Nonetheless, this new module opens opportunities to study how TKE affects nutrient availability (Rosman *et al.* 2010), oxygen dynamics (Murie & Bourdeau, 2020), and larval transport (Pakhomov *et al.* 2022) in kelp forest regions.

3.6 CONCLUSIONS

The *canopy* method presented in this paper to simulate kelp forests including the canopy is a new and relatively simple way to represent kelp forests in *COAWST*. The module modifies the plant thickness and plant diameter to decrease spacing in the last meter of the water column to mimic the effects of the kelp canopy. The revised module slightly improved fits to velocity and greatly improved fits to TKE depth profiles over the default vegetation module provided in *COAWST*. While both *canopy* and *standard* modules simulated similar time-averaged velocity profile when compared against *in situ* data, the difference in the turbulence created near the surface due to the presence of the kelp canopy is greatly improved and could have significant effects on air-sea fluxes, biogeochemical processes, and larval dispersion within the kelp forest. This model provides improved opportunities to study the impacts of kelp forests around flows and can further

be used to understand larvae dispersal and biogeochemistry in a kelp environment using hydrodynamic models.

CHAPTER 4

DEVELOPMENT OF A SIMPLE OXYGEN FLUX RATE MODEL FOR KELP FORESTS[2]

[2] Fagundes, Matheus and Woodson, C. B. To be submitted to *Ocean Modeling journal*.

ABSTRACT

Several observational studies have been done in kelp forest domains; however, the conclusions are generally for a small area compared to the total kelp forest area. It is also hard to have good biogeochemistry measurements in the canopy region and within the kelp forest. Here we report for the first time a model development for Dissolved Oxygen (DO) with an offline pH estimation model for kelp forest biogeochemistry modeling. We used 2-1/2 years of *in situ* data covering periods with and without kelp forests around Isla Natividad (Baja CA, MX). This dataset was used to validate the DO model for the main tidal constituents. We tested three scenarios and compared the simulations for present and under Fossil-fueled development with 8.5 W/m^2 radiative forcing (hereafter SSP585) scenario conditions. Results showed that the combination of the hydrodynamic module developed previously that captures the turbulence within kelp forests and the DO model (hereafter full model, FM) gave the best semi-diurnal and diurnal DO variability compared to the mooring in Punta Prieta - MX. The FM also represented well the difference between inside and outside kelp forest pH described in the literature. The DO ratio between simulations and the SSP585 scenario showed an increase between 2 and 3-fold at the canopy region and 1.5 and 2-fold at the bottom, demonstrating that kelp forest regions could help mitigate hypoxia and ocean acidification. Overall, kelp forests could offset the average decrease of 0.3 pH units by the end of the century. This new DO model coupled with the hydrodynamics module that simulates TKE within kelp forests could have great potential for studying the present and future impacts of climate change on local and global scales.

4.1 INTRODUCTION

Coastal ecosystems are highly dynamic and greatly affected by climate change (Booth *et al.* 2014). Within Eastern Boundary Upwelling Systems (EBUS), upwelling events bring low pH and deoxygenated waters to the coastal zones (Gruber, 2011). Upwelling has been intensifying due to climate change (Grantham *et al.* 2004). However, much of what is known about trends in Dissolved Oxygen (DO) and ocean acidification is based upon open-ocean conditions (Frieder *et al.* 2012) and few nearshore regions along the coasts have been studied with high spatial and temporal resolution to understand DO and pH dynamics. However, these biogeochemical studies are generally done by using long-term moorings in specific regions (Pfister *et al.* 2019; Low *et al.* 2021) giving a localized perspective of the ecosystem. For example, to study biogeochemical processes in canopy-forming giant kelp forests (*Macrocystis pyrifera*; kelp forests hereafter) most measurements are done using point sensors (e.g., Pfister *et al.* 2019; Traiger *et al.* 2022).

Global surface pH has decreased by roughly 0.11 units since 1770 (Jiang *et al.* 2019) and ocean oxygen content has decreased by over 2% (Schmidtko *et al.* 2017). As a result, oxygen minimum zones (OMZs) have expanded in all oceans (Stramma *et al.* 2010). The DO change accounts for approximately 40% of the total percentage of DO globally in the North and Equatorial Pacific (Schmidtko *et al.* 2017). The California Current System (CCS) also exhibits one of the largest declines in pH, ~0.15 units, since 1770 (Jiang *et al.* 2019). The CCS already experiences natural seasonal upwelling (Kekuewa *et al.* 2022), and consequently, declines in DO and pH raise concerns about the function of ecosystems on the continental and inner shelf of the CCS (Grantham *et al.* 2004). However, vegetated coastal habitats can ameliorate some of the impacts of climate change (Duarte, 2017) through the uptake of CO_2 and release of O_2. For example, kelp beds can locally increase pH and DO (Pfister *et al.* 2019).

Marine vegetated habitats (e.g., seagrasses, mangroves, salt-marshes, macroalgae), while occupying less than 0.5% of the ocean surface, are responsible for removing 50% of the CO_2 (Duarte *et al.* 2013) and represent up to 10% of the global marine net primary production (Duarte, 2017). Out of the four marine vegetated habitats, seaweed ecosystems are the largest vegetated coastal ecosystem on the planet (Pessarrodona *et al.* 2022). Seaweed ecosystems can produce up to 6 kg C m^{-2} $year^{-1}$ in net primary production (NPP) in some regions, which is around 3-fold more than ocean phytoplankton (Pessarrodona *et al.* 2022). Out of 8 vegetation types in the seaweed ecosystem category, kelp forests are responsible for most of the total NPP (Pessarrodona *et al.* 2022).

Kelp forests cover approximately 1/4 of the total coastal regions of the World (Wernberg *et al.* 2018). In the California Current System (CCS), they are found from 55°N to 25°N (Wu *et al.* 2017; Valle-Levinson *et al.* 2022) and have been studied extensively in some specific areas (Frieder *et al.* 2012; Koweek *et al.* 2017; Traiger *et al.* 2021). However, because of their high density and canopy-formation, biogeochemical observations become limited to *in situ* data collection (Traiger *et al.* 2021). Kelp forests also provide shelter to macroinvertebrates (Dayton, 1985), uptake carbon (Macreadie *et al.* 2021), are highly productive (Gerard, 1986), and elevate pH and Dissolved Oxygen (DO) relative to surrounding areas (Frieder *et al.* 2012). For instance, Pfister *et al.* (2019) analyzed samples in the Northern CCS both inside and outside kelp forests at 1 m depth, and found differences of almost 2.5 mg/L and 0.2 units for DO and pH, respectively. In Central California, Koweek *et al.* (2017) found a difference inside kelp of over 0.5 pH units between the top and bottom. Traiger *et al.* (2022) found that daily variability inside kelp could be as high as 7 mg/L and 0.36 pH units for a Central California region, similar to Frieder *et al.* (2012).

Until now, no numerical simulations have been done to understand how these ecosystems modify the DO dynamics and pH within their region. In this chapter, I developed a simple kelp photosynthesis and respiration model based on Scully (2010) to assess how the three-dimensional structure that kelp creates can impact DO dynamics and further used an offline model approach to calculate pH based on DO. An offline model is defined here as a model that does not interact directly with the actual model. For instance, the offline model only receives "fixed" datasets (e.g.: outputs from models or observational data) that are used to calculate a variable (e.g.: pH), and consequently, does not affect in any way the original values used. A semi-idealized high-resolution circulation model was used to conduct a detailed study to assess the combined response of kelp hydrodynamics, and photosynthesis and respiration on DO and pH within a kelp forest domain under Fossil-fueled development with 8.5 W/m^2 radiative forcing (hereafter SSP585) scenario.

4.2 THEORY

4.2.1 Simple biological kelp model

Kelp respiration is added by modifying the model developed in Scully (2010), which simulates how physical processes modulate DO in the water column. The model uses a 3D respiration rate (mmol/m^3/day) that can be provided as a constant input or a daily forcing variable. Following Scully (2010), the equation for the conservation of DO with the proposed kelp forest net primary production (NPP) added gives:

$$\frac{\partial DO}{\partial t} + (\frac{u\partial}{\partial x} + \frac{v\partial}{\partial y} + \frac{w\partial}{\partial z})DO = \frac{\partial}{\partial z}K_z\frac{\partial DO}{\partial z} - R_{kelp} + NPP_{kel} \quad \textbf{(1)}$$

Where $\frac{\partial DO}{\partial t}$ is the time rate of change of DO, the second term is the advection of DO, the terms on the right side are the vertical diffusion, nocturnal respiration rate of kelp forests (R_{kelp}), and a new term for the net photosynthetic rate of kelp forests (NPP_{resp}) respectively.

4.2.2 Empirical calculations of Dissolved Inorganic Carbon (DIC) and Total Alkalinity (TA)

I utilized an offline calculation for pH using the method proposed by Chen *et al.* (2017) to calculate the difference between a reduced physics model (RP, *canopy* module off) and a full model (FM, *canopy* module on) simulations. A better description of the simulations for RP and FM can be found in the Scenarios section below. Calculations were done for slices in two patches present in the model (see dashed regions in Fig. 4.1). This method used Apparent Oxygen Utilization (AOU) to calculate DIC and TA. Assuming that the Redfield ratio is the same in the kelp forest domain as it is in the open ocean, yields:

$$(CH_2O)_{106}(NH_3)_{16}H_3PO_4 + 138O_2 \rightarrow 106CO_2 + 122H_2O + 17H^+ + 16NO_3^- + H_2PO_4^- \quad \textbf{(2)}$$

for the decomposition of organic matter. DIC can be described as:

$$DIC = DIC^0 + \Delta \sum CO_2 + \Delta DIC_{org} + \Delta DIC_{ic} \quad \textbf{(3)}$$

Where excess $\Delta \sum CO_2$ is considered null given the small region of the model simulation, leading to:

$$DIC = DIC^0 + \Delta DIC_{org} + \Delta DIC_{ic}$$

where DIC^0 is the monthly mean DIC taken from a global climate model for the period simulated, DIC_{org} is calculated using eq. 2, and using the relationship between DIC_{org} and DIC_{ic} found by Chen *et al.* (1996), yields:

$$\Delta DIC_{org} = (106/138)\Delta AOU_{model}$$

$$\Delta DIC_{ic} = R_{ic:org}(z) * \Delta DIC_{org}$$

Where, $R_{ic:org}(z) = 0.212 + 0.0238z$ (Chen *et al.* 1996), after some manipulations DIC can be calculated as follows (eq. 4):

$$DIC = DIC^0 + (106/138) * (AOU - AOU^0) * (1 + R_{ic:org}) \quad \textbf{(4)}$$

And following the same approach, I can estimate TA (eq. 5), where TA^0 is the monthly mean TA from a global climate model for the period simulated, TA_{org} is found by the relationship between H^+ and O_2 in eq. 2, TA_{ic} production is 2-fold the production of DIC_{org}, thus:

$$\begin{gathered} TA = TA^0 + \Delta TA_{org} + \Delta TA_{ic} \\ \Delta TA_{org} = (-17/138)\Delta AOU \\ \Delta TA_{ic} = 2R_{ic:oc}(z) * \Delta DIC_{org} \end{gathered} \quad \textbf{(5)}$$

Finally yielding,

$$TA = TA^0 + ([AOU - AOU^0]/138) * (-17 + 212R_{ic:org}) \quad \textbf{(6)}$$

Converting Apparent Oxygen Utilization (AOU) from O_2 modeled:

$$\Delta AOU = AOU - AOU^0 \quad \textbf{(7)}$$

For this study, BM was considered AOU^0:

$$AOU_{model} = O_2sat - O_2model$$

$$AOU^0_{BM} = O_2sat(BM) - O_2(BM)$$

Where O_{2sat} is calculated using coefficients found by Benson & Krause (1984) and fitted by Garcia & Gordon (1992). The O_{2sat} equation present in GSW-python function is based on practical

salinity and potential temperature referenced to the sea pressure. I used the same python package to convert the temperature of the model to potential temperature at sea level.

4.2.3 Calculating pH_{sim} using TA_{sim} and DIC_{sim} data

Hourly pH_{sim} was calculated using CO_2 System Calculations Program (CO2SYS) (Pierrot, Lewis, & Wallace, 2006) python version (PyCO2SYS v1.8; Humphreys *et al.* 2022). Hourly TA_{sim}, DIC_{sim}, temperature, and salinity were used as parameters. The parameters for PyCO2SYS are shown in Table 4.1.

Table 4.1 - Constants applied to calculate pH by using PyCO2SYS.

Author	K_1	K_2	Boric Acid	Sulfate Acid
Mehrbach *et al.* (1973)	$6x10^{-3}$	$1x10^{-2}$		
Dickson (1990)			$7.25x10^{-9}$	$1.2x10^{-2}$

4.3 METHODS

4.3.1 Scenarios

The model for the present-day scenario was initialized at rest with a well-mixed domain where temperature and salinity are 19°C and 34 PSU in the entire domain, respectively (Low *et al.* 2021). To examine the role of kelp hydrodynamics in modulating dissolved oxygen, 3 numerical experiments are conducted using the model configuration described above (Table 4.2). For the base model run (BM), the simulation ran for 3 months with both the biological kelp and hydrodynamics models deactivated. To examine the effects of the simple biological kelp model (RP), a simulation using the same profiles based on literature was conducted. The last simulation

(FM) is combining the biological kelp model with the hydrodynamic kelp model to understand the impacts on local dissolved oxygen. These simulations did not include winds, and considered the same kelp respiration and oxygen production profiles over the 3 months period. This study also did not include kelp growth, change in kelp biomass, change in kelp density.

Table 4.2 - Description of model runs.

Model ID	Model description
BM	Base model run with no kelp hydrodynamics or the simple biological kelp model, only dissolved oxygen.
RP	Base model and simple biological kelp model, kelp hydrodynamics not activated.
FM	Simple biological kelp model and kelp hydrodynamics (*canopy* module) activated.

4.3.2 Numerical Model Description

The model used in this study was the *Coupled Ocean-Atmosphere-Wave-Sediment-Transport model (COAWST V3.3*; Warner *et al.* 2008). The ocean component of *COAWST* is the *Regional Ocean Modeling System (ROMS)* (Haidvogel *et al.* 2008). ROMS is a 3-D, free-surface model, which solves the primitive equations using hydrostatic and Boussinesq approximations with topography-following sigma layers (Shchepetkin and McWilliams, 2005; Haidvogel *et al.* 2008). For the momentum equations, splines vertical advection and logarithmic bottom friction were selected to keep stability and better represent the environment, respectively. The model used the

Mellor-Yamada level 2.5 turbulence closure scheme (MY-2.5). All boundaries (N, S, E, W) were open to allow along- and cross-shore flows. A periodic boundary condition was applied for free-surface, a Flather condition for 2D u- and v-momentum, and a Radiation-Nudging condition for 3D u- and v-momentum. The barotropic time-step was set at 10 s. Bottom roughness (z_{ob}) was 0.03 m and surface roughness (z_{os}) was 0.4 m with a no-slip condition along the bottom to provide a best fit for the no-kelp simulations to observed velocity profiles. The model had 40 sigma-layers splitting the 13 meters of water column with surface stretching (θ_s) = 1, bottom stretching (θ_b) = 2, and thermocline depth (Tcline) = 0. The domain was approximately 14 km long by 3 km wide with a grid size of 25 meters x 25 meters (Fig. 4.1). Hydrodynamic conditions of the domain were simulated for 3 months.

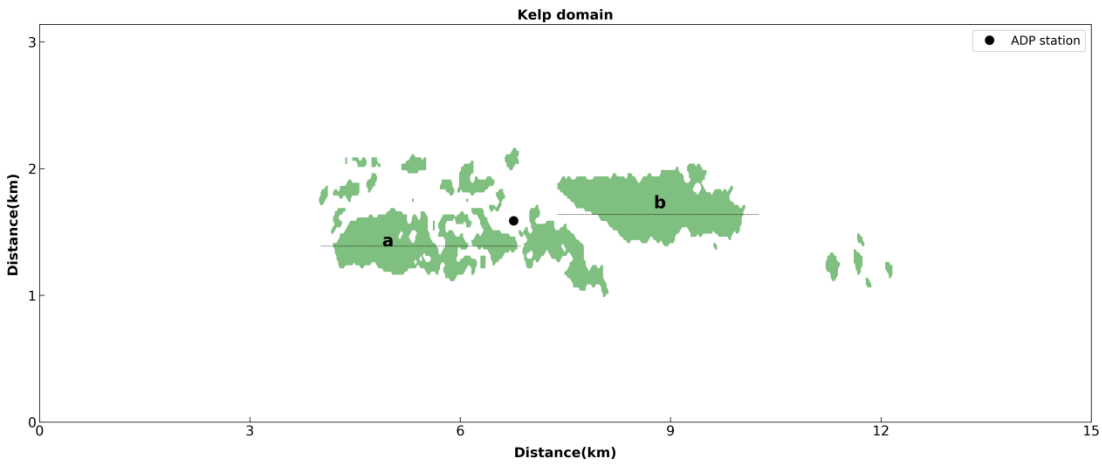

Figure 4.1 - Model domain for the region of study. The ADP station is used for model validation, two main patches a and b for a fragmented kelp and a continuous kelp, respectively. The points a and b also represent the location where I calculated time-averaged DO profiles. Dashed-lines show the slices used to calculate DIC, TA, and pH.

4.3.3 Forcings

4.3.3.1 Currents

The mooring at Punta Prieta for the Winter 2015 period (henceforth adp15) was chosen to force this simulation (see chapter 3 or Monismith *et al.* 2022). *In situ* current data was collected every 0.5 meter starting from 0.65 meters above the bottom to the surface (~14 m). The depth of the ADP data used for this simulation was from 2.65-12.65 meters from the bottom to remove errors in the first couple meters due to side-lobe interference (Monismith *et al.* 2022). Alongshore and cross-shore velocities are 10-minute profiles, rotated to the true shore.

4.3.3.2 Daily kelp Respiration (R_{kelp}) and Net Primary Production (NPP_{kelp})

For this experiment I modified respiration and photosynthesis for *Macrocystis pyrifera* found in the literature (Gerard,1986) from μmol O_2 cm^{-2} h^{-1} to mmol O_2 m^{-3} day^{-1} (Table 4.3). No values were available after 9 meters from the surface, and consequently, these parameters were set to zero. The highest values are in the last meter to the surface where kelp canopy is present. The values were then interpolated to the depth of the idealized model and assigned only for the region where the kelp forest is present (see Fig. 4.1). The final interpolated values are shown in Fig. 4.2. This model did not considered respiration from bottom organisms present in kelp forests regions.

Table 4.3 - Respiration and Photosynthesis for *Macrocystis pyrifera* in mmol O_2 m^{-3} day^{-1}.

	Surface	**0.5 m**	**4 m**	**8 m**	**bottom**
Respiration	792.0	48.0	15.6	20.4	0.0
Photosynthesis	2952.0	240.0	120.0	43.2	0.0

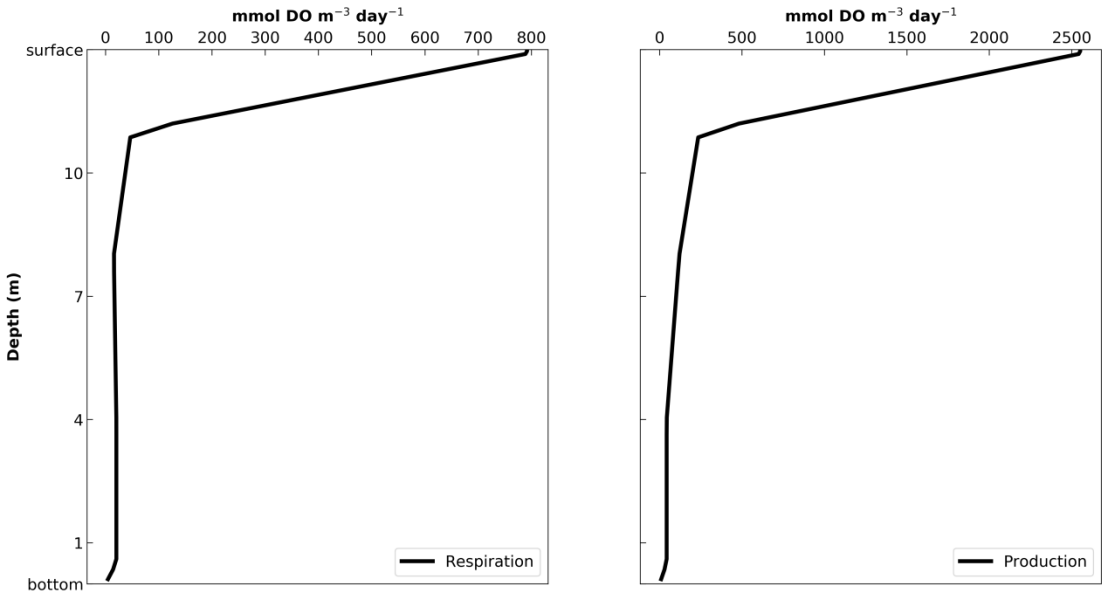

Figure 4.2 - Initial and Boundary conditions for Respiration and Production for kelp forest region.

4.3.3.3 Dissolved Oxygen

The DO used is from The Operational Mercator Ocean biogeochemical global analysis and forecast system (Von Schuckmann *et al.* 2018). This dataset provides a daily/monthly temporal resolution from 1993-present and a 1/4°x1/4° spatial resolution. The global biogeochemical output has 75 vertical levels and has seven variables available: chlorophyll (chl), dissolved oxygen (DO), nitrate (NO_3), silicate (Si), iron (Fe), and net primary production (NPP). Daily DO was interpolated to 10-min input to match the velocities inputs. It was forced on all the boundaries using Summer 2015 data; the same year as the observed currents used.

4.3.3.4 DIC^0, TA^0, and pH_{out}

Historical Canadian Earth System Model version 5 (CanESM5) was selected (Swart *et al.* 2022) for this experiment. This historical global scenario uses NEMO 3.4.1 with 1° horizontal resolution and 45 vertical levels, the biogeochemistry model is the Canadian Model of Ocean

Carbon (CMOC) with NPZD ecosystem, and the output is monthly. For DIC^0 and TA^0, I considered a 30-year mean value for the months of June and July (Fig. 4.3a-b). The mean of three nearest grid-points in latitude and longitude to the location of the model were used. The pH_{out} for the analysis was from the Global Ocean Biogeochemistry Hindcast (Von Schuckmann *et al.* 2018), that covers 1993-2020, with a horizontal resolution is 0.25° x 0.25° and 75 levels in depth. I used the period of 1993-2014, and as previously I did for DIC^0 and TA^0, I also estimated pH_{out} by using the nearest 3 grid points in latitude and longitude from the model domain for the months of June and July (Fig. 4.3c). All the variables were then interpolated to the depth of the model.

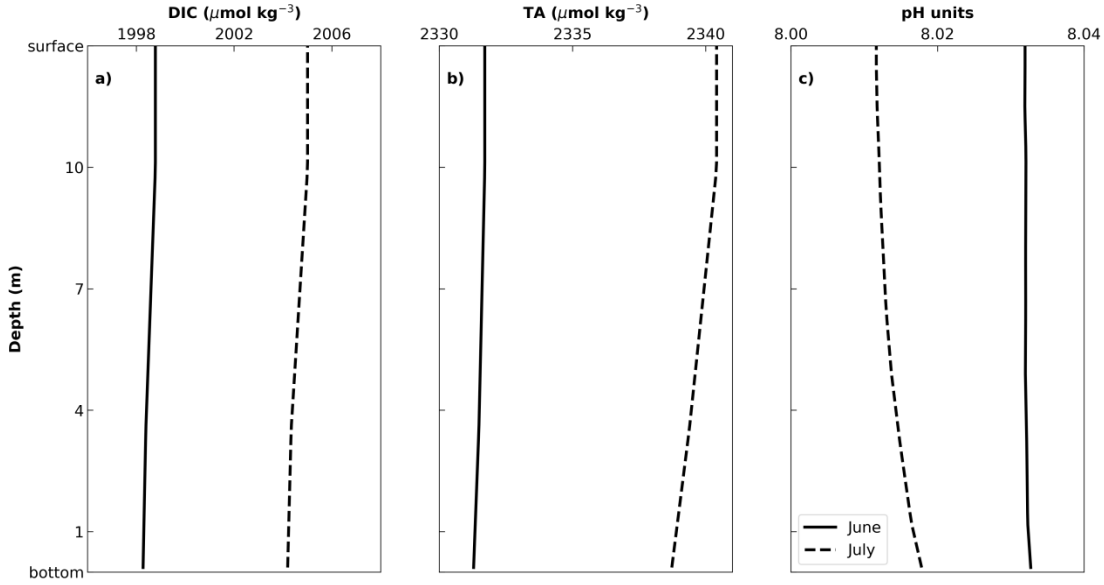

Figure 4.3 - Climatological mean DIC_0, TA_0, and pH_{out} for the months of June (solid line) and July (dashed line).

4.3.4 Pseudo-Global Warming (PGW) scenario

To understand the impact of climate change on the oxygen dynamics in kelp forest environments, I used the Pseudo-Global Warming (PGW) approach (Schär *et al.* 1996). This method was first introduced to study the atmospheric response in Europe to a pseudo-global

warming of 2 K (Schär *et al.* 1996). This "time-slice" approach generates climate variability between historical period and future scenarios and has been applied to several regional climate simulations studies (Lynn *et al.* 2009; Denamiel *et al.* 2020; Kessouri *et al.* 2021) (eq. 8). Several factors were used to select the global climate model for this experiment such that it needed to have historical CO_2 and SSP585 experiments, the same variant label, and have all the three monthly variables selected to be downscaled salinity, temperature and DO. As a result, only CanESM5 (Swart *et al.* 2022) was selected for this experiment. Because of its coarse resolution, three grid points in latitude and longitude were selected to represent an average of the region around Isla Natividad, MX. To calculate the PGW, 30-year periods for historical (1980-2010) ($Var[monthly,z]_{Hist}$) and future (2070-2100) ($Var[monthly,z]_{Fut}$) scenarios were used. The difference between median monthly datasets resulted in a median variability for each depth ($\Delta var[monthly,z]$). The result was then interpolated to the depth of the domain and added to each corresponding month simulated (Fig. 4.4). The greatest difference is observed in the range of the depth-averaged DO for SSP585 compared to the control (CTRL; Fig. 4.4c). As expected DO decreases in future scenarios, probably due to decreases in oxygen saturation as ocean temperatures rise (see Fig. 4.5; Giomi *et al.* 2019).

$$\Delta var(monthly, z) = Var(monthly, z)_{Fut} - Var(monthly, z)_{Hist}$$

$$PGW_{var} = Var(daily, z) \pm \Delta var(monthly, z) \qquad \textbf{(8)}$$

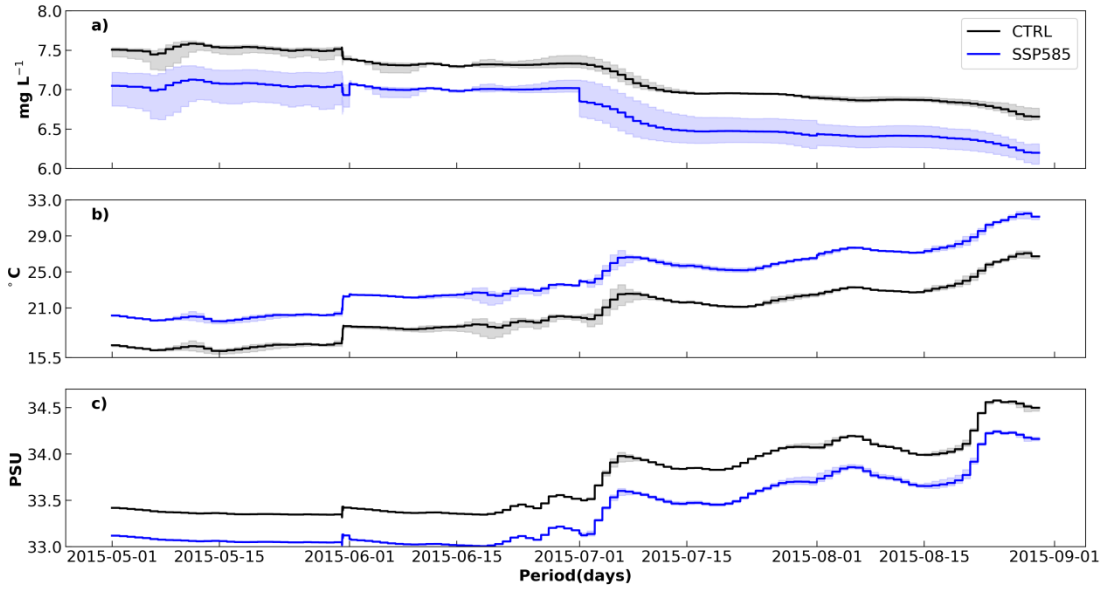

Figure 4.4 - Time-series of depth-averaged Dissolved Oxygen (a), Temperature (b), and Salinity (c) for CTRL (black line) and PGW using SSP585 (blue line).

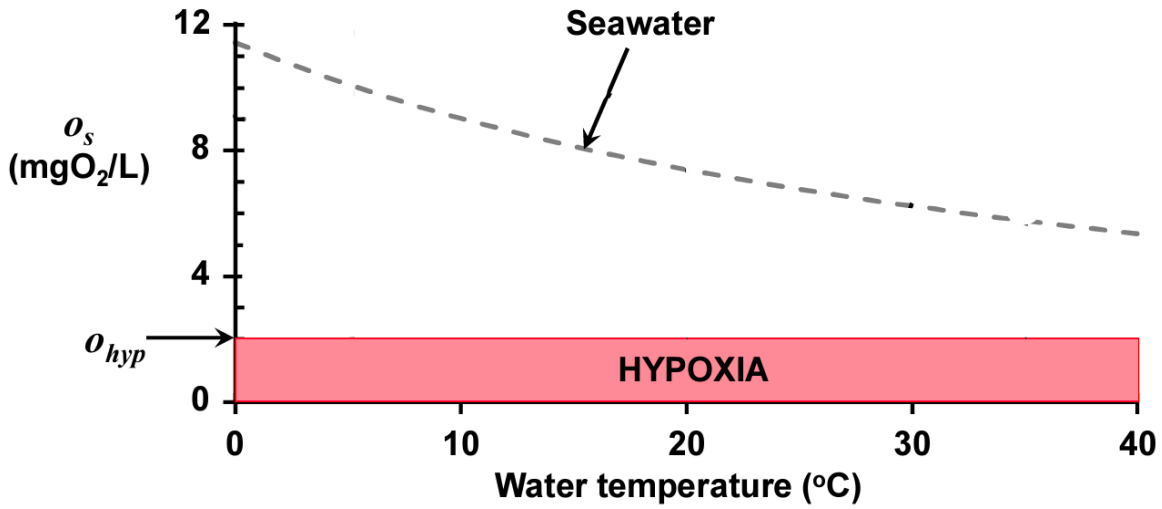

Figure 4.5 - Dissolved Oxygen saturation versus temperature for seawater modified from Chapra *et al.* (2021).

4.3.5 Statistical Analysis

I conducted an analysis of variances (ANOVA) to examine the effects of the turbulence and hydrodynamics between the different DO models. ANOVA is a suitable statistical method for

comparing means across multiple groups. The assumptions of ANOVA were checked before the analysis. I verified that the mean variability between the two models met the assumptions of independence, normality, and homogeneity of variances. To compare the volume difference between the BM and the other two models, I performed a one-way ANOVA to determine whether there were statistically significant differences in mean DO volume between the RP and FM models. The null hypothesis is that there are no significant differences between the volume variability of DO between RP and FM models, while the alternative hypothesis is that the volume variability in the model with the *canopy* module off is different than the FM with the *canopy* module on. I used a 95% significance level ($p < 0.05$) to determine whether the two models are significantly different and reject the null hypothesis.

4.4 RESULTS

Before analysis, the model needs to reach a stable condition. Therefore, I used the depth-averaged DO in the middle of the domain for the second month of simulation to establish when transient oscillations had decayed (Fig. 4.6). The Base Model (BM) stayed around 7.6 mg/l, resulting from the lower complexity. For the RP and FM simulations, the DO adjustment took over a month to stabilize. Consequently, the analysis was based solely on the last 6 weeks of the simulation.

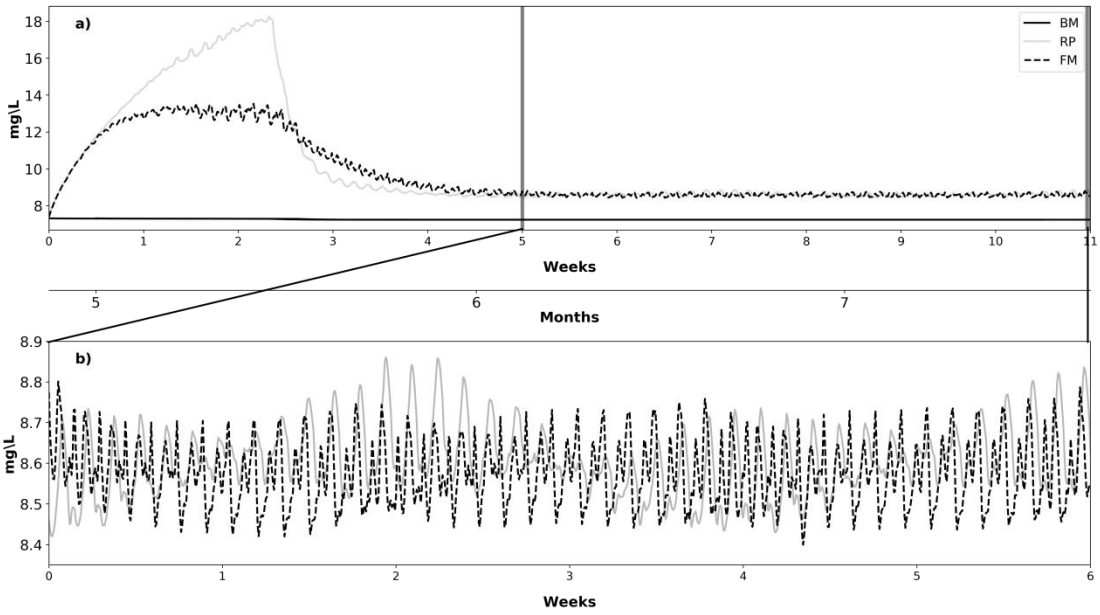

Figure 4.6 - Spin up of DO for BM, RP, and FM. Gray line represents the time-step where all models finish the spin-up.

I estimated power spectra using Fast Fourier Transform (FFT) with hourly windowing to validate temporal variability in the simulations (Fig. 4.7). This method was chosen due to its robustness for static data. FFT allowed us to quantify the variability by frequency of the two main tidal constituents (M2, K1) observed in the kelp forest region for the June 2014 period with the highest biomass concentration (Monismith *et al.* 2022)**.** I applied the analysis only for the period after spin-up for all scenarios. The *in situ* dataset was averaged from 10-minutes output to hourly to match the hourly results from the simulations. The spectral analysis was used to ascertain the dominant temporal constituents of DO for all simulations between 12- and 24-h periods for Isla Natividad - MX (Monismith *et al.* 2022). Not all scenarios showed the observed variability found at 12 m depth (Fig. 4.7a). Only two scenarios simulate diurnal and semi-diurnal variability in DO for Punta Prieta (Fig 4.7-b,c). However, the RP scenario showed DO variability twice double observed values (Fig. 4.7b). The FM model accurately simulates the diurnal and semi-diurnal

variability observed. However, some frequencies (e.g., 8 and 48 hours) observed are not present in either RP or FM, but could be due to regional forcing and variability in wave field which are not accounted for in the current model.

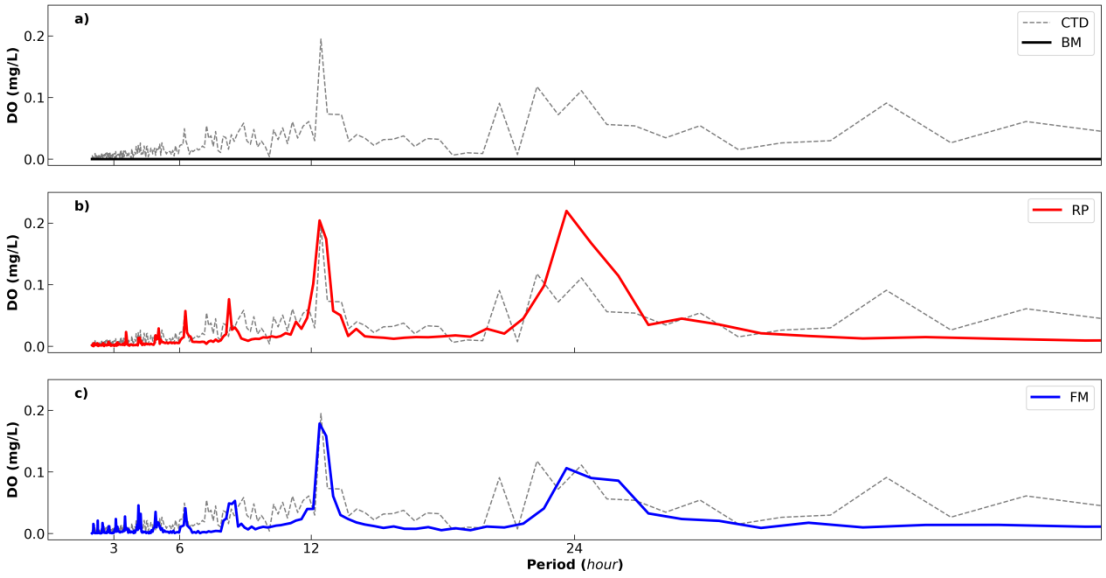

Figure 4.7 - FFT of the DO dataset close to the bottom for BM (a); RP (b); and FM (c). The dashed line represents the ADP dataset for Summer 2014.

Amplitudes for diurnal and semi-diurnal DO variability for PP were also calculated using t-tide **(**Pawlowicz *et al.* 2002; Table 4.4). I found that amplitudes for the dataset at the 12 m were 0.2 and 0.09 mg/L for M2 and K1, respectively, as expected BM did not have either diurnal or semi-diurnal variability. The two signals show up when daily respiration and DO production are added to the domain. However, the signals present in the RP simulation are approximately 2-fold higher for K1 and 1.2-fold higher for M2. The FM simulation shows the best agreement for diurnal and semi-diurnal amplitudes. It is interesting to notice how daily respiration/production of O_2 combined with kelp forest hydrodynamics can generate amplitudes for M2 and K1, similar to what is found in the ADP station.

Table 4.4 - DO amplitude for the two main tide constituents in Punta Prieta - MX.

	ADP Station	Base Model	Only Respiration	Full Model
M2	0.20	0.00	0.30	0.22
K1	0.09	0.00	0.25	0.13

The time-averaged profiles are based on the alongshore slice in the middle of the domain and masked to only account for the DO from the kelp forest domain (Fig. 4.8). BM showed a constant DO of 7.2 mg/L throughout the water column. When DO flux is imposed without the kelp forest hydrodynamic module, the maximum variability in the DO is about 1 mg/L, with a mean DO of approximately 8.5 mg/L. Mean DO increases by about 0.5 mg/L more when the *canopy* module is activated allowing for kelp-flow interactions. Although the mean DO difference between RP and FM scenarios was only 0.5 mg/L, the variability was 3.5-fold greater for FM.

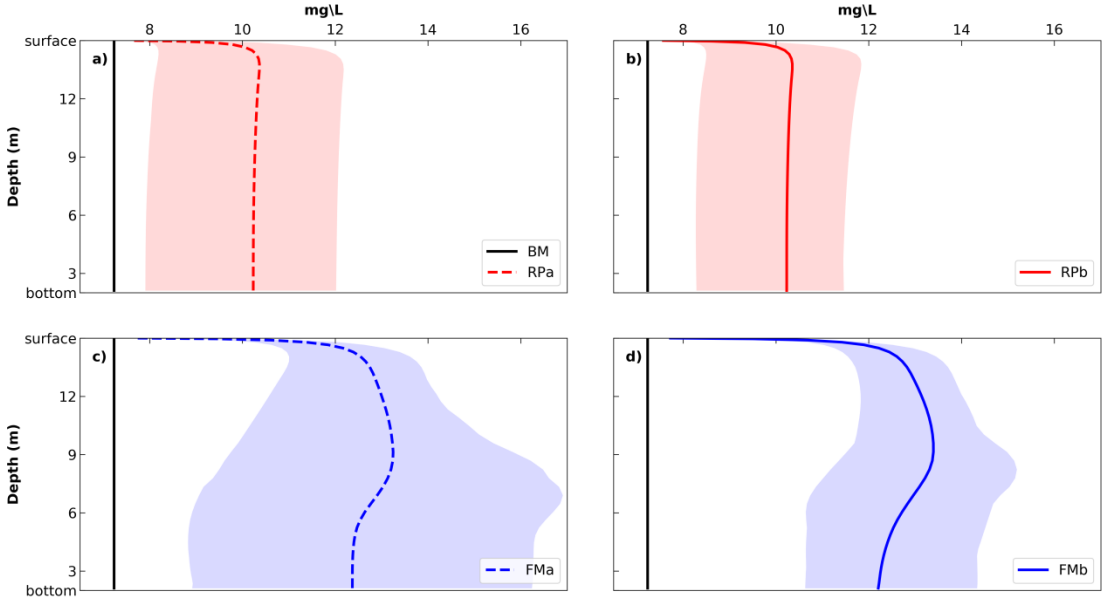

Figure 4.8 - Time-averaged DO in the middle of the domain for two regions shown in Fig. 4.1 for RP (a and b) and FM (c and d).

The alongshore depth and time-averaged values for DO were calculated using minima and maxima (Fig. 4.9; also see Fig. 4.1). The kelp forest region is plotted in green to illustrate where the peak of depth-averaged DO falls relative to kelp presence. For both simulations, the first kilometer of the domain is close to the BM scenario, as expected. Although both RP and FM scenarios were forced with the exact shape of R_{kelp} and NPP_{kelp}, they showed different maximum depth-averaged DO, and the maximum values found were also in different locations along the sliced area. The FM shape corresponds better with how the DO production would behave in a kelp forest area. For example, DO is expected to have a more significant concentration around the center of a patch due to the attenuation of currents as they go through a high-density kelp forest (elevated vegetation-induced drag) (Gaylord *et al.* 2007), resulting in a higher residence time compared to regions near the edge of the kelp forests, resulting in an increase of DO and pH. The DO variability for the RP scenario (Fig. 4.9a) ranged from 7.2 mg/L to 11 mg/L, where the maximum variability was found between 5.5 and 8.5 km. In the FM scenario (Fig. 4.9b) DO varied between approximately 7mg/L to 14 mg/L in agreement with Gaylord *et al.* (2007).

Interestingly, the highest concentration is between 5-5.5 km in patch a. As the alongshore current goes through and reaches fragmented parts, the DO concentration decreases significantly due to increased advection. The lowest DO within the kelp forest is also where a significant channel is found and where there is an increase in cross-shore and alongshore velocities (Fagundes *et al. in preparation)* due to flow ducting around kelp patches (Valle-Levinson *et al.* 2022). There is also a rapid increase in DO concentration after this channel in patch **b**.

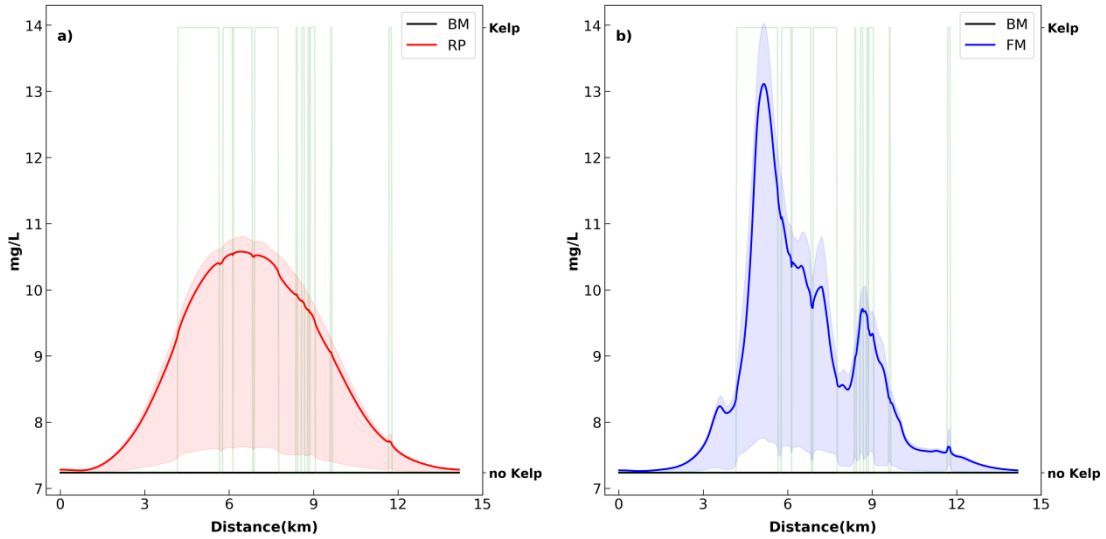

Figure 4.9 - Depth-averaged DO for RP (a) and FM (b) at 1.5 km alongshore the model domain. Black line represents the Depth-averaged DO for BM. Green lines represent the kelp distribution for that region.

Fig. 4.10 shows distribution of the volume difference between BM and FM/RP and hourly volume of DO in the kelp environment for the 6-week period analyzed. I employed ANOVA (Analysis of Variance) to analyze the effects of the *canopy* module developed by Fagundes *et al.* (*in preparation*) when coupled with the DO model developed in this chapter. The ANOVA analysis produced a p-value<0.001. Since the p-value was less than the predetermined significant value (α=0.95), I can reject the null hypothesis and concluded that there were statistically significant differences when *canopy* module is in the model, this can also be seen by comparing Δ(FM-BM) = 2.92 mg L^{-1} h^{-1} and Δ(RP-BM) = 2.28 mg L^{-1} h^{-1} (Fig. 4.10-c). Fig. 4.10c shows an almost 2-fold higher range of DO volume going through the kelp forest region for RP (~1.2 mg L^{-1} h^{-1}) than for FM (~0.7 mg L^{-1} h^{-1}). The rate of DO change shows that FM is 2-fold higher compared to what Low *et al.* (2021) found for Punta Prieta-MX. I assume that this difference could be caused by two factors: a) I am calculating variability for the entire kelp forest area while they

used only one point; b) other physical and biological factors were not include in the model. When kelp hydrodynamics are accounted for in the biogeochemical model the variability decreases by 1/2 which can be important when daily variability creates refuges for organisms from climate change (Woodson *et al* 2018).

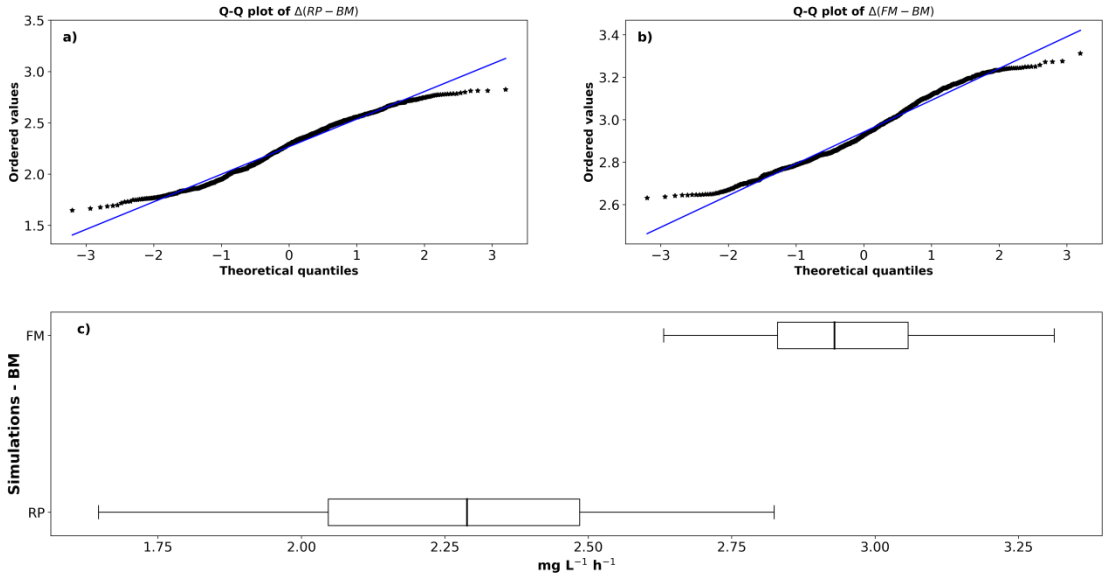

Figure 4.10 - Kelp forest volume variability per hour for FM and RP minus the BM.

The six weeks used for calculating DIC_{sim} did not show a strong gradient for RP, but a strong gradient towards the middle of the domain for both patches in the FM simulation (Fig. 4.11). The DIC_{sim} calculated for RP patches varied from 1945±35 μmol kg^{-1} for a slice in patch **a** and 1957±34 μmol kg^{-1} for the slice in patch **b**. The lowest DIC_{sim} concentration (approximately 1915 μmol kg^{-1}) for Fig. 10a was near the end of the patch and close to the surface. The reason that the minimum value is not located in the center of the patch is that this patch contains fragmentation. For patch **b** (Fig. 14.11b), the region with the lowest DIC_{sim} concentration (~ 1925 μmol kg^{-1}) is located near the middle of the domain. This pattern was expected since the patch in region **b** is continuous, meaning no fragmentation.

For the regions in the Full Model (FM) (Fig. 4.11c-d), the mean low DIC_{sim} concentration is in the middle of the domain. Both regions show the lowest DIC_{sim} concentration right below the canopy region. These low concentrations could result from the depth being a transition zone between high and low turbulence (Fagundes *et al. in preparation*). For the fragmented patch (Fig. 4.11c), low DIC_{sim} spreads out in the first 3m to the surface for almost 1 km in line with the current direction. The continuous patch (Fig. 4.11d) does not show the same pattern. Instead, it shows a gradient towards the middle of the domain (between 8.5-9km), where it reaches the lowest DIC_{sim} values; this demonstrates that continuous patches can decrease the concentration of DIC_{sim} by almost 88% compared to outside regions. A constant patch can have a broader area of low DIC_{sim} at the bottom compared to fragmented patches, which can help shelter organisms against acidification. Values for DIC, when compared for a similar depth region in the high-wave kelp forest site in Traiger *et al.* (2022), show that patch **b** for FM simulation has the lowest difference, 6 µmol kg^{-1} while patch **b** for RP simulation was the worst (36 µmol kg^{-1}). The DIC calculated changes for the low-wave kelp forest site. Patch **b** for RP shows the best scenario, 3 µmol kg^{-1}, and patch **a** for FM had the most significant difference compared with the study by Traiger *et al.* (2022).

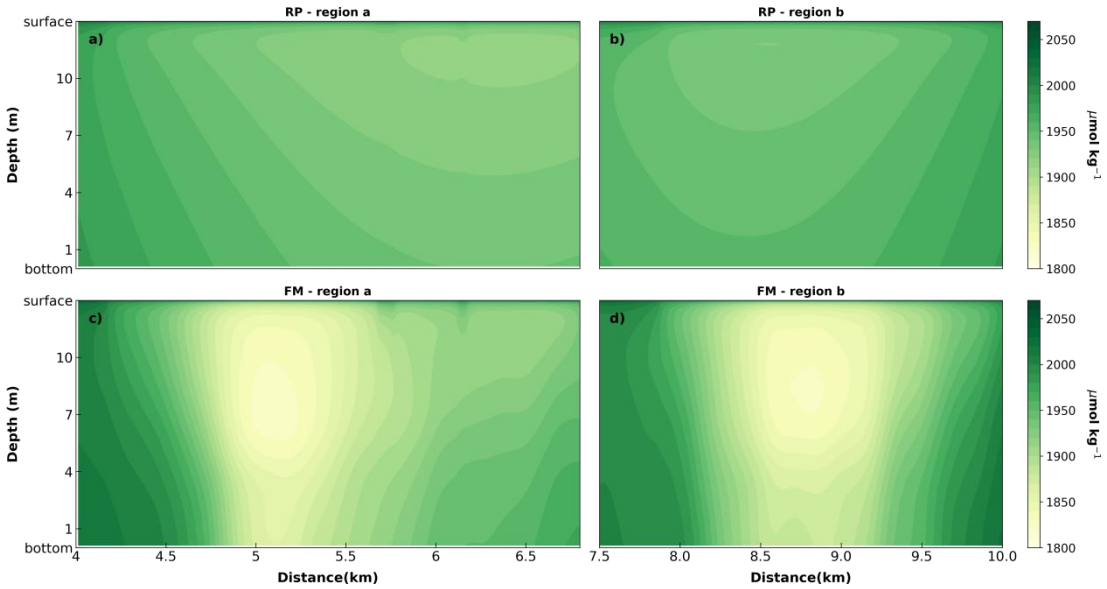

Figure 4.11 - DIC_{sim} calculated for regions a and b shown in Fig. 4.1 without kelp hydrodynamics (a and b) and with kelp hydrodynamics (c and d).

Overall TA_{sim} calculated (Fig. 4.12) followed the same patterns as DIC_{sim}. TA_{sim} showed a mean value equal to 2314 ± 20 μmol kg^{-1}; the lowest temporal mean value is found around the canopy between 5.5 - 7 km (Fig. 4.12a). The lowest TA_{sim} values are in the last 2 m from the surface, the region has a mean value of 2320 ± 20 μmol kg^{-1}. The region is similar to DIC_{sim} (Fig. 4.11a) because TA is directly related to DIC_{org}. However, some differences could be related to AOU^0_{BM} being higher than AOU_{RP}. For the slice in patch **b**, the lowest region is confined around the middle of the domain but also not as low as in region **a**. The depth gradient in Figs. 4.12a-b resembles the depth gradient calculated in Fig. 10a-b; however, I speculate that AOU could be the main factor controlling TA_{sim}. The same pattern is found for the lowest TA_{sim} in the same regions from the FM simulation (Figs. 4.12c-d). One big difference compared to DIC_{sim} is that the lowest TA_{sim} is shifted towards the canopy region**,** while for DIC_{sim}**,** the region is below the canopy. The mean TA is approximately 2305 ± 30 μmol kg^{-1} (Fig. 4.12c); higher TA is present in bottom

regions for the fragmented patch. A weaker along-shore gradient is present around the surface region for patch **a**. For patch **b** (Fig. 4.12d), the lowest TA_{sim} region is shifted more towards the surface. Higher TA_{sim} regions are located on the edges of the continuous patch for approximately 500 m near the bottom. On the other hand, the fragmented patch **a** (Fig. 4.121c) shows that for the continuous region (between 4 - 4.5km), the same pattern of high TA_{sim} is observed. However, there is an intrusion of higher TA_{sim} on the fragmented side (between 5.5 - 7km) near the bottom.

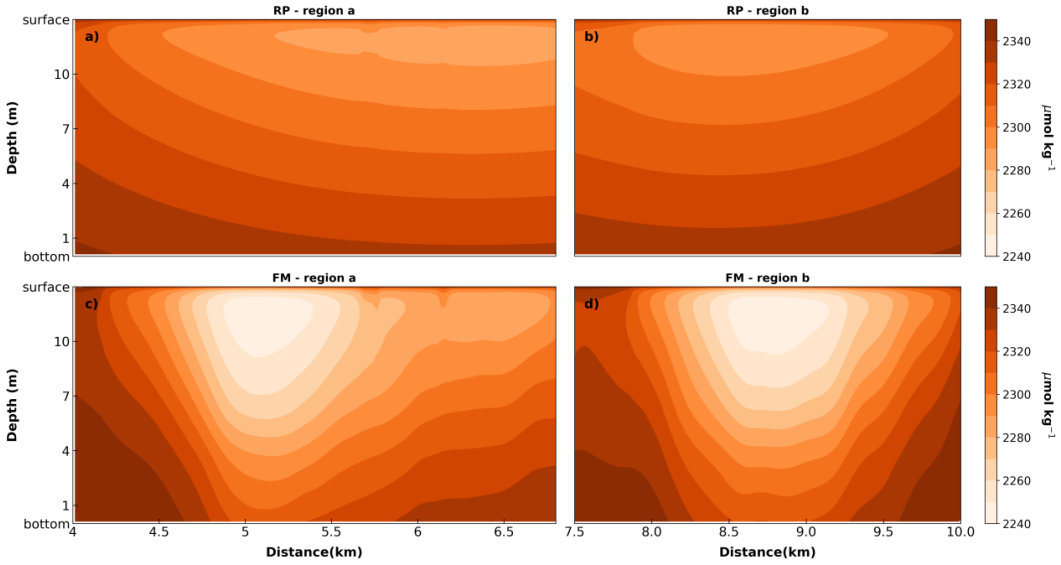

Figure 4.12 - TA_{sim} calculated for regions a and b shown in Fig. 4.1 without kelp hydrodynamics (a and b) and with kelp hydrodynamics (c and d).

The pH results of this simulation were calculated using the offline approach done by Chen *et al.* (2017) and modified for this study to understand the patterns of pH throughout fragmented and continuous patches of kelp between two different simulations (Fig. 4.13). The highest pH is at the same depth, near the bottom, around 6-6.5 km for region **a** and about 8-8.5 km for region **b**. Figs. 4.13c-d followed about the same patterns as DIC_{sim} (Fig. 4.11c-d) and TA_{sim} (Fig. 4.12c-d). Figures 4.13c and d show an along-shore gradient in pH going from around 8.12 to

8.35 for region **a** and 8.12 to 8.30 for region **b**. The highest values are found between 4-7 m and the last meter from the surface near the center of region **a.** These two regions are also observed for patch **b**; however, they are not as clear. For patch **a**, the fragmentation increases the region with a pH equal to 8.25 further, while for patch **b,** the same pH covers a much smaller region. The increase in the size of the increased pH region could indicate that even when kelp is fragmented, the pH could still be high agreeing with Murie *et al.* (2020).

The temporal mean pH calculated is similar to the max pH (8.2-8.35) found in the literature for kelp forest regions (Hofmann *et al.* 2011; Britton *et al.* 2016; Koweek *et al.* 2017). For the patches in the RP simulation (Figs. 4.13a-b), pH is high (~8.20-8.25) and almost constant throughout both patches. Although I observed that the mean pH for both simulations was .10 units above the mean value found by Hirsh *et al.* (2020) at 6.1 m from the bottom, the FM simulations reached the closest variability of 0.06 and 0.07 for patches **a** and **b**, respectively, compared to 0.09 (Hirsh *et al.*2020). The surface value, however, showed only a difference of 0.05 units for FM when compared with the same study. The mean pH at approximately 11.8 m depth for both simulations and patches closely agrees with Traiger *et al.* (2022) for high-wave and low-wave kelp forest sites. The difference ranged from 0.06 ± 0.02 units for RP patch **b** and 0.02 ± 0.019 units for FM patch **a**.

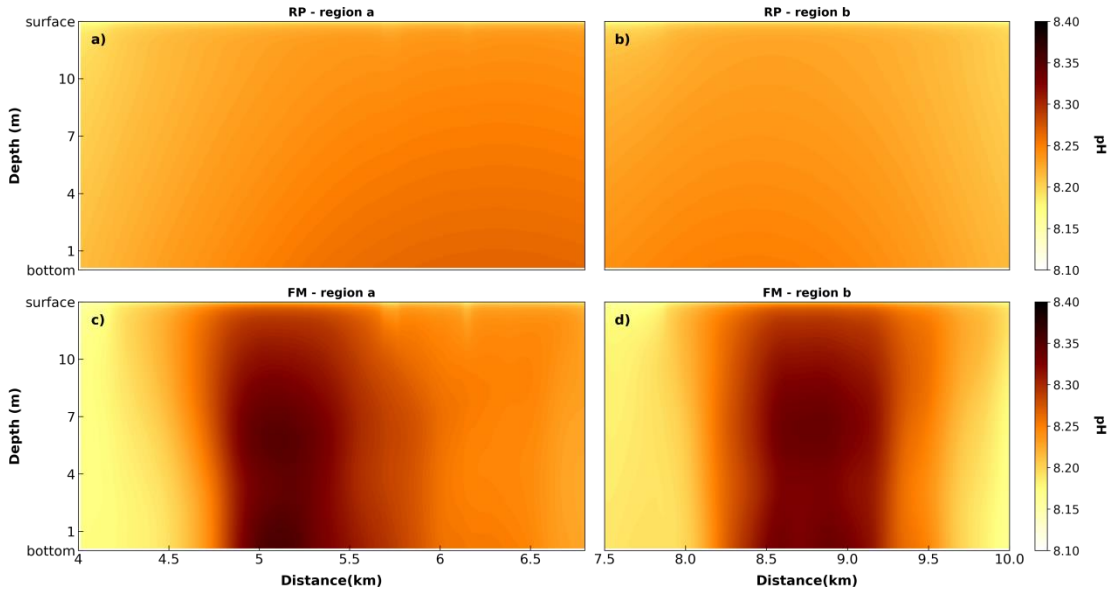

Figure 4.13- pH_{sim} calculated for regions a and b shown in Fig. 4.1 without kelp hydrodynamics (a and b) and with kelp hydrodynamics (c and d).

Differences between pH_{calc} and monthly global model outputs for three regions in the water column for patch **a** (Table 4.5) and patch **b** (Table 4.6) show similar patterns. Surface pH difference showed the slightest change, while the bottom region exhibited the most considerable variability for both simulations and patches (Tables 4.5-4.6). Pfister *et al.* (2019) found a difference in pH of 0.024 from 1 m to the surface between the inside and outside of the kelp bed. From the results calculated for the last meter to the surface, patch **a** from the FM simulation showed the best result and is comparable with what they found. Likewise, the surface value calculated for patch **a** in the simulation is similar. However, the mean and variance differ significantly from the FM simulation (Table 4.5). Both patches indicated that the means and variances for FM and RP significantly differ throughout the water column.

Table 4.5 - Difference between pH_{calc} and Global model for patch a divided into surface, bottom, and total water column. Non-parametric tests are calculated between simulations.

Simulation	pH region	Inside vs Global model median difference	Mann-Whitney U test (alternative=two-sided)	Fligner's test (center=median)	number of grid points
FM	**Surface**	0.024±0.005	p-value <0.05	p-value <0.05	$8x10^5$
RP		0.023±0.004			$8x10^5$
FM	**Bottom**	0.028±0.008	p-value < 0.05	p-value < 0.05	$47x10^5$
RP		0.029±0.004			$47x10^5$
FM	**Total**	0.028±0.007	p-value < 0.05	p-value <0.05	$46x10^6$
RP		0.027±0.005			$46x10^6$

4.4.1 Nearshore biogeochemistry impacts due to climate change

The temporal averaged DO ratios show the strong effect of kelp forests on the low DO scenario used here (Fig. 4.14). Overall, all simulations showed an increase in DO when compared against the SSP585 scenario. Interestingly, by increasing the model's resolution and adding tides, the DO model was almost 6% higher than the GCM simulation. Regions **a** and **b** for the RP scenario showed that if a simulation added only R_{kelp} and NPP_{kelp} to understand the impact in climate change scenarios, there would be roughly 2-fold more DO production within 1 meter below the surface for fragmented kelp forest and 2.1-fold more DO production for a non-fragmented kelp forest region at the same depth. However, when high drag environment is present, this maximum difference in DO for the environment jumps to 2.9 and 3.15-fold for areas **a** and **b**, respectively. The gradient between the surface and bottom is stronger for FM simulation. This peak within the

first meter could be due to the high TKE caused due to the presence of a canopy in the model (Fagundes *et al. in preparation*).

Table 4.6 - Difference between pH_{calc} and Global model for patch b divided into surface, bottom, and total water column. Non-parametric tests are calculated between simulations.

Simulation	pH region	Inside vs Global model median difference	Mann-Whitney U test (alternative=two-sided)	Fligner's test (center=median)	number of grid points
FM	**Surface**	0.022±0.006	p < 0.001	p < 0.001	$8.1x10^5$
RP		0.021±0.004			$8.1x10^5$
FM	**Bottom**	0.025±0.009	p < 0.001	p < 0.001	$46.5x10^5$
RP		0.027±0.004			$46.5x10^5$
FM	**Total**	0.025±0.008	p <0.001	p < 0.001	$46.5x10^6$
RP		0.025±0.004			$46.5x10^6$

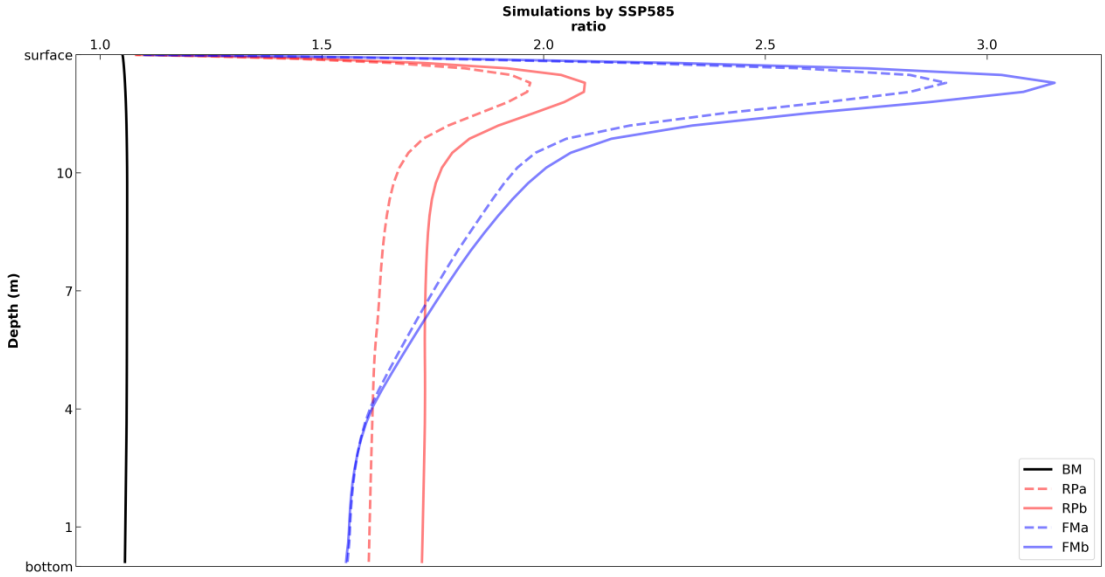

Figure 4.14 - Temporal averaged DO ratio profiles between PGW simulations and SSP585 scenario. BM simulation DO without kelp forests, RP simulation has *canopy* module off, and FM simulation has *canopy* module on.

The pH difference between pH_{sims} and climatogical pH for the southern California region (pH_{ref}) showed a projected pH for kelp forests higher than the SSP585 (Fig. 4.15), indicating that kelp forests could help mitigate climate change (Britton *et al.* 2016). In addition, the Kruskal-Wallis H-test with a Post hoc pairwise test for multiple comparisons of mean rank sums (Conover´s test) was used to understand if the mean pH between Global, RP, and FM scenarios were the same. All the scenarios for both months showed that the means were statistically different (p-values <0.01). The 30 years climatology for both months showed a similar mean, 7.72±0.17 for June and 7.71±0.17. June had a higher mean pH difference for the total water column and 1 meter above the bottom than July for both simulations.

Furthermore, the RP scenario showed the same mean pH for both regions with no large variability difference between fragmented and non-fragmented kelp forests (Fig. 4.15a). The pH difference between FM and pH_{ref} remained relatively constant in both fragmented and non-fragmented kelp forests. In contrast, the RP scenario showed more variation in June (Fig. 4.15a). The lower variability could be explained by the net slowdown of the currents in the water column when entering the high drag environment caused by the kelp. For July, the minimum values for both simulations reached close to the mean value for the SSP585 scenario (Fig. 4.15d). The spread for the FM simulation increased for July (Fig. 4.15d) compared to June for the total water column. In Fig. 14b, the pH range for the RP scenario at 1 meter above the bottom is similar to the pH variance for the entire water column in Fig. 14a. The spread for the FM scenario decreased in both fragmented and non-fragmented kelp forests, as shown in Fig. 14b. In July, the mean pH for both simulations decreased, as seen in Fig. 4.15e.

The pH is different between months of June and July for the FM scenario. The fragmented kelp forest had a higher mean pH than the non-fragmented region. Still, the non-fragmented kelp

forests had a lower minimum at the first meter above the bottom for the FM. For the canopy region, fragmented kelp forests for FM had similar mean pH compared to both RP regions (Fig. 4.15c). The FM non-fragmented kelp forest region had the highest mean pH than the other regions and simulations. There is no difference in pH between regions for RP. The most significant results are shown in Fig. 4.15f. The variability for FM patches for the canopy region is more significant than the RP. At the same time, all had a minimum pH close to the mean global pH. The dispersion for RP kept closely the same compared to the first meter above the bottom and in the whole water column. Similarly, the pH for FM regions in July showed the most significant spread among all the regions in the water column. The mean pHs are higher, and the maximum pH found for both FM patches is comparable with RP non-fragmented patch in Fig. 4.15a. I am unsure why there is such a big jump for the canopy region in July, which needs further investigation.

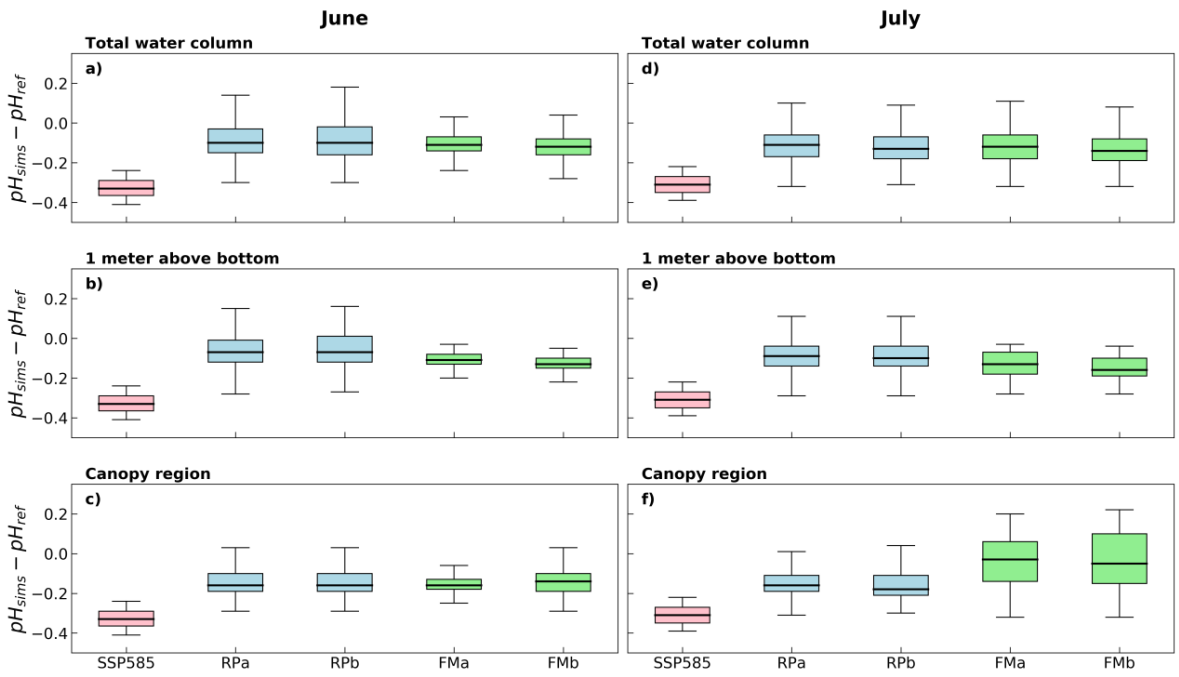

Figure 4.15 - Difference pH between historical southern California pH (pH_{ref}) and SSP585, RP, and FM simulations for total water column (a,d), 1 meter above the bottom (b,e), and 1 meter below the surface (c,f).

4.5 DISCUSSION

The Coupled Ocean-Atmosphere-Wave-Sediment transport (*COAWST*) modeling system has been successfully applied to characterize wave-flow-seagrass interactions (Beudin *et al.* 2016). The new module described in this paper expands *COAWST*'s capability to simulate flow-vegetation-biogeochemistry interactions for canopied vegetation, specifically kelp forests (Fagundes *et al. in preparation*). The combination of this new module and offline pH calculation captures the tidally-driven fluctuations of DO in the presence of kelp forests and provides good results for understanding pH via DO dynamics. Some assumptions were made to control the experiment. For example, constant kelp respiration, constant kelp photosynthesis, fixed plant density, and no winds or atmospheric forcings were imposed. In spite of these assumptions, the model well reproduced biogeochemical variability observed in kelp forests (Traiger *et al.* 2022).

The influence of kelp forests on the modification of local biogeochemistry has been studied in different regions of the World (Krause-Jensen *et al.* 2016; Filbee-Dexter & Wernberg, 2020; Hirsh *et al.* 2020; Kekuewa *et al.* 2022). However, all of these studies, while showing the importance of kelp forests in ameliorating climate change effects (Krause-Jensen *et al.* 2016), are generally located in a few points, which give a limited understanding of kelp hydrodynamics and kelp forest CO_2 system chemistry (Koweek *et al.* 2017). The kelp forest CO_2 system chemistry is highly complex, and therefore, several factors of variability can affect the measurements, such as kelp biomass (Koweek *et al.* 2017), kelp type (Britton *et al.* 2016), fragmentation (Krause-Jensen *et al.* 2016), bathymetry (Leary *et al.* 2017), internal waves (McPhee-Shaw *et al.* 2007), and currents (Monismith *et al.* 2022). The development of this model using the *canopy* module developed by Fagundes *et al.* (*in preparation*) to simulate kelp forests and kelp canopies enables novel views of kelp forest biogeochemistry and highlights the importance of kelp-flow interactions

in determining observed variability. Some caveats should be mentioned for this biogeochemistry module, such as that R_{kelp} and NPP_{kelp} are forced daily and constant throughout the three months of model simulation, kelp biomass is invariant, biogeochemistry variables represent the closest overall region of the study domain, phytoplankton is not present which can add to the NPP production in the domain. Even so, the model does well represent natural variability in DO, pH, and carbon constituents.

The FM simulation (Fig. 4.7c) presented here shows good agreement for the semi-diurnal and diurnal DO variability at PP for the 2015 period when kelp was the highest (Monismith *et al.* 2022). This variability was confirmed by using FFT (Fig. 4.7c) and t-tide (table 4.4) at 12m. The only difference between FM and RP simulations was the presence of a high-drag environment represented by the *canopy*. The *canopy* may have damped the diurnal signal of $Resp_{kelp}$ plus NPP_{kelp} in the FM simulation, resulting in frequencies similar to observed.

I do not expect to simulate the same DO values observed for PP or any other region on the West Coast of the US. I did not force the model with the DO dataset for the PP region since only bottom values are available. However, surface and subsurface values range between 8 to 12 mg/L along the West Coast (Murie & Bourdeau, 2020; Traiger *et al.* 2022), which agrees with FM simulation (Fig. 7c-d). Frieder *et al.* (2012) found values for DO around 9.4 mg/L at 7 m below the surface in 20 m water depth during winter. However, in wintertime, kelp biomass is the lowest on the CCS (Monismith *et al.* 2022), which could explain the difference between FM simulation and their dataset. While not the same region, but controlled by tides, Krause-Jensen *et al.* (2016) measured DO variability going from 12 mg/L to 18 mg/L at 1 meter above the bottom. In PP during the Summer of 2018, Low *et al.* (2021) found mean DO values close to 10 mg/L at the station outside the kelp forest domain. These values represent the low end of FM simulation (Fig. 4.8c-d)

for the time-averaged DO for patches **a** and **b**. The RP simulation (Fig. 4.8a-b) has a mean time-averaged DO close to 10 mg/L for both patches, close to what Low *et al.* (2021) observed outside the kelp forest region. Adjusting our model to account for diurnal variability in photosynthesis may also bring our results closer to some of these higher observed values, especially at the surface where DO is often super-saturated during the day (Koweek *et al.* 2017).

In this study, a method proposed by Chen *et al.* (2017) was used to calculate TA and DIC in the Sea of Japan, which was effective in kelp forest regions. The DIC estimates were comparable to Traiger *et al.* (2022) reported in Monterey Bay, CA. However, it is challenging to compare pH values directly due to variability within the same site but in different years (Hirsh *et al.* 2020 vs. Traiger *et al.* 2022), measurement differences, or estimation methods used by other studies. Based on the validated pH estimates, the FM model represents the closest approximation to observed results and better defines the change in chemistry at the middle of a kelp domain due to high drag causing water to stagnate in the middle of a patch, resulting in a modification of the chemistry within the kelp environment. Based on this study, the increase in pH region could indicate that even when kelp is fragmented, the pH could still be high agreeing with Murie *et al.* (2020).

A PGW approach was made to understand the impact of the new DO model proposed with kelp hydrodynamics on climate change (Fig. 4.14-4.15). The DO simulated for the future showed to increase in the canopy region. The increase in DO was more significant in the FM model than the RP model. As a result, the turbulent kinetic energy generated by the kelp hydrodynamics distribution the higher DO production in the canopy into the interior water column. The projected pH is expected to drop between 0.3-0.4 units by the end of the 21st century (Doney *et al.* 2009) (see SSP585 in Fig. 4.15). The mean values for both RP and FM simulations showed that climate change would still affect kelp forest domains. However, pH values would be close to the pH_{ref}

values, providing significant potential climate refuge. From the FM model, the mean pH difference at the bottom is smaller than found in the canopy.

4.6 CONCLUSIONS

The combination of *canopy* model that simulates TKE in kelp domain and new DO model combined with an offline pH estimation represents well the dynamics and variability of the biogeochemistry in kelp forests. This DO in kelp model along with this method to calculate pH opens the opportunity to study biogeochemical variability in kelp forest including how climate change can change the DO and pH dynamics in these ecologically important regions. While RP and FM simulations show good agreement with observational studies, FM model gives the best variability when compared against observational studies.

As shown previously, the combination of kelp hydrodynamics and DO kelp model gave the best results for DO and pH when compared against *in situ* datasets and the literature. Furthermore, kelp forests have been suggested as a habitat that can serve as refugia against acidification and hypoxia in the future (Hofmann *et al.* 2011; Frieder *et al.*2012; Britton *et al.* 2016; Koweek *et al.* 2017; Murie *et al.* 2020). The PGW simulation was done to test the new DO kelp forest model and understand the future impact on the local ecosystem (Fig. 4.14). As studies previously pointed out and our model showed, kelp forests can mitigate ocean acidification and hypoxia even when fragmented (Murie *et al.* 2020; e.g., Fig.4.1 - region **a**). Furthermore, when comparing DO between fragmented and non-fragmented patches for FM, I observed they are similar at the bottom, and the non-fragmented kelp forest domain produces more DO at the canopy region. However, the pH calculation showed that fragmentation could benefit benthic organisms more than the non-fragmented kelp forest domain in the future. Therefore, future studies utilizing

the FM model should be done to understand the impact of fragmentation in mixing and biogeochemistry in kelp forest domains in the present and future scenarios.

CHAPTER 5

EFFECTS OF KELP FOREST FRAGMENTATION ON NEARSHORE PROCESSES[3]

[3] Fagundes, Matheus and Woodson, C. B. To be submitted to *Limnology & Oceanography journal.*

ABSTRACT

Fragmentation is one of the main effects of climate change on coastal vegetation ecosystems. As a result, local physics and chemistry changes happen, and effects on the global carbon cycle are expected. Most studies about fragmentation in kelp forests have focused on the ecology of the organisms. On the other hand, studies have been done to understand the change in physics and biogeochemistry are only for a small region of the entire kelp forest domain. This paper focused on understanding how different levels of fragmentation can affect spatial and temporal aspects of the physics and chemistry of an idealized region. Using the Coupled Ocean-Atmosphere-Wave-Sediment transport (*COAWST*) coupled with the *canopy* module and the DO model developed previously. I was able to show changes in the ratio of TKE due to the increase in fragmentation, an increase in flow ducting in simulations with fewer patches, and changes in stratification. For biogeochemistry, all scenarios showed a decrease in DO production compared to the non-fragmented scenario at the bottom and an increase in DO production within the canopy region. I also showed that pH would be relatively higher in the inner area of a domain if the fragmentation were weak. This idealized study shows the capabilities of these two new models and the potential for studying present and future impacts on the local scale.

5.1 INTRODUCTION

One of the factors that can lead to change in biodiversity, benthic community composition, ecosystem function, and biogeochemistry is habitat fragmentation (Bodkin, 1988; Norderhaug *et al.* 2020). Habitat fragmentation process can be caused by an increase in stress (Bryan-Brown *et al.* 2020; Murie & Bourdeau, 2020) that can be either natural (Monismith *et al.* 2022) or

anthropogenic (Tegner *et al.* 1995). For example, fragmentation has increased in mangrove and kelp forests due to climate change (Bryan-Brown *et al.* 2020; Murie & Bourdeau, 2020).

Fragmentation is a process that can affect local chemistry (Murie & Bourdeau, 2020) and biodiversity (Fahrig, 2003) on land and in the water. These impacts occur due to the three-dimensional variability in the flow (Poëtte *et al.* 2017), generating turbulence in the interior, an increase in the flow on the edges (Dupont & Brunet, 2008), and a change in bulk drag (Monismisth *et al.* 2022), and stratification (Hirsh *et al.* 2020) in fragmented regions. For example, in kelp forests, fragmentation was shown to generate flow ducting and headland upwelling (Valle-Levinson *et al.* 2022), which could impact larval recruitment (Deza & Anderson, 2010) and biogeochemistry (Murie & Bourdeau, 2020). However, these fragmentation studies have been done on point-source locations and extrapolated for the entire kelp forest domain.

Ecological disruption in coastal regions is anticipated to be more frequent and severe in the future (Norderhaug *et al.* 2020). One reason for increased disturbances in these environments is the increased frequency of extreme events (Dayton, 1985). For instance, fragmentation in kelp forests can be worsened due increases in hurricanes (Filbee-Dexter & Scheibling, 2012) and more frequent marine heatwaves (Cavanaugh *et al.* 2019).

While the majority of these studies point out the negative change of fragmentation in kelp forests, Murie & Bourdeau (2020) showed that fragmented kelp forests can still modify the biogeochemistry locale. In Chapter 4, I showed that Dissolved Oxygen (DO) and pH in both fragmented kelp and non-fragmented kelp forests would still be able to increase DO and pH in nearshore regions for the SSP585 global climate scenario. While my results agreed with the the suggestsions of Murie & Bourdeau (2020), my results focused on two different patches in different regions of the domain and fragmentation level was not controlled in the simulation.

To-date only my chapter 4 has used a complex model to understand biogeochemistry in the water column for a kelp forest domain. Although, my previous chapter showed almost no difference between a fragmented and non-fragmented kelp forest domain, it did not include a broad overview on the impact of fragmentation in the physics and biogeochemistry. As a result, this chapter comes with the intention to bring both modules previously described to understand the physics and biogeochemistry in three different regions (canopy, bottom, and middle of the water column) of fragmentation scenarios in a kelp domain.

5.2 THEORY

5.2.1 Kelp Hydrodynamics

The modified vegetation module (henceforth *canopy*) was activated (developed in Chapter 3). I decided to use the full canopy model (eq. 1):

$$\begin{cases} pt = pd = 0.3m & if\ h \leq H - 1m \\ pt = pd = 2.3h - 27.3 & if\ h > H - 1m \end{cases} \quad \textbf{(1)}$$

5.2.2 Kelp Dissolved Oxygen model

The model used for understanding DO dynamics in fragmented kelp forests is briefly described below. This model simulates how physical processes modulate DO in kelp forests regions (eq. 2). The model uses a 3D kelp respiration rate (mmol/m^3/day) and 3D NPP kelp rate that can be forced as input or daily as a forcing.

$$\frac{\partial DO}{\partial t} + (\frac{u\partial}{\partial x} + \frac{v\partial}{\partial y} + \frac{w\partial}{\partial z})DO = \frac{\partial}{\partial z}K_z\frac{\partial DO}{\partial z} - R_{kelp} + NPP_{kelp} \quad \textbf{(2)}$$

Where $\frac{\partial DO}{\partial t}$ is the time rate of change of DO, the second term is the advection of DO, the terms on the right side are the vertical diffusion, nocturnal respiration rate of kelp forests (R_{kelp}), and a new term for the net photosynthetic rate of kelp forests (NPP_{kelp}), respectively.

5.2.3 Empirical calculations of Dissolved Inorganic Carbon (DIC) and Total Alkalinity (TA)

I utilized an offline calculation for pH using the method proposed by Chen *et al.* (2017) to calculate the difference between a reduced physics model (RP, *canopy* off) and a full model (FM, *canopy* on) simulations. A better description of the simulations for RP and FM can be found in the Scenarios section below. This method used Apparent Oxygen Utilization (AOU) to calculate DIC and TA. Assuming that the Redfield ratio is the same in the kelp forest domain as it is in the open ocean, yields:

$$(CH_2O)_{106}(NH_3)_{16}H_3PO_4 + 138O_2 \rightarrow 106CO_2 + 122H_2O + 17H^+ + 16NO_3^- + H_2PO_4^- \quad \textbf{(2)}$$

for the decomposition of organic matter. DIC can be described as:

$$DIC = DIC^0 + \Delta \sum CO_2 + \Delta DIC_{org} + \Delta DIC_{ic} \quad \textbf{(3)}$$

Where excess $\Delta \sum CO_2$ is considered null given the small region of the model simulation, leading to:

$$DIC = DIC^0 + \Delta DIC_{org} + \Delta DIC_{ic}$$

where DIC^0 is the monthly mean DIC taken from a global climate model for the period simulated, DIC_{org} is calculated using eq. 2, and using the relationship between DIC_{org} and DIC_{ic} found by Chen *et al.* (1996), yields:

$$\Delta DIC_{org} = (106/138)\Delta AOU_{model}$$

$$\Delta DIC_{ic} = R_{ic:org}(z) * \Delta DIC_{org}$$

Where, $R_{ic:org}(z) = 0.212 + 0.0238z$ (Chen *et al.* 1996), after some manipulations DIC can be calculated as follows (eq. 4):

$$DIC = DIC^0 + (106/138) * (AOU - AOU^0) * (1 + R_{ic:org}) \quad \textbf{(4)}$$

And following the same approach, I can estimate TA (eq. 5), where TA^0 is the monthly mean TA from a global climate model for the period simulated, TA_{org} is found by the relationship between H^+ and O_2 in eq. 2, TA_{ic} production is 2-fold the production of DIC_{org}, thus:

$$\begin{gathered} TA = TA^0 + \Delta TA_{org} + \Delta TA_{ic} \\ \Delta TA_{org} = (-17/138)\Delta AOU \\ \Delta TA_{ic} = 2R_{ic:oc}(z) * \Delta DIC_{org} \end{gathered} \quad \textbf{(5)}$$

Finally yielding,

$$TA = TA^0 + ([AOU - AOU^0]/138) * (-17 + 212R_{ic:org}) \quad \textbf{(6)}$$

Converting Apparent Oxygen Utilization (AOU) from O_2 modeled:

$$\Delta AOU = AOU - AOU^0 \quad \textbf{(7)}$$

For this study, BM was considered AOU^0:

$$AOU_{model} = O_2sat - O_2model$$

$$AOU^0_{BM} = O_2sat(BM) - O_2(BM)$$

Where O_{2sat} is calculated using coefficients found by Benson & Krause (1984) and fitted by Garcia & Gordon (1992). The O_{2sat} equation present in GSW-python function is based on practical salinity and potential temperature referenced to the sea pressure. I used the same python package to convert the temperature of the model to potential temperature at sea level.

5.3 METHODS

5.3.1 Numerical Model Description

The model used in this study was the *Coupled Ocean-Atmosphere-Wave-Sediment-Transport model (COAWST V3.3*; Warner *et al.* 2008). The ocean component of *COAWST* is the *Regional Ocean Modeling System (ROMS)* (Haidvogel *et al.* 2008). ROMS is a 3-D, free-surface model, which solves the primitive equations using hydrostatic and Boussinesq approximations with topography-following sigma layers (Shchepetkin and McWilliams, 2005; Haidvogel *et al.* 2008). For the momentum equations, splines vertical advection and logarithmic bottom friction were selected to keep stability and better represent the environment, respectively. The model used the Mellor-Yamada level 2.5 turbulence closure scheme (MY-2.5). All boundaries (N, S, E, W) were open to allow along- and cross-shore flows. A periodic boundary condition was applied for free-surface, a Flather condition for 2D u- and v-momentum, and a Radiation-Nudging condition for 3D u- and v-momentum. The barotropic time-step was set at 10 s. Bottom roughness (z_{ob}) was 0.03 m and surface roughness (z_{os}) was 0.4 m with a no-slip condition along the bottom to provide a best fit for the no-kelp simulations to observed velocity profiles. The model had 40 sigma-layers splitting the 13 meters of water column with surface stretching (θ_s) = 1, bottom stretching (θ_b) = 2, and thermocline depth (Tcline) = 0. The domain was approximately 14 km long by 3 km wide with a grid size of 25 meters x 25 meters.

5.3.2 pH calculations

The pH calculations followed the same steps described in Chen *et al.* (2017) and modifications made in chapter 4. This method used Apparent Oxygen Utilization (AOU) to calculate DIC and TA. Three assumptions were made. The first one is that the Redfield ratio is the same inside and outside kelp forests. Secondly, that the DIC_{org} and DIC_{ig} follows the equation described by Chen *et al.* (1996). Lastly, excess $\Delta \sum CO_2$ is null for a small region like the one in study. Hourly pH_{sim} was calculated using CO_2 System Calculations Program (CO2SYS) (Pierrot, Lewis, & Wallace, 2006) python version (PyCO2SYS v1.8; Humphreys *et al.* 2022). Hourly TA_{sim}, DIC_{sim}, temperature, and salinity were used as parameters.

5.3.3 Forcings

5.3.3.1 Initial Patches

There is a total of 6 fragmentation scenarios (Fig. 5.1): 1 patch (Fig. 5.1a), 2 patches (Fig. 5.1b), 4 patches (Fig. 5.1c), 6 patches (Fig. 5.1d), 8 patches (Fig. 5.1e), and 10 patches (Fig. 5.1f). The curves were randomly generated by using Bezier curves and the total area for these curves calculated using shoelace formula. To keep the same number of plants as in Fig. 5.1a and a plant density equal to 1, the sum of total area for the other fragmentation scenarios could not exceed 50% of the total area in Fig. 5.1a. Scenarios Fig. 5.1a and Fig. 5.1c represent advanced fragmentation while Fig. 5.1f represents a scenario where fragmentation is only in the beginning. As a result, these scenarios could offer a broad and interesting aspect of fragmentation phases in a kelp forest region and how it could change physical and biogeochemistry aspects in this nearshore environment.

In Fig. 5.2, the darker green regions show the region selected to analyze DO and calculate pH for all patches. This approach was done to understand the inside of the domain which is the region with the slowest alongshore velocity (Jackson, 1977), and consequently, the longest residence time. I assumed that the inner area is large enough to still represent the impacts of fragmentation.

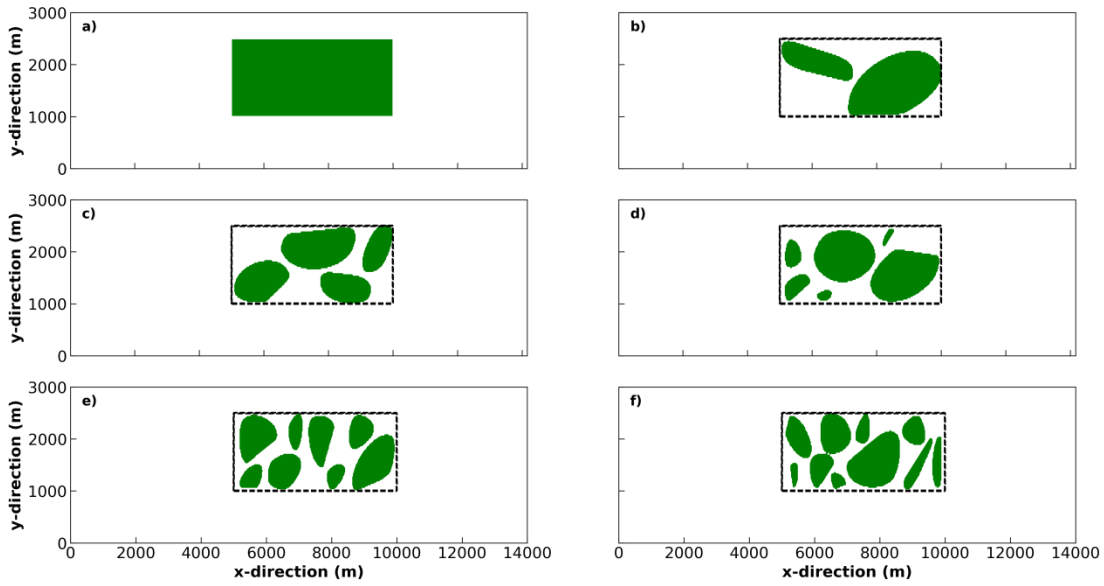

Figure 5.1 - Top-down view of fragmented domains representing approximately 50% of the total area shown in a).

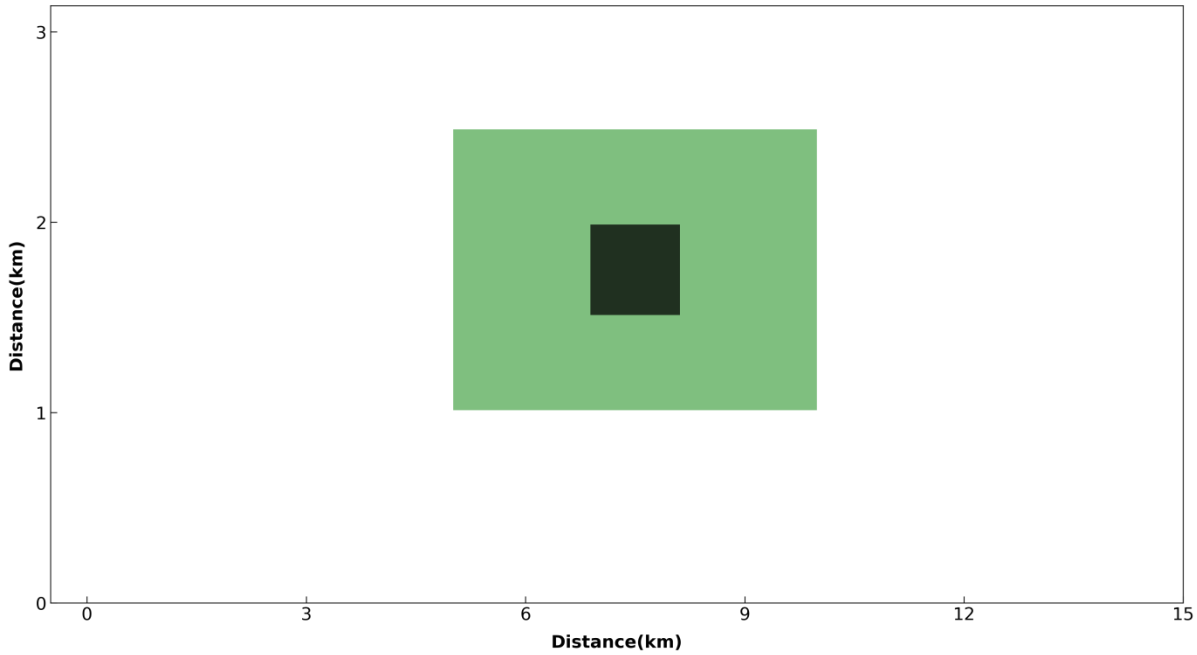

Figure 5.2 - Top-down view showing the center of possible climate change refugia and used for analysis of DO and pH.

5.3.3.2 Currents

The mooring at Punta Prieta for the Winter 2015 (henceforth adp15) period was chosen to force this simulation (see chapter 3 or Monismith *et al.* 2022). *In situ* current data was collected every 0.5 meter starting from 0.65 meters above the bottom to the surface (~14 m). The depth of the ADP data used for this simulation was from 2.65-12.65 meters from the bottom to remove errors in the first couple meters due to side-lobe interference (Monismith *et al.* 2022). Alongshore and cross-shore velocities are 10-minute profiles, rotated to the true shore.

5.3.3.3 Vegetation Parameters

The vegetation module is a standard component in *COAWST* (Beudin *et al.* 2017). This module receives *u* and *v* from *ROMS* and returns both the drag force (F_d) and vertical turbulent

mixing (Beudin *et al.* 2017). The vegetation module requires 4 parameters: plant height (m), plant density (plants/m^2), plant diameter (m), and plant thickness (m) (Table 3.1). The other settings are number of vegetation types, Young's modulus (10^7), vegetation mass density (1000.0), additional horizontal viscosity coefficient (0.0), and drag coefficient used was 0.35.

Table 5.1 - Vegetation module initial parameters.

	Plant height(m)	**Plant Density (plants/m^2)**	**Plant diameter (m)**	**Plant thickness (m)**	**Vegetation drag**
Canopy	13	0.9*	See equation 1	See equation 1	0.35

*(GAYLORD *et al.* 2007).

5.3.3.4 R_{kelp} and NPP_{kelp}

For these simulations, I applied the values measured by Gerard (1986) in the kelp forests (Table 5.2). The values were then interpolated to the depth of the idealized fragmented models and assigned only for the region where the kelp forest is present (see Fig. 5.3).

Table 5.2 - Respiration and Photosynthesis for Macrocystis pyrifera in mmol O_2 m^{-3} day^{-1}.

	Surface	**0.5 m**	**4 m**	**8 m**	**bottom**
Respiration	792.0	48.0	15.6	20.4	0.0
Photosynthesis	2952.0	240.0	120.0	43.2	0.0

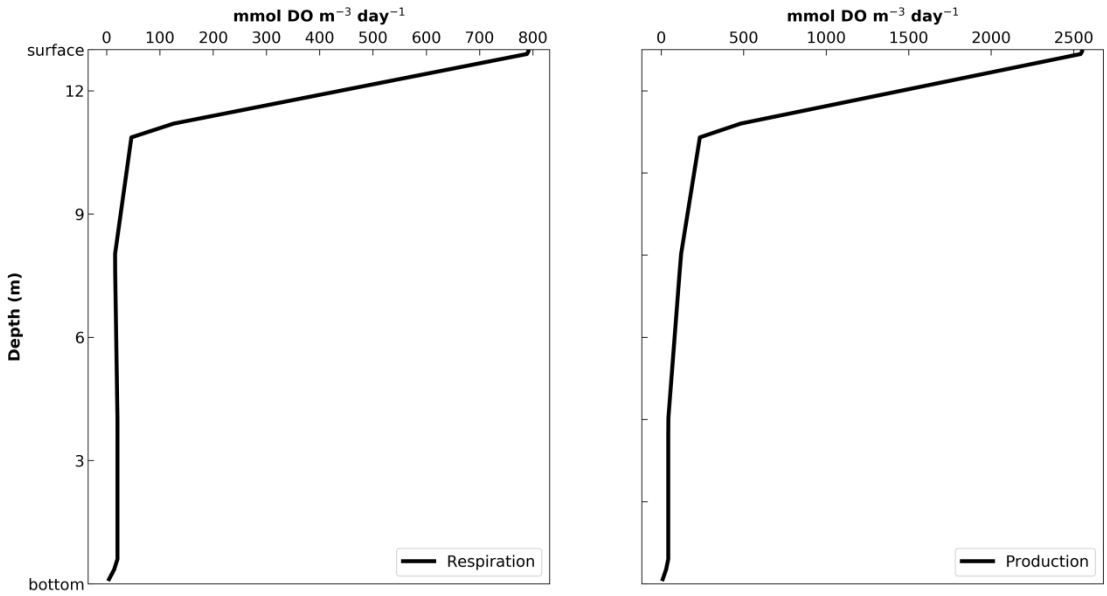

Figure 5.3 - Initial and Boundary conditions for Respiration and Production for kelp forest region.

5.3.3.5 Dissolved Oxygen

The DO used is from The Operational Mercator Ocean biogeochemical global analysis and forecast system (Von Schuckmann *et al.* 2018). This dataset provides a daily/monthly temporal resolution from 1993-present and a 1/4°x1/4° spatial resolution. The global biogeochemical output has 75 vertical levels and has seven variables available: chlorophyll (chl), dissolved oxygen (DO), nitrate (NO3), silicate (Si), iron (Fe), and net primary production (NPP). Daily DO was interpolated to 10-min input to match the velocities inputs. The model was forced on all the boundaries using Summer 2015 data; the same year as the observed currents used.

5.3.3.6 DIC^0, TA^0, and pH_{sim}

Historical Canadian Earth System Model version 5 (CanESM5) was selected (Swart *et al.* 2022) for this experiment. This historical global scenario uses NEMO 3.4.1 with 1° horizontal

resolution and 45 vertical levels, the biogeochemistry model is the Canadian Model of Ocean Carbon (CMOC) with NPZD ecosystem, and the output is monthly. For DIC^0 and TA^0, I considered a 30-year mean value for the months of May, June, and July. The mean of three nearest grid-points in latitude and longitude to the location of the model were used. pH_{out} for the analysis is from the Global Ocean Biogeochemistry Hindcast (Von Schuckmann *et al.* 2018), that covers 1993-2020, with a horizontal resolution is 0.25° x 0.25° and 75 levels in depth. I used the period of 1993-2014, and as previously I estimated the pH_{out} by using the nearest 3 grid points in latitude and longitude from the model domain for the months of June and July. All the variables were then interpolated to the depth of the model (Fig. 5.4).

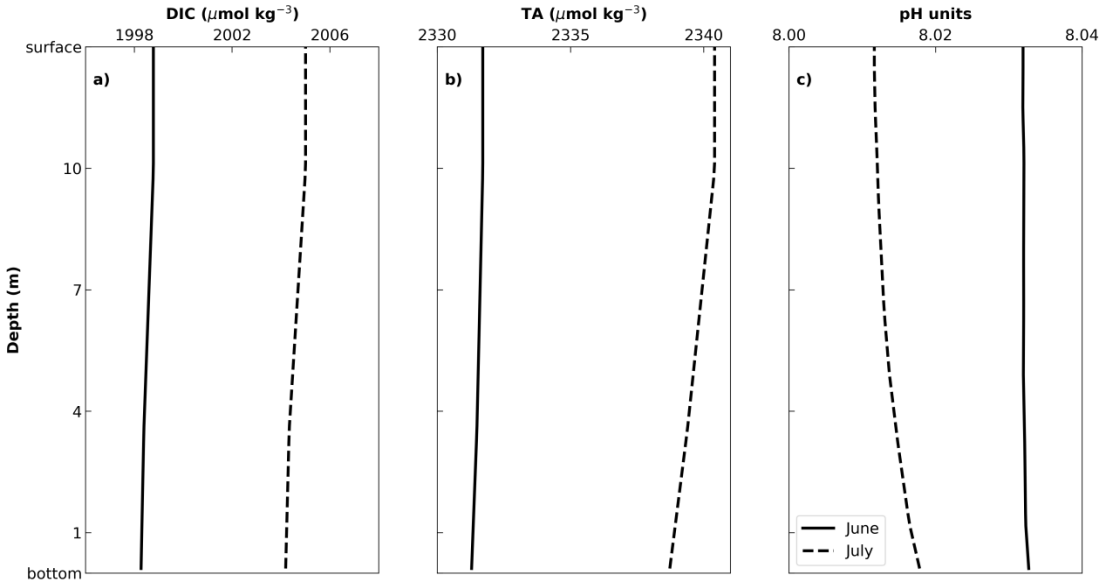

Figure 5.4 - Climatological mean DIC^0, TA^0, and pH_{out} for the months of June (solid line) and July (dashed line).

5.4 RESULTS

Before analyzing the results, the model needs to reach a stable state by allowing for transient oscillations to dissipate (Fig. 5.5). The x-axis shows the result in weeks and y-axis shows

the amplitude of the sea surface elevation in centimeters. Besides the first week of adjustment, all the simulations had approximately the same amplitude throughout the length of the simulation. I decided to use from week 4 to week 9 because, week 4 is when the currents are 100% and up to week 9 because it feels the change in variability was not as abrupt as past the week 9. All the analysis was based on 5 weeks (week 4 to week 9) with hourly dataset.

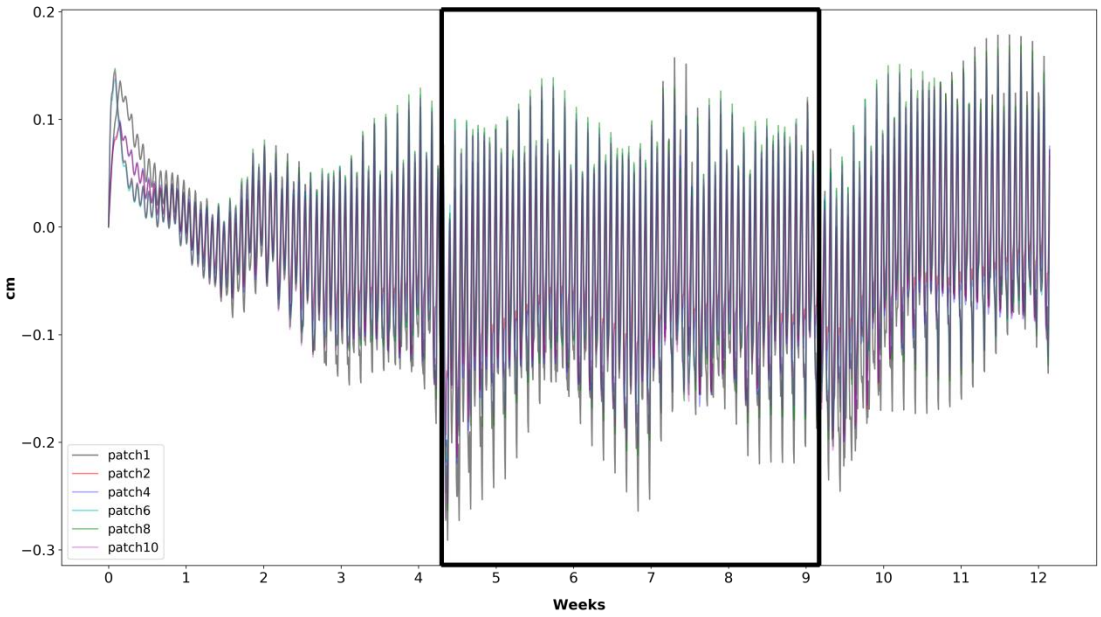

Figure 5.5 - Spin up of the different patches. Square box indicates the length of the simulation utilized to do the calculations.

5.4.2 Turbulent Kinetic Energy (TKE)

Profiles of the ratio of TKE to the velocity magnitude squared (hereafter TKE ratio) by total velocity for all scenarios further illustrate the effects of fragmentation on flows (Fig. 5.6). TKE is generally described by the intensity of the turbulent motion. The canopy region is believed to be an important region that dissipates TKE ratio (Rosman *et al.* 2010; Fagundes *et al. in preparation*). The solid gray line represents the average TKE outside the kelp forest domain close to the west

boundary region. The model without kelp forest showed an almost TKE ratio equals 0 within 4 meters to the surface. The TKE ratio increased to a maximum equal approximately 2.5 for the outside region. The only time TKE ratio was the same for all scenarios was between 8-9m from the bottom. The non-fragmented region was in principle the same way Rosman *et al.* (2010) represented dense kelp forest in the laboratory experiment. The result at the canopy region is for 1 patch experiment had a maximum TKE ratio is 4.5 while Rosman *et al.* (2010) found TKE ratio equals 4 which indicates that 100% coverage adopted (eq. 1) could produce roughly the same turbulence as a laboratory experiment. While Fagundes *et al.* (*in preparation*) found that they had to reduce the coverage by 50% to reach close to what Rosman *et al.* (2010) found. Bottom TKE ratio for non-fragmented scenario also showed similar values to Rosman *et al.* (2010). As a result, I can assume the model is representing well the turbulence created due to kelp forests in a regional ocean model.

The relative percentage difference between non-fragmented and fragmented scenarios increase from 66% for scenarios with 8 and 10 patches to as much as an 80% decrease in turbulence dissipation. The simulation with 4 patches dissipates more turbulence than 6 patches. It is interesting to observe an inversion in TKE ratio within the first 2.5 m from the bottom. Although, 2 patches showed the lowest TKE ratio at the canopy region, it showed a 33% increase in turbulence dissipation compared to 1 patch at the bottom layer. The scenarios with 8 and 10 patches showed similar TKE ratio as the non-fragmented region at the bottom layer.

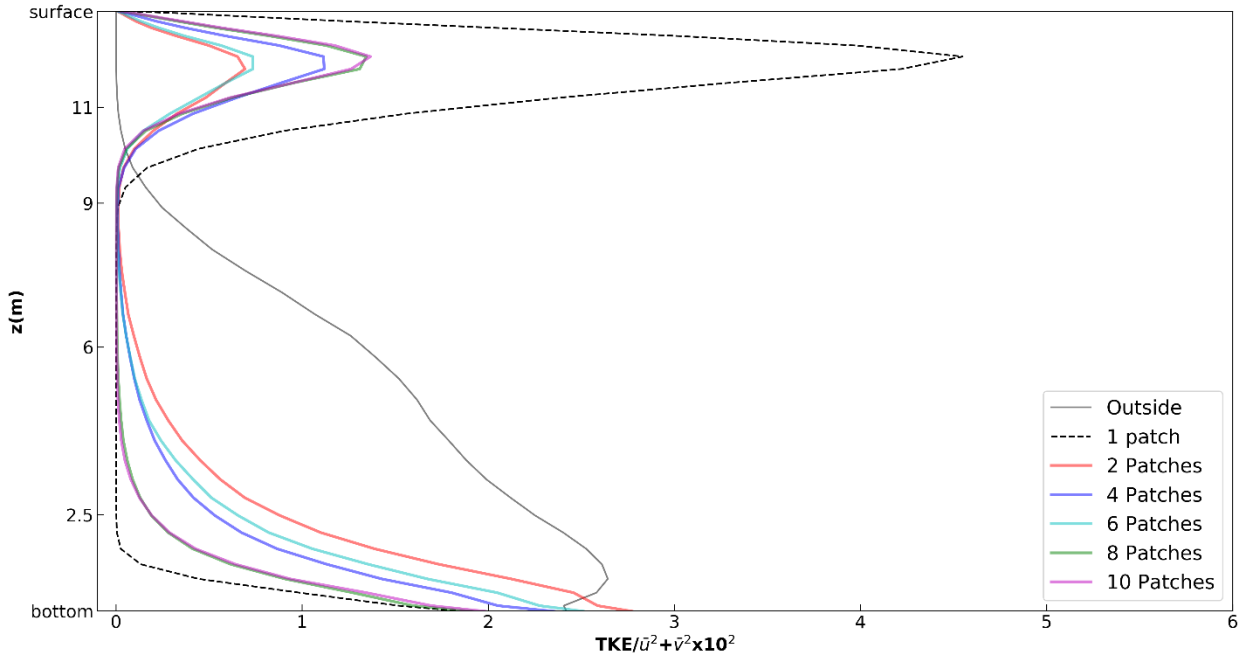

Figure 5.6 - Averaged normalized TKE for the area of 1 patch scenario.

5.4.3 Depth-averaged velocities

The positive mean depth-averaged velocity calculated for the 5 weeks is shown in Fig. 5.7. As expected the middle of the non-fragmented patch (Fig. 5.7a) is where mean along-shore velocities reached values close to zero. This result is expected as Jackson (1997) observed similar patterns in a kelp forest region that was almost completely non-fragmented. The shapes and maximum mean depth-averaged velocity varied among the simulations, though. Mean along-shore velocity reached the maximum absolute value in the beginning and on the east side of the 1 patch simulation. Maximum flow-ducting was also observed especially for scenarios with 2 and 4 patches. As the spaces between kelp patches decrease, and therefore, more attenuation of along-shore velocities, weaker mean flows occur in between the patches (Fig. 5.7e-f).

All negative mean along-shore velocities showed an opposite pattern in the flow (Fig. 5.8) and mirrored Fig. 5.7. Accordingly with Gaylord *et al.* (2007) a flow reversal is generally formed as a

flow passes a solid object or region and it is generally developed in the wake of the forests. Flow ducting did not occur in Fig. 5.8b which could be due to the larger patch blocked the flow. However, some flow ducting still occurred for Fig. 5.8c and Fig. 5.8f surprisingly had some flow increase inside the domain.

Along-shore depth-averaged variability inside the kelp forest patches decreased (Fig. 5.9). The outer boundary flow region decreased but the outer depth-averaged along-shore variability increased by a minimum of 4.2-fold and maximum of 5.9-fold for 10 patches and 2 patches, respectively. The wakes generated east of the flow were between 1.2 to 1.4-fold greater than the 1 patch scenario. The only scenario that had a similar outer flow on the North and South regions was the 10 patches simulation.

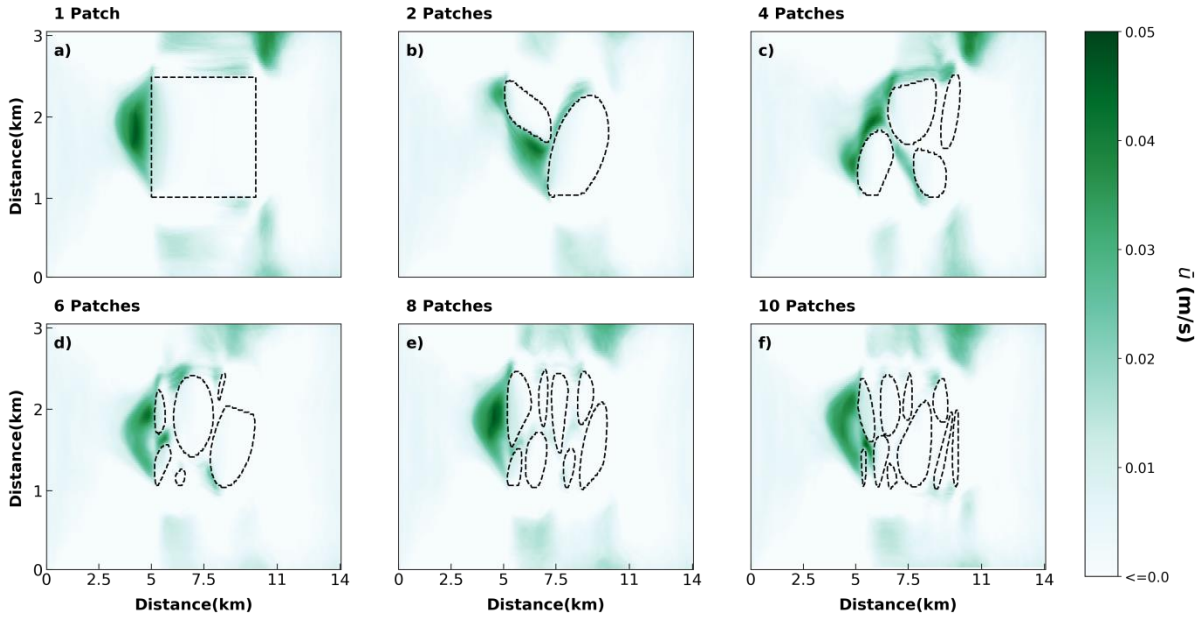

Figure 5.7 - Positive mean depth-averaged along-shore velocity calculated for the 5 weeks in study. Dotted lines represent the kelp forests patches for a better visualization.

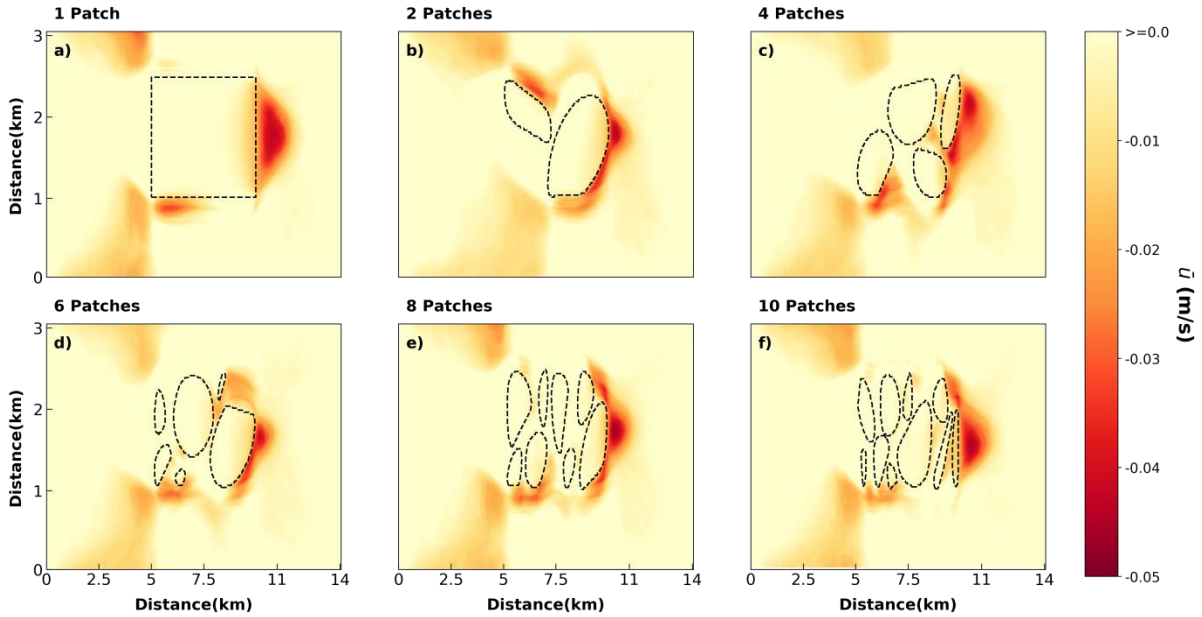

Figure 5.8 - Negative mean depth-averaged along-shore velocity calculated for the 5 weeks in study. Dotted lines represent the kelp forests patches for a better visualization.

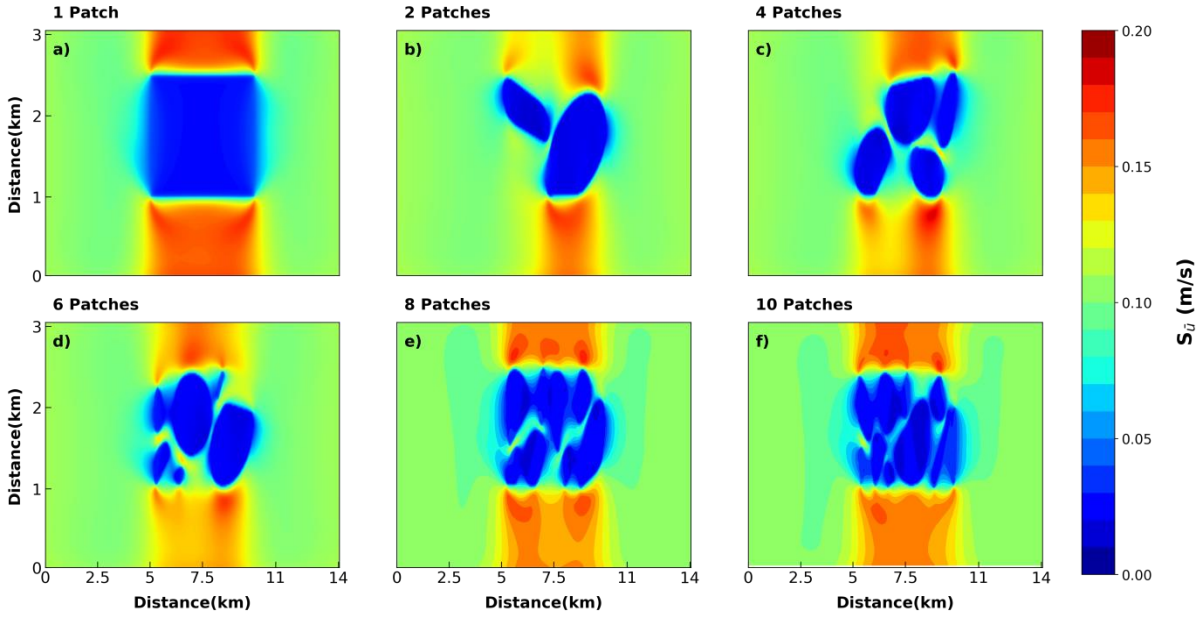

Figure 5.9 - Variability of the along-shore depth-averaged velocity for all fragmentation scenarios. The y-axis represents East-West boundaries and x-axis represents North-South boundaries.

5.4.4 Bulk Drag

The mean bulk drag for all scenarios is summarized in table 5.3. The non-fragmented simulation had a mean C_D of 1.49 which corresponded to an increase between 3.5-fold for the most fragmented simulation (10 patches) to almost 8-fold for the simulation with 6 patches. While these bulk drag values are higher than found in the observational experiments, they are similar to what Liu *et al.* (2021) found running LES scenarios for submerged vegetation patches. The highest mean C_D they found was 1.237 and corresponds to the 1 patch simulation here. It is also good to point it out that in order to keep the same number of plants found in 1 patch to the other scenarios I had to increase the plant density for the other scenarios to 1 plant/m^2 which represents the highest plant density scenario found in the literature. The Kruskal-Wallis H-test for independent samples was applied to understand whether or not the mean C_D found for patches 2 to 10 were the same. The result showed $p < 0.001$ indicating that the mean C_D calculated were statistically significant. However, only the Kruskal-Wallis H-test does not show which particular pair are significant different, and therefore, a posthoc test was applied. The posthoc chosen was Conover's test (Conover & Iman, 1979) to do pairwise comparison. All mean C_D bulk drags were statistically significant with exception of bulk drag for 4 patches and 10 patches with p-value equals 0.4.

Table 5.3 - Averaged bulk drag for different kelp fragmentation scenarios.

	Number of Patches					
	1	**2**	**4**	**6**	**8**	**10**
Mean C_D	1.49	0.26	0.38	0.20	0.33	0.42

5.4.5 Stratification

Buoyancy frequency ($N = \sqrt{-\frac{g}{\rho_0}\frac{d\rho}{dz}}$), where g is the gravity (m s^{-2}), is the fluid density (kg m^{-3}), and z is the depth. *N* was calculated outside the simulation and only for the total area regions with for entire domain corresponding to the area of the one patch domain for all the fragmentation scenarios (Fig. 5.10). Brunt-Väisälä represents the strength of stratification in the water column. As a result, the greater the value of *N* more stratified the water column is (Woodson, 2018). Typical values are between 10^{-3} to 10^{-2} s^{-1}. Stratification for non-kelp region (solid black line) peaked within the last 3 meters to the surface with the maximum value of $.3x10^{-2}$ s^{-1}.

The net Brunt-Väisälä for the non-fragmented (1 patch) simulation showed two stratification peaks, one below the canopy depth and one in the first 3 meters from the bottom. The peak buoyancy frequency around 10 meters in depth could result from the higher residence time at the canopy region, creating more mixing and less stratification. The highest stratification was at the bottom for the non-fragmented area. Koweek *et al.* (2017) found that the bottom was the major contributor affecting the carbon system via increased stratification. Overall, the fragmented simulations (e.g., 2, 4, 6, 8, and 10 patches) showed higher stratification in the canopy region. Also, those simulations showed a slightly upward shift of the stratification peaks. Simulations with 2 and 4 patches showed the lowest net stratification in the canopy region, and both were the closest to the outside profile in stratification strength indicating that less fragmentation could affect benthic organisms more often in the future. Simulated patches 6, 8, and 10 showed the most immediate stratification strength to the profile with no kelp.

Furthermore, the same scenarios had stronger buoyancy in the non-fragmented scenario compared to those with 2 and 4 patches. The closest was the simulation with ten patches. I assume this happened because there are so many patches in one region that they can have a similar effect

in stratification, like when there is no fragmentation and which is the beginning of fragmentation in a kelp forest domain.

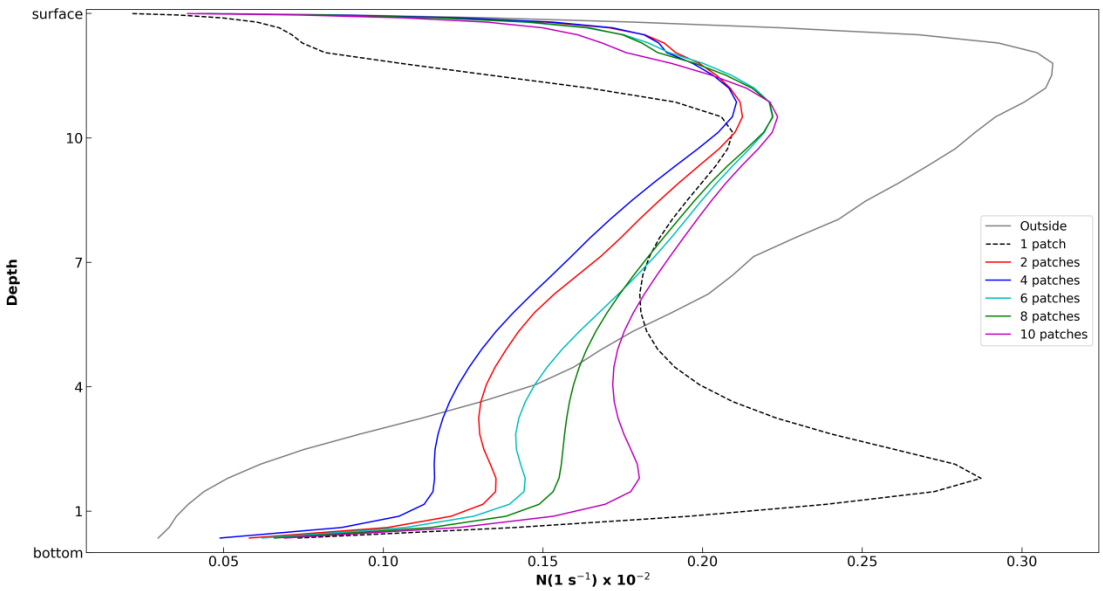

Figure 5.10 - Brunt-Väisälä frequency profiles of simulated kelp forest fragmentation.

5.4.5.1 Percentage relative DO change - bottom

Although, all scenarios showed a decline in DO content at the first meter from the bottom compared to the non-fragmented simulation (Fig. 5.11), they also showed an increase in DO production on both the east and west edges. The middle of the domain represented the region with the lowest DO content compared to the non-fragmented scenario. Scenarios got relatively better as they approached the non-fragmented simulation. For example, scenario with 2 patches showed a minimum decline in DO content of approximately 50% while scenario with 10 patches had a maximum decline in DO of 39%. However, this pattern cannot be applicable to the increase in DO along the edges. The least fragmented scenario (2 patches) showed the highest increase in DO

production on the edges, followed by 6 patches, and 8 patches. Both 4 and 10 patches showed only a decrease in DO compared to 1 patch scenario.

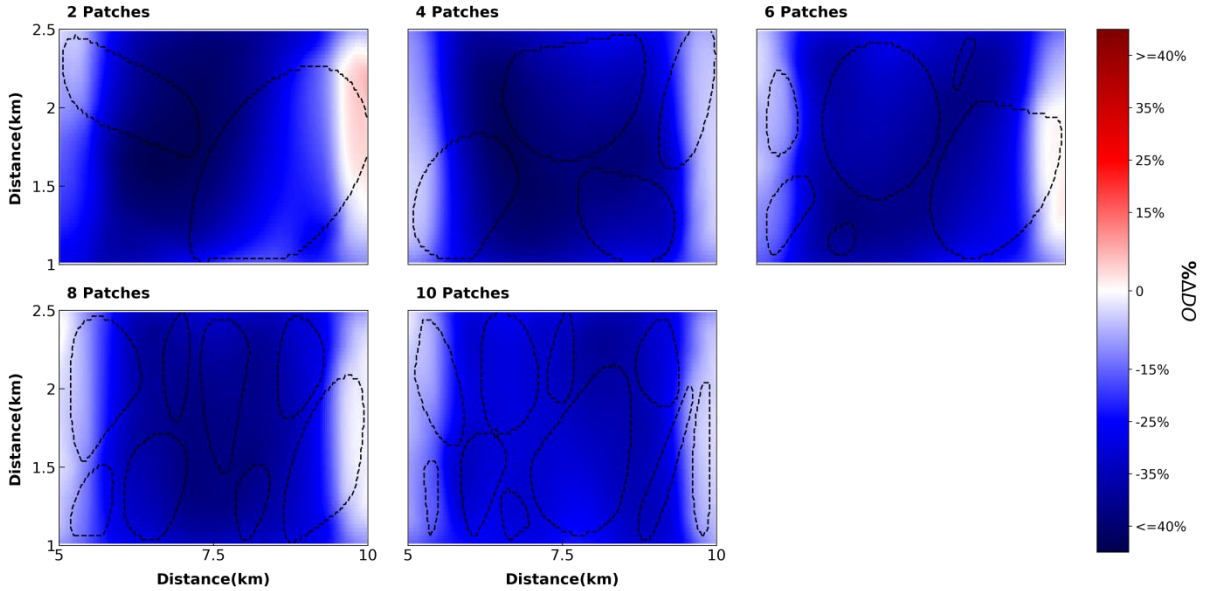

Figure 5.11 - Percentage relative change in DO between non-fragmented and fragmented simulations for 1 meter above bottom.

5.4.5.2 Percentage relative DO change - surface

The decrease in DO relative to the non-fragmented scenario followed more or less same pattern as the bottom relative DO change (Fig. 5.12). The region selected corresponded to the last 3 meters to the surface. This region was selected because it is the region with the highest turbulence observed in Fig. 5.6. The total overall relative DO change for all simulations showed a mean decrease of approximately 9%. The lowest total relative change was found for 6, 8, and 10 patches simulations. The highest decrease was found for the 2 patches simulation with 40% change while 8 patches had the lowest decrease of 20%. One interesting thing to observe is that the regions where there was a decrease in DO for all scenarios corresponded to the channel regions where flow ducting occurs (Valle-Levinson *et al.* 2022). The maximum DO increase was observed for the least

fragmentation scenario (2 patches) with patch regions reaching almost 14% more DO. I suspect that the reason is because the 2 patches has the largest patch among all scenarios. The maximum increase can be observed in patches that are larger than the others in the simulations. As a result, patch size is important for ecology and important for local biogeochemistry or patch size affects biogeochemistry in result affecting larvae that are sensitive to changes.

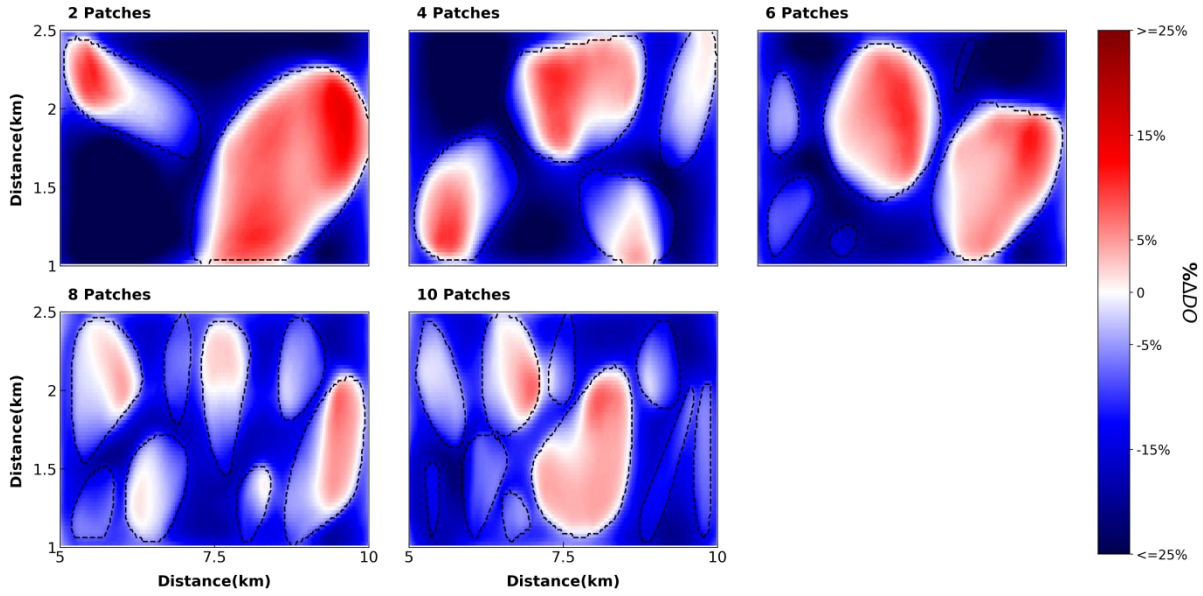

Figure 5.12 - Percentage relative change in DO between non-fragmented and fragmented simulations for the last 3 meters from the surface.

5.4.5 Interior DO and pH

The DO ratio, the ratio between the variance of each fragmented patch scenario to the variance of the non-fragmented scenario for the inner region, is shown in Fig. 5.13. While no actual pattern is observed, no matter how strong is the fragmentation of a kelp forest region, regions below the canopy would have roughly close to 1:1 variability. The lowest variance occurred for the region with 8 patches which had 5-fold more variability than a non-fragmented region. The highest

variability occurred for the simulation with 6 patches being almost 8-fold more variability than the non-fragmented region. The 4 patches simulation showed a 6-fold variability in the DO content within the canopy region. For 2 patches, the variability of DO was 0.5-fold higher than observed in the simulation with 4 patches. Ten patches decreased the variability compared to 6 patches, like mentioned before this could have been the effect that several patches together in the same area almost become a non-fragmented region. This effect is lowered because most of the inner area is a kelp patch region for the simulation with 10 patches.

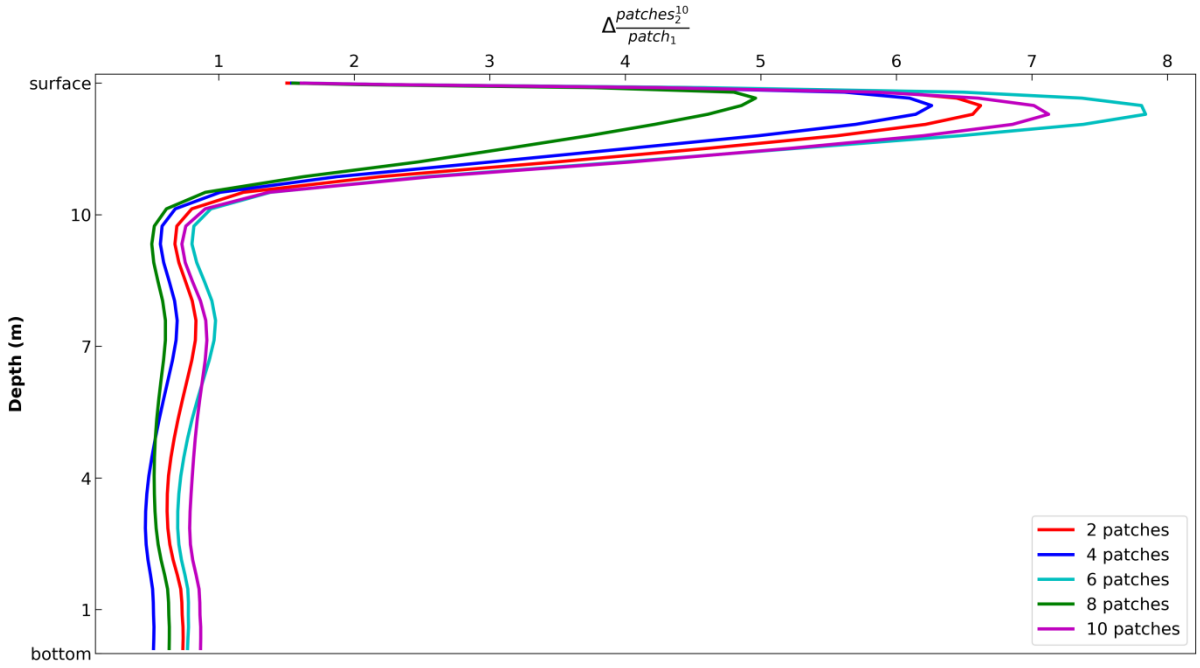

Figure 5.13 - Ratio of the DO variability from the inner region in Fig. 5.2.

The pH calculated for the inner area for all the patches scenarios are shown in Fig. 5.14. The non-fragmented region (1 patch scenario) was used as AOU^0 to calculate DIC and TA for the other scenarios. As a result, if Apparent Oxygen Utilization (AOU) between non-fragmented and fragmented are similar, pHs calculated will be higher. The inner regions had around the same patterns throughout the time in study. There was a strong vertical gradient between 7-14 days for

all scenarios. For the days between 19 and 22 an upwelling-like formation was observed for all scenarios. Around the same period, the 6 patches (Fig. 5.14c) and 10 patches scenarios (Fig. 5.14e) had a blob-like formation of high pH near the canopy region. The pH started moving downwards after day 22 where 2 and 4 patches simulations brought lower pH than the other scenarios. This could be a result of a higher residence time causing DO to decrease which would linearly affect the pH. pH values lower than 8 were observed for the rest of the time in study. The worst-case scenarios were simulations with 2 and 4 patches (Fig. 5.14a-b) as expected since the open area between patches increases. It could also be due to the flow-ducting formation (Fig. 5.7b-c), causing lower residence time, and lower DO and pH from the open ocean.

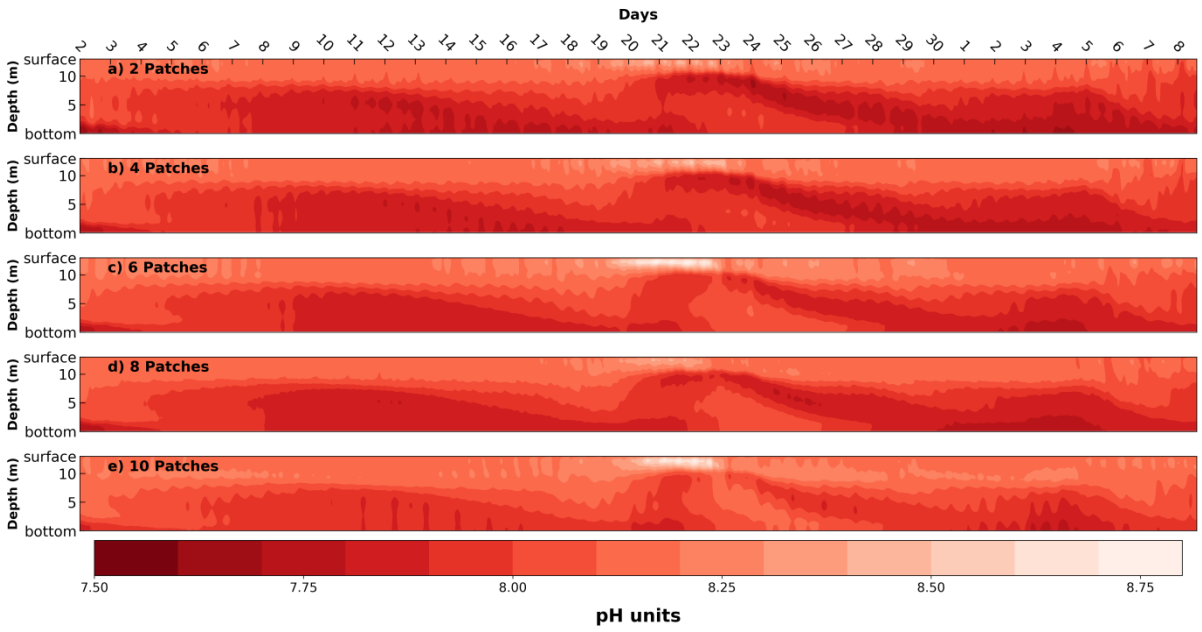

Figure 5.14 - pH time series for the inner region of the kelp forest domain.

5.5 DISCUSSION

The Coupled Ocean-Atmosphere-Wave-Sediment transport (*COAWST*) modelling system has been successfully applied to characterize the effects of fragmentation in the physics and biogeochemistry within kelp forest domains. This new study brought together both *canopy* module and DO model developed previously to understand the concerns of climate change stresses on kelp forests, and consequently, the increase in fragmented kelp forests regions (Murie & Bourdeau, 2020). This study also looked into the biogeochemistry difference between canopy and bottom in fragmented kelp forests regions which have had different conclusions based on field observations.

Observational studies have been the main way to analyze physics and biogeochemistry in the water column in kelp forest domains (Monismith *et al.* 2022a; Low *et al.* 2021). Most of the fragmentation studies have focused on either the ecological impact on organisms (Efird & Konar, 2014; Rogers-Bennett *et al.* 2016) or indirectly via physical or biogeochemistry measurements in already fragmented regions (Murie & Bourdeau, 2020; Valle-Levinson *et al.* 2022). While these studies were important they were conditioned to how the kelp forest domain was shaped at the time of the data collection, and therefore, no directly effect of increased in fragmentation was measured.

As expected, there is an increase in flow through channels, which could result in increased dispersion (Nepf, 2012). Valle-Levinson *et al.* (2022) speculated that these channels could also have positive ecological implications. The mean along-shore depth-averaged for the non-fragmented scenario showed damping in the alongshore velocities as published by Jackson (1997). All the scenarios also showed wake formation downstream of the flow. This is a region where turbulence is generated and reverse-flows are formed (Gaylord *et al.* 2007; Rosman *et al.* 2010). Wu *et al.* (2017) also observed the formation of wakes in a non-fragmented kelp bed simulation.

My results indicate that the maximum fragmentation simulated could increase stratification by 10% compared to non-fragmented domains in the canopy region. However, it would have the lowest change at the bottom with a 41% decrease compared to the 1 patch simulation. The highest reduction in stratification occurs with four patches close to 60% of the original. This could indicate that not even canopy regions would provide natural refugia against temperature variability.

Bottom regions are going to be more affected than canopy regions in the future in agreement with Koweek *et al.* (2017) that suggested that only canopy regions could become a natural refugia against hypoxia. While there is not a large change compared to the non-fragmented scenario, canopy regions showed a positive change in DO in agreement with Murie & Bourdeau (2020) that observed that kelp canopy could alter local biogeochemistry.

5.6 CONCLUSION

This modeling study demonstrated the potential in using the *canopy* and DO model together to study the effects of fragmentation on physics and biogeochemistry in kelp forests using *COAWST*. Fragmentation is a process that is expected to increase in kelp forests under climate change. As a result, this first study utilizing 1 non-fragmented simulation and 5 different levels of fragmentation showed that there is a possibility that less mixing within the canopy region and increase in mixing at the bottom will occur. Additionally, the higher the fragmentation the higher the chances of flow ducting. Mixing will approach a non-kelp scenario even for regions more fragmented, for example, 10 patches. Bottom regions will have a higher decrease in DO production compared to the canopy region. Depending on the fragmentation level low pH would be less likely to occur in the interior regions. For instance, the most fragmented scenario (10 patches) showed less occurrence of low pH compared to the least fragmented scenario (2 patches). I hypothesized

that the 10 patches scenario has so many patches that they almost act as one full single patch. As a result, not so much fragmentation but depending on the patch size and patch distribution in the domain, the domain could still represent a climate refugia in the future.

CHAPTER 6

CONCLUSION AND FUTURE WORK

Kelp forests are present in over 25% of the coastlines in the world. They vary their size, density, and patchiness both seasonally and/or due to large-scale events (marine heatwaves, El Niño, storms; climate change; Dayton & Tegner, 1984; Dayton, 1985; Gaylord *et al.* 2007; Dalmau *et al.* 2020; Monismith *et al.* 2022a). They have been studied extensively using observational methods that, while important, can only provide limited insight into the overall ecology, physics, and biogeochemistry of the kelp forest domain (Koweek *et al.* 2017; Wernberg *et al.* 2018; Monismith *et al.* 2022a). Additionally, inferences about the effects of kelp forests in future climate scenarios are constrained to speculations based on present observations or laboratory experiments (Rosman *et al.* 2010; Murie & Bourdeau, 2020). For example, little is known about how fragmentation will alter local DO and pH and global carbon uptake at the end of the 21st century (Murie & Bourdeau, 2020). This research has developed valuable tools that I used to answer some of the critical questions around the effects of flow-vegetation interactions in kelp forests on their ecology and biogeochemistry. The main findings of this study are:

1) A hydrodynamic module for kelp forests was developed for a regional ocean model. This new module was able to simulate temporally averaged velocity with and without kelp forests, and mean bulk drag was comparable to values from the literature; this module also simulated patterns in the currents (e.g., flow ducting) for the region in study, the ratio of TKE to the velocity magnitude squared observed in the laboratory. 2) The interaction between the DO model and the previously

developed hydrodynamic module could simulate observed DO variability for the study site. The offline approach for pH calculation looks promising for kelp forest environments. Based on these results, kelp forests could offset climate change acidification and hypoxia, which is especially true for the canopy regions.

3) Fragmentation has an enormous impact on turbulence in the water column within kelp forest domains; the least fragmentation (e.g., two patches scenario) produces more and stronger flow ducting. Stratification tends towards non-kelp scenario for more fragmented simulations at the canopy level, and for less fragmented simulations at the bottom. Fragmented simulations are not expected to increase DO at the bottom compared to the non-fragmented scenario; within the canopy regions, the highest decrease and highest increase in DO are anticipated for less fragmented scenarios such as those with 2 and 4 patches. Finally, pH is expected to be higher for simulations with more fragmentation (e.g., ten-patch simulation in the inner region), while simulations with more space between patches had lower pH.

ENGINEERING APPLICATIONS

This work has several contributions and applications to engineering. For example, kelp forests and farming have been suggested as one of the marine carbon dioxide removal (Macreadie *et al.* 2019). However, little is known about the impacts of nutrient cycling, which could change current patterns depending on the size of the kelp farm. The modules developed here show a great potential to understand these impacts before the applications in the oceans. Nowadays, it is estimated that around 40% of the entire population lives within 100 km of the coast (SEDAC, 2011), and 25% of the coastlines in the world have at least one type of kelp forest (Wernberg *et al.* 2019); with that in mind, pollutants could potentially get strained within 5 and 30 meters where these ecosystems are found affecting water quality and important economic species, for example, and having a model

that could understand that is important. This module could also be used to understand the larvae transport of organisms essential to the local economy (Watson *et al.* 2010; Reid *et al.* 2016).

FUTURE WORK

Future work could improve the hydrodynamic module developed in Chapter 3. Despite the module reproducing critical physical aspects, this was done for a specific period with a constant kelp size and density. However, kelp forests are susceptible to seasonality, extreme events, and climate change (Dayton & Tegner, 1984; Dayton, 1985; Gaylord *et al.* 2007; Dalmau et al 2020; Monismith *et al.* 2022). This variability is not present in the module currently, but could be added relatively easily through a time-variant boundary condition. A study exploring the means C_D found in the last chapter to understand the impact of kelp forests in the different resolutions using *COAWST* would also improve the model and advance our understanding of kelp-flow interactions. Also, changes in biomass could also be developed further in the model over seasonal and inter-annual timescales to evaluate potential impacts of extreme events and climate change. Additionally, including the pH model directly to receive feedback from the hydrodynamic and oxygen modules could also give a better understanding view when applying for submesoscale or mesoscale resolutions.

REFERENCES

Anderson, T. W. (1994). Role of macroalgal structure in the distribution and abundance of a temperate reef fish. *Marine ecology progress series. Oldendorf*, *113*(3), 279-290.

Arafeh-Dalmau, N., Montaño-Moctezuma, G., Martínez, J. A., Beas-Luna, R., Schoeman, D. S., & Torres-Moye, G. (2019). Extreme marine heatwaves alter kelp forest community near its equatorward distribution limit. *Frontiers in Marine Science*, *6*, 499.

Beas-Luna, R., Micheli, F., Woodson, C. B., Carr, M., Malone, D., Torre, J., & Torres-Moye, G. (2020). Geographic variation in responses of kelp forest communities of the California Current to recent climatic changes. *Global Change Biology*, *26*(11), 6457-6473.

Bannister, E. J., MacKenzie, A. R., & Cai, X. M. (2022). Realistic Forests and the Modeling of Forest-Atmosphere Exchange. *Reviews of Geophysics*, *60*(1), e2021RG000746.

Beudin, A., Kalra, T. S., Ganju, N. K., & Warner, J. C. (2017). Development of a coupled wave-flow-vegetation interaction model. *Computers & Geosciences*, *100*, 76-86.

Benson, B. B., & Krause Jr, D. (1984). The concentration and isotopic fractionation of oxygen dissolved in freshwater and seawater in equilibrium with the atmosphere 1. *Limnology and oceanography*, *29*(3), 620-632.

Boch, C. A., Micheli, F., AlNajjar, M., Monismith, S. G., Beers, J. M., Bonilla, J. C., ... & Woodson, C. B. (2018). Local oceanographic variability influences the performance of juvenile abalone under climate change. *Scientific reports*, *8*(1), 1-12.

Bodkin, J. L. (1988). Effects of kelp forest removal on associated fish assemblages in central California. *Journal of Experimental Marine Biology and Ecology*, *117*(3), 227-238.

Booth, J. A. T., Woodson, C. B., Sutula, M., Micheli, F., Weisberg, S. B., Bograd, S. J., ... & Crowder, L. B. (2014). Patterns and potential drivers of declining oxygen content along the southern California coast. *Limnology and Oceanography*, *59*(4), 1127-1138.

Britton, D., Cornwall, C. E., Revill, A. T., Hurd, C. L., & Johnson, C. R. (2016). Ocean acidification reverses the positive effects of seawater pH fluctuations on growth and photosynthesis of the habitat-forming kelp, Ecklonia radiata. *Scientific reports*, *6*(1), 26036.

Bryan-Brown, D. N., Connolly, R. M., Richards, D. R., Adame, F., Friess, D. A., & Brown, C. J. (2020). Global trends in mangrove forest fragmentation. *Scientific reports*, *10*(1), 1-8.

Buschmann, A. H., Camus, C., Infante, J., Neori, A., Israel, Á., Hernández-González, M. C., ... & Critchley, A. T. (2017). Seaweed production: overview of the global state of exploitation, farming and emerging research activity. *European Journal of Phycology*, *52*(4), 391-406.

Campbell, N. A., & Atchley, W. R. (1981). The geometry of canonical variate analysis. *Systematic Biology*, *30*(3), 268-280.

Carter, G. S., Gregg, M. C., & Lien, R. C. (2005). Internal waves, solitary-like waves, and mixing on the Monterey Bay shelf. *Continental Shelf Research*, *25*(12-13), 1499-1520.

Cavanaugh, K. C., Reed, D. C., Bell, T. W., Castorani, M. C., & Beas-Luna, R. (2019). Spatial variability in the resistance and resilience of giant kelp in southern and Baja California to a multiyear heatwave. *Frontiers in Marine Science*, *6*, 413.

Cavanaugh, K. C., Siegel, D. A., Kinlan, B. P., & Reed, D. C. (2010). Scaling giant kelp field measurements to regional scales using satellite observations. *Marine Ecology Progress Series*, *403*, 13-27.

Chapra, S. C., Camacho, L. A., & McBride, G. B. (2021). Impact of global warming on dissolved oxygen and BOD assimilative capacity of the world's rivers: Modeling analysis. *Water*, *13*(17), 2408.

Chen, C. T. A., Gong, G. C., Wang, S. L., & Bychkov, A. S. (1996). Redfield ratios and regeneration rates of particulate matter in the Sea of Japan as a model of closed system. *Geophysical Research Letters*, *23*(14), 1785-1788.

Chen, C. T. A., Lui, H. K., Hsieh, C. H., Yanagi, T., Kosugi, N., Ishii, M., & Gong, G. C. (2017). Deep oceans may acidify faster than anticipated due to global warming. *Nature Climate Change*, *7*(12), 890-894.

Colombo-Pallotta, M. F., García-Mendoza, E., & Ladah, L. B. (2006). Photosynthetic performance, light absorption, and pigment composition of macrocystis pyrifera (laminariales, phaeophyceae) blades from different depths 1. *Journal of Phycology*, *42*(6), 1225-1234.

Dayton, P. K. (1985). Ecology of kelp communities. *Annual review of ecology and systematics*, *16*(1), 215-245.

Dayton, P. K., & Tegner, M. J. (1984). Catastrophic storms, El Niño, and patch stability in a southern California kelp community. *Science*, *224*(4646), 283-285.

Denamiel, C., Pranić, P., Quentin, F., Mihanović, H., & Vilibić, I. (2020). Pseudo-global warming projections of extreme wave storms in complex coastal regions: the case of the Adriatic Sea. *Climate Dynamics*, *55*, 2483-2509.

Deza, A. A., & Anderson, T. W. (2010). Habitat fragmentation, patch size, and the recruitment and abundance of kelp forest fishes. *Marine Ecology Progress Series*, *416*, 229-240.

Dickson, A. G. (1990). Standard potential of the reaction: AgCl(s) + 0.5 H_2(g) = Ag(s) + HCl(aq), and the standard acidity constant of the ion HSO_4^- in synthetic sea water from 273.15 to 318.15 K. *Journal of Chemical Thermodynamics* 22, 113–127.

Doney, S. C., Fabry, V. J., Feely, R. A., & Kleypas, J. A. (2009). Ocean acidification: the other CO2 problem. *Annual review of marine science*, *1*, 169-192.

Duarte, C. M., Losada, I. J., Hendriks, I. E., Mazarrasa, I., & Marbà, N. (2013). The role of coastal plant communities for climate change mitigation and adaptation. *Nature climate change*, *3*(11), 961-968.

Duarte, C. M. (2017). Reviews and syntheses: Hidden forests, the role of vegetated coastal habitats in the ocean carbon budget. *Biogeosciences*, *14*(2), 301-310.

Dupont, S., & Brunet, Y. (2008). Edge flow and canopy structure: a large-eddy simulation study. *Boundary-Layer Meteorology*, *126*(1), 51-71.

Edwards, M. S. (2004). Estimating scale-dependency in disturbance impacts: El Niños and giant kelp forests in the northeast Pacific. *Oecologia*, *138*, 436-447.

Efird, T. P., & Konar, B. (2014). Habitat characteristics can influence fish assemblages in high latitude kelp forests. *Environmental biology of fishes*, *97*, 1253-1263.

Eger, A. M., Marzinelli, E. M., Beas-Luna, R., Blain, C. O., Blamey, L. K., Byrnes, J. E., ... & Vergés, A. (2023). The value of ecosystem services in global marine kelp forests. *nature communications*, *14*(1), 1894.

Elias, S.A. (2013). Rise of Human Influence on the World's Biota.

Fahrig, L. (2003). Effects of habitat fragmentation on biodiversity. *Annual review of ecology, evolution, and systematics*, *34*(1), 487-515.

Filbee-Dexter, K., & Scheibling, R. E. (2012). Hurricane-mediated defoliation of kelp beds and pulsed delivery of kelp detritus to offshore sedimentary habitats. *Marine Ecology Progress Series*, *455*, 51-64.

Filbee-Dexter, K., & Wernberg, T. (2020). Substantial blue carbon in overlooked Australian kelp forests. *Scientific Reports*, *10*(1), 1-6.

Frieder, C. A., Nam, S. H., Martz, T. R., & Levin, L. A. (2012). High temporal and spatial variability of dissolved oxygen and pH in a nearshore California kelp forest. *Biogeosciences*, *9*(10), 3917-3930.

Garcia, H. E., & Gordon, L. I. (1992). Oxygen solubility in seawater: Better fitting equations. *Limnology and oceanography*, *37*(6), 1307-1312.

Gaylord, B., Reed, D. C., Raimondi, P. T., Washburn, L., & McLean, S. R. (2002). A physically based model of macroalgal spore dispersal in the wave and current-dominated nearshore. *Ecology*, *83*(5), 1239-1251.

Gaylord, B., Rosman, J. H., Reed, D. C., Koseff, J. R., Fram, J., MacIntyre, S., ... & Mardian, B. (2007). Spatial patterns of flow and their modification within and around a giant kelp forest. *Limnology and Oceanograpy*, *52*(5), 1838-1852.

Gerard, V. A. (1986). Photosynthetic characteristics of giant kelp (Macrocystis pyrifera) determined in situ. *Marine Biology*, *90*, 473-482.

Giomi, F., Barausse, A., Duarte, C. M., Booth, J., Agusti, S., Saderne, V., ... & Fusi, M. (2019). Oxygen supersaturation protects coastal marine fauna from ocean warming. *Science advances*, *5*(9), eaax1814.

Gordon, T. A., Radford, A. N., Simpson, S. D., & Meekan, M. G. (2020). Marine restoration projects are undervalued. *Science*, *367*(6478), 635-636.

Grantham, B. A., Chan, F., Nielsen, K. J., Fox, D. S., Barth, J. A., Huyer, A., ... & Menge, B. A. (2004). Upwelling-driven nearshore hypoxia signals ecosystem and oceanographic changes in the northeast Pacific. *Nature*, *429*(6993), 749-754.

Gruber, N. (2011). Warming up, turning sour, losing breath: ocean biogeochemistry under global change. *Philosophical Transactions of the Royal Society A: Mathematical, Physical and Engineering Sciences*, *369*(1943), 1980-1996.

Haidvogel, D. B., Arango, H., Budgell, W. P., Cornuelle, B. D., Curchitser, E., Di Lorenzo, E., ... & Wilkin, J. (2008). Ocean forecasting in terrain-following coordinates: Formulation and skill assessment of the Regional Ocean Modeling System. *Journal of computational physics*, *227*(7), 3595-3624.

Hirsh, H. K., Nickols, K. J., Takeshita, Y., Traiger, S. B., Mucciarone, D. A., Monismith, S., & Dunbar, R. B. (2020). Drivers of biogeochemical variability in a central California kelp forest: implications for local amelioration of ocean acidification. *Journal of Geophysical Research: Oceans*, *125*(11), e2020JC016320.

Hofmann, G. E., Smith, J. E., Johnson, K. S., Send, U., Levin, L. A., Micheli, F., ... & Martz, T. R. (2011). High-frequency dynamics of ocean pH: a multi-ecosystem comparison. *PloS one*, *6*(12), e28983.

Humphreys, M. P., Lewis, E. R., Sharp, J. D., & Pierrot, D. (2022). PyCO2SYS v1. 8: marine carbonate system calculations in Python. *Geoscientific Model Development*, *15*(1), 15-43.

Jackson, G. A. (1997). Currents in the high drag environment of a coastal kelp stand off California. *Continental Shelf Research*, *17*(15), 1913-1928.

Jiang, L. Q., Carter, B. R., Feely, R. A., Lauvset, S. K., & Olsen, A. (2019). Surface ocean pH and buffer capacity: past, present and future. *Scientific reports*, *9*(1), 18624.

Kalra, T. S., Aretxabaleta, A., Seshadri, P., Ganju, N. K., & Beudin, A. (2017). Sensitivity analysis of a coupled hydrodynamic-vegetation model using the effectively subsampled quadratures method (ESQM v5. 2). *Geoscientific Model Development*, *10*(12), 4511-4523.

Kekuewa, S. A., Courtney, T. A., Cyronak, T., & Andersson, A. J. (2022). Seasonal nearshore ocean acidification and deoxygenation in the Southern California Bight. *Scientific Reports*, *12*(1), 17969.

Kessouri, F., McWilliams, J. C., Bianchi, D., Sutula, M., Renault, L., Deutsch, C., ... & Weisberg, S. B. (2021). Coastal eutrophication drives acidification, oxygen loss, and ecosystem change in a major oceanic upwelling system. *Proceedings of the National Academy of Sciences*, *118*(21), e2018856118.

Koweek, D. A., Nickols, K. J., Leary, P. R., Litvin, S. Y., Bell, T. W., Luthin, T., ... & Dunbar, R. B. (2017). A year in the life of a central California kelp forest: physical and biological insights into biogeochemical variability. *Biogeosciences*, *14*(1), 31-44.

Krause-Jensen, D., Marbà, N., Sanz-Martin, M., Hendriks, I. E., Thyrring, J., Carstensen, J., ... & Duarte, C. M. (2016). Long photoperiods sustain high pH in Arctic kelp forests. *Science Advances*, *2*(12), e1501938.

Ladah, L. B., Zertuche-González, J. A., & Hernández-Carmona, G. (1999). Giant kelp (Macrocystis pyrifera, Phaeophyceae) recruitment near its southern limit in Baja California after mass disappearance during ENSO 1997–1998. *Journal of Phycology*, *35*(6), 1106-1112.

Leary, P. R., Woodson, C. B., Squibb, M. E., Denny, M. W., Monismith, S. G., & Micheli, F. (2017). "Internal tide pools" prolong kelp forest hypoxic events. *Limnology and Oceanography*, *62*(6), 2864-2878.

Liu, Y., MacCready, P., Hickey, B. M., Dever, E. P., Kosro, P. M., & Banas, N. S. (2009). Evaluation of a coastal ocean circulation model for the Columbia River plume in summer 2004. *Journal of Geophysical Research: Oceans*, *114*(C2).

Liu, M., Huai, W., Ji, B., & Han, P. (2021). Numerical study on the drag characteristics of rigid submerged vegetation patches. *Physics of Fluids*, *33*(8), 085123.

Løvås, S. M., & Tørum, A. (2001). Effect of the kelp Laminaria hyperborea upon sand dune erosion and water particle velocities. *Coastal Engineering*, *44*(1), 37-63.

Low, N. H., Micheli, F., Aguilar, J. D., Arce, D. R., Boch, C. A., Bonilla, J. C., ... & Woodson, C. B. (2021). Variable coastal hypoxia exposure and drivers across the southern California Current. *Scientific reports*, *11*(1), 1-10.

Lynn, B. H., Healy, R., & Druyan, L. M. (2009). Investigation of Hurricane Katrina characteristics for future, warmer climates. *Climate Research*, *39*(1), 75-86.

Macreadie, P. I., Anton, A., Raven, J. A., Beaumont, N., Connolly, R. M., Friess, D. A., ... & Duarte, C. M. (2019). The future of Blue Carbon science. *Nature communications*, *10*(1), 3998.

Mancilla-Peraza, M., Palacios-Hernández, E., & López-Castillo, G. (1993). Hydrographic Variability In Bahia Vizcaino, Baja California, Mexico. *Ciencias marinas*, *19*(3), 265-284.

McPhee-Shaw, E. E., Siegel, D. A., Washburn, L., Brzezinski, M. A., Jones, J. L., Leydecker, A., & Melack, J. (2007). Mechanisms for nutrient delivery to the inner shelf: Observations from the Santa Barbara Channel. *Limnology and Oceanography*, *52*(5), 1748-1766.

McPherson, M. L., Finger, D. J., Houskeeper, H. F., Bell, T. W., Carr, M. H., Rogers-Bennett, L., & Kudela, R. M. (2021). Large-scale shift in the structure of a kelp forest ecosystem co-occurs with an epizootic and marine heatwave. *Communications biology*, *4*(1), 298.

Mehrbach, C., Culberson, C. H., Hawley, J. E., & Pytkowicx, R. M. (1973). Measurement of the apparent dissociation constants of carbonic acid in seawater at atmospheric pressure 1. *Limnology and oceanography*, *18*(6), 897-907.

Micheli, F., Saenz-Arroyo, A., Greenley, A., Vazquez, L., Espinoza Montes, J. A., Rossetto, M., & De Leo, G. A. (2012). Evidence that marine reserves enhance resilience to climatic impacts. *PloS one*, *7*(7), e40832.

Monismith, S. G., Alnajjar, M. W., Woodson, C. B., Boch, C. A., Hernandez, A., Vazquez-Vera, L., ... & Micheli, F. (2022a). Influence of kelp forest biomass on nearshore currents. *Journal of Geophysical Research: Oceans*, *127*(7), e2021JC018333.

Monismith, S., Alnajjar, M., Daly, M., Valle-Levinson, A., Juarez, B., Fagundes, M., ... & Woodson, C. B. (2022b). Kelp forest drag coefficients derived from tidal flow data. *Estuaries and Coasts*, *45*(8), 2492-2503.

Mork, M. (1996). The effect of kelp in wave damping. *Sarsia*, *80*(4), 323-327.

Murie, K. A., & Bourdeau, P. E. (2020). Fragmented kelp forest canopies retain their ability to alter local seawater chemistry. *Scientific reports*, *10*(1), 11939.

Nepf, H. M. (1999). Drag, turbulence, and diffusion in flow through emergent vegetation. *Water resources research*, *35*(2), 479-489.

Nepf, H. M. (2012). Flow and transport in regions with aquatic vegetation. *Annual review of fluid mechanics*, *44*, 123-142.

Norderhaug, K. M., Filbee-Dexter, K., Freitas, C., Birkely, S. R., Christensen, L., Mellerud, I., ... & Steen, H. (2020). Ecosystem-level effects of large-scale disturbance in kelp forests. *Marine Ecology Progress Series*, *656*, 163-180.

Pandolfi, J. M., Bradbury, R. H., Sala, E., Hughes, T. P., Bjorndal, K. A., Cooke, R. G., ... & Jackson, J. B. (2003). Global trajectories of the long-term decline of coral reef ecosystems. *Science*, *301*(5635), 955-958.

Pakhomov, E., Kaehler, S., & McQuaid, C. (2002). Zooplankton community structure in the kelp beds of the sub-Antarctic Prince Edward Archipelago: are they a refuge for larval stages?. *Polar Biology*, *25*, 778-788.

Pawlowicz, R., Beardsley, B., & Lentz, S. (2002). Classical tidal harmonic analysis including error estimates in MATLAB using T_TIDE. *Computers & geosciences*, *28*(8), 929-937.

Pessarrodona, A., Assis, J., Filbee-Dexter, K., Burrows, M. T., Gattuso, J. P., Duarte, C. M., ... & Wernberg, T. (2022). Global seaweed productivity. *Science Advances*, *8*(37), eabn2465.

Pierrot, D. E., Wallace, D. W. R., & Lewis, E. (2011). MS Excel program developed for CO2 system calculations. *Carbon Dioxide Information Analysis Center*.

Poëtte, C., Gardiner, B., Dupont, S., Harman, I., Böhm, M., Finnigan, J., ... & Brunet, Y. (2017). The impact of landscape fragmentation on atmospheric flow: a wind-tunnel study. *Boundary-Layer Meteorology*, *163*, 393-421.

Raffaelli, D., & Hawkins, S. J. (1996). *Intertidal ecology*. Springer Science & Business Media.

Reed, D., Rassweiler, A., & Arkema, K. (2009). Density derived estimates of standing crop and net primary production in the giant kelp Macrocystis pyrifera. *Marine Biology*, *156*, 2077-2083.

Reed, D., Washburn, L., Rassweiler, A., Miller, R., Bell, T., & Harrer, S. (2016). Extreme warming challenges sentinel status of kelp forests as indicators of climate change. *Nature Communications*, *7*(1), 13757.

Reid, J., Rogers-Bennett, L., Vasquez, F., Pace, M., Catton, C. A., Kashiwada, J. V., & Tanigushi, L. (2016). The economic value of the recreational red abalone fishery. *California Fish and Game*, *102*(3), 119-130.

Rogers-Bennett, L., Dondanville, R. F., Catton, C. A., Juhasz, C. I., Horii, T., & Hamaguchi, M. (2016). Tracking larval, newly settled, and juvenile red abalone (Haliotis rufescens) recruitment in Northern California. *Journal of Shellfish Research*, *35*(3), 601-609.

Rogers-Bennett, L., & Catton, C. A. (2019). Marine heat wave and multiple stressors tip bull kelp forest to sea urchin barrens. *Scientific reports*, *9*(1), 15050.

Rosman, J. H., Koseff, J. R., Monismith, S. G., & Grover, J. (2007). A field investigation into the effects of a kelp forest (Macrocystis pyrifera) on coastal hydrodynamics and transport. *Journal of Geophysical Research: Oceans*, *112*(C2).

Rosman, J. H., Monismith, S. G., Denny, M. W., & Koseff, J. R. (2010). Currents and turbulence within a kelp forest (Macrocystis pyrifera): Insights from a dynamically scaled laboratory model. *Limnology and Oceanography*, *55*(3), 1145-1158.

Rosman, J. H., Denny, M. W., Zeller, R. B., Monismith, S. G., & Koseff, J. R. (2013). Interaction of waves and currents with kelp forests (Macrocystis pyrifera): Insights from a dynamically scaled laboratory model. *Limnology and Oceanography*, *58*(3), 790-802.

Russell, P., & Vennell, R. (2017). High-resolution observations of secondary circulation and tidally synchronized upwelling around a coastal headland. *Journal of Geophysical Research: Oceans*, *122*(2), 890-913.

Seas, U. R. (2011). Percentage of total population living in coastal areas.

Smale, D. A., Burrows, M. T., Evans, A. J., King, N., Sayer, M. D., Yunnie, A. L., & Moore, P. J. (2016). Linking environmental variables with regional-scale variability in ecological structure and standing stock of carbon within UK kelp forests. *Marine Ecology Progress Series*, *542*, 79-95.

Smale, D. A., Epstein, G., Hughes, E., Mogg, A. O., & Moore, P. J. (2020). Patterns and drivers of understory macroalgal assemblage structure within subtidal kelp forests. *Biodiversity and Conservation*, *29*, 4173-4192.

Schär, C., Frei, C., Lüthi, D., & Davies, H. C. (1996). Surrogate climate-change scenarios for regional climate models. *Geophysical Research Letters*, *23*(6), 669-672.

Schmidtko, S., Stramma, L., & Visbeck, M. (2017). Decline in global oceanic oxygen content during the past five decades. *Nature*, *542*(7641), 335-339.

Shchepetkin, A. F., & McWilliams, J. C. (2005). The regional oceanic modeling system (ROMS): a split-explicit, free-surface, topography-following-coordinate oceanic model. *Ocean modelling*, *9*(4), 347-404.

Schlenger, A. J., Beas-Luna, R., & Ambrose, R. F. (2021). Forecasting ocean acidification impacts on kelp forest ecosystems. *PloS one*, *16*(4), e0236218.

Scully, M. E. (2010). Wind modulation of dissolved oxygen in Chesapeake Bay. *Estuaries and coasts*, *33*, 1164-1175.

Steneck, R. S., Graham, M. H., Bourque, B. J., Corbett, D., Erlandson, J. M., Estes, J. A., & Tegner, M. J. (2002). Kelp forest ecosystems: biodiversity, stability, resilience and future. *Environmental conservation*, *29*(4), 436-459.

Stramma, L., Schmidtko, S., Levin, L. A., & Johnson, G. C. (2010). Ocean oxygen minima expansions and their biological impacts. *Deep Sea Research Part I: Oceanographic Research Papers*, *57*(4), 587-595.

Swart, Neil Cameron; Cole, Jason N.S.; Kharin, Viatcheslav V.; Lazare, Mike; Scinocca, John F.; Gillett, Nathan P.; Anstey, James; Arora, Vivek; Christian, James R.; Jiao, Yanjun; Swart, N. C., Cole, J. N., Kharin, V. V., Lazare, M., Scinocca, J. F., Gillett, N. P., ... & Sigmond, M. (2019). IPCC DDC: CCCma CanESM5-CanOE model output prepared for CMIP6 ScenarioMIP.

Swart, N. C., Cole, J. N., Kharin, V. V., Lazare, M., Scinocca, J. F., Gillett, N. P., ... & Sigmond, M. (2019). IPCC DDC: CCCma CanESM5-CanOE model output prepared for CMIP6 ScenarioMIP.

Tegner, M. J., Dayton, P. K., Edwards, P. B., Riser, K. L., Chadwick, D. B., Dean, T. A., & Deysher, L. (1995). Effects of a large sewage spill on a kelp forest community: Catastrophe or disturbance?. *Marine Environmental Research*, *40*(2), 181-224.

Thomson, R. E., & Emery, W. J. (2014). *Data analysis methods in physical oceanography*. Newnes.

Thurstan, R. H., Brittain, Z., Jones, D. S., Cameron, E., Dearnaley, J., & Bellgrove, A. (2018). Aboriginal uses of seaweeds in temperate Australia: an archival assessment. *Journal of Applied Phycology*, *30*, 1821-1832.

Traiger, S. B., Cohn, B., Panos, D., Daly, M., Hirsh, H. K., Martone, M., ... & Nickols, K. J. (2022). Limited biogeochemical modification of surface waters by kelp forest canopies: Influence of kelp metabolism and site-specific hydrodynamics. *Limnology and Oceanography*, *67*(2), 392-403.

Trenberth, K. E. (1997). The definition of el nino. *Bulletin of the American Meteorological Society*, *78*(12), 2771-2778.

Utter, B. D., & Denny, M. W. (1996). Wave-induced forces on the giant kelp Macrocystis pyrifera (Agardh): field test of a computational model. *Journal of experimental Biology*, *199*(12), 2645-2654.

Valle-Levinson, A., Daly, M. A., Juarez, B., Tenorio-Fernandez, L., Fagundes, M., Woodson, C. B., & Monismith, S. G. (2022). Influence of kelp forests on flow around headlands. *Science of the Total Environment*, *825*, 153952.

von Schuckmann, K., Le Traon, P. Y., Smith, N., Pascual, A., Brasseur, P., Fennel, K., ... & Zuo, H. (2018). Copernicus marine service ocean state report. *Journal of Operational Oceanography*, *11*(sup1), S1-S142.

Walter, R. K., Woodson, C. B., Arthur, R. S., Fringer, O. B., & Monismith, S. G. (2012). Nearshore internal bores and turbulent mixing in southern Monterey Bay. *Journal of Geophysical Research: Oceans*, *117*(C7).

Watson, J. R., Mitarai, S., Siegel, D. A., Caselle, J. E., Dong, C., & McWilliams, J. C. (2010). Realized and potential larval connectivity in the Southern California Bight. *Marine Ecology Progress Series*, *401*, 31-48.

Warner, J. C., Geyer, W. R., & Lerczak, J. A. (2005). Numerical modeling of an estuary: A comprehensive skill assessment. *Journal of Geophysical Research: Oceans*, *110*(C5).

Warner, J. C., Sherwood, C. R., Signell, R. P., Harris, C. K., & Arango, H. G. (2008). Development of a three-dimensional, regional, coupled wave, current, and sediment-transport model. *Computers & geosciences*, *34*(10), 1284-1306.

Wernberg, T., Smale, D. A., Tuya, F., Thomsen, M. S., Langlois, T. J., De Bettignies, T., ... & Rousseaux, C. S. (2013). An extreme climatic event alters marine ecosystem structure in a global biodiversity hotspot. *Nature Climate Change*, *3*(1), 78-82.

Wernberg, T., Krumhansl, K., Filbee-Dexter, K., & Pedersen, M. F. (2019). Status and trends for the world's kelp forests. In *World seas: An environmental evaluation* (pp. 57-78). Academic Press

Willmott, C. J. (1981). On the validation of models. *Physical geography*, *2*(2), 184-194.

Woodson, C. B. (2018). The fate and impact of internal waves in nearshore ecosystems. *Annual review of marine science*, *10*, 421-441.

Wu, Y., Hannah, C. G., O'Flaherty-Sproul, M., & Thupaki, P. (2017). Representing kelp forests in a tidal circulation model. *Journal of Marine Systems*, *169*, 73-86.